Remote Sensing Series 65

Philip Claudio Jörg

Assessment of Glacial Changes, Surface Properties, and Related Uncertainties Based on Airborne Laser Scanning

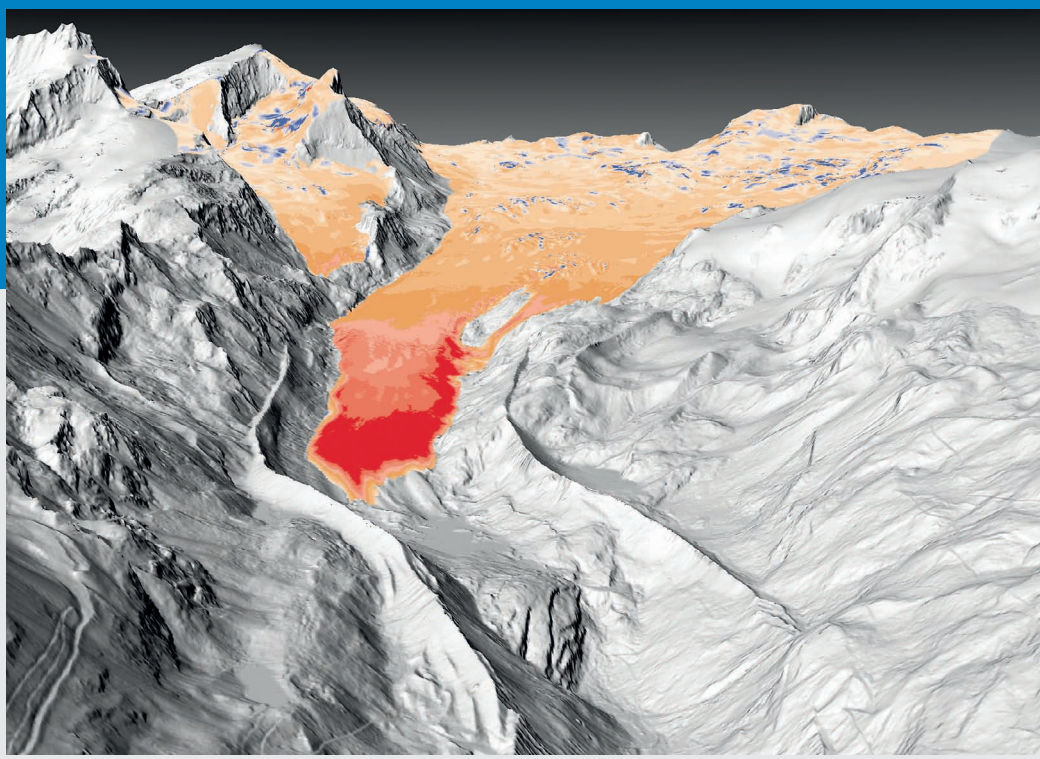

Remote Sensing Laboratories
Department of Geography
University of Zurich, 2014

Remote Sensing Series 65

Philip Claudio Jörg

Assessment of Glacial Changes, Surface Properties, and Related Uncertainties Based on Airborne Laser Scanning

Remote Sensing Laboratories
Department of Geography
University of Zurich, 2014

Front page: 3-dimensional rendering of the Findelengletscher, Valais, Switzerland, and surroundings using airborne laser scanning digital elevation models. Colors indicate the change in elevation of the glacier from 2005 to 2010, ranging from more than 24 meters elevation decrease at the tongue (dark red) to little elevation change (light yellow and light blue), and areas of elevation gain in the accumulation area in the range of few meters (blue).

Jörg, Philip Claudio

Assessment of Glacial Changes, Surface Properties, and Related Uncertainties Based on Airborne Laser Scanning.

Remote Sensing Series, Vol. 65
Remote Sensing Laboratories, Department of Geography, University of Zurich
Switzerland, 2014

ISBN: 978-3-03703-031-8

This work was approved as a PhD thesis by the Faculty of Science of the University of Zurich in the fall semester 2014. Doctorate committee: Prof. Dr. Michael E. Schaepman (chair), Prof. Dr. Wilfried Haeberli, PD Dr. Michael Zemp (dissertation supervisor), Dr. Felix Morsdorf. External examiner: Prof. Dr. Bernhard Höfle (Heidelberg University, Germany).

SUMMARY

Glaciers are unique and obvious natural indicators of climate change. Long-term shifts in temperature or precipitation regimes result in alterations in the shape and volume of a glacier. The consequences of such glacier changes are far-reaching and concern both the immediate and distant environment, both today and in the future. In Switzerland, there have been few positive consequences, but most implications are negative, including less water available for energy production, drinking water, and irrigation, as well as increased risks of natural hazards. Observing glacier changes and assessing the related measurement uncertainties are essential requirements for secondary impact studies and are investigated in-depth in this PhD thesis.

The thesis consists of four peer-reviewed scientific publications evaluating digital elevation models and albedo measurements using airborne laser scanning (ALS). These contributions focus on investigations of systematic and stochastic uncertainties of ALS and its benefits for glaciology.

In the first paper, the volume change in the Findelengletscher in the Swiss Canton of Valais was calculated with the ALS digital elevation models. In addition, a physical error model was developed to enable the assessment of uncertainties in the volume change and the allocation of errors at any location in the study site which can then be used to calculate the overall error. At the same time, the observed errors could be traced back to their sources.

The ALS elevation models evaluated were subsequently used in a second publication as reference data sets to evaluate the limitations of traditional and established methods to measure glacier volume changes. The scale and method-dependent limitations and uncertainties in these methods were identified and recommendations for their application given. The third paper addressed the seasonal volume balance, i.e. the winter snow accumulation, resulting in a distributed accumulation map of the Findelengletscher. This provided insights into the accumulation distribution and the dynamic glacier processes involved, which could then be used to enhance glaciological energy and mass balance models.

To accurately model the glacier mass balance, not only is it important to understand glacier processes, but also the surface albedo, which is a paramount factor. Up to now, the values from the literature used are mostly approximate and not based on any field measurements. In the fourth study, we evaluated ways of extracting the distributed albedo from ALS intensity data. This albedo approximation can serve as the initialization point for glacier mass balance models and benefits from reflectance ALS information in addition to the topographic products.

The results of these papers demonstrate the benefits and successful application of ALS in glaciology. In addition, the limitations of the methods are discussed and potential future developments of the data and methods described as part of a general outlook.

ZUSAMMENFASSUNG

Gletscher sind einzigartige und augenfällige natürliche Indikatoren der Klimaänderung. Längerfristige Veränderungen von Temperatur- und Niederschlagsregime resultieren in einer Anpassung der Form und des Volumens eines Gletschers. Die Folgen dieser Gletscheränderungen sind weitreichend und betreffen ihre nähere und fernere Umwelt, jetzt und in der Zukunft. In der Schweiz sind, neben wenigen positiven, vor allem negative Konsequenzen absehbar wie die verringerte Verfügbarkeit von Wasser zur Gewinnung von Energie, als Trinkwasser, zur Bewässerung sowie das steigende Risiko von Naturgefahren. Die exakte Feststellung von Gletscheränderungen und zugehörigen Messunsicherheiten stellen deshalb entscheidende Voraussetzungen für Untersuchungen zur Folgenabschätzung dar und werden in dieser Dissertation vertieft untersucht.

Die vorliegende Arbeit befasst sich, basierend auf vier wissenschaftlichen Publikationen, mit digitalen Höhenmodellen und Albedomessungen aus Airborne Laser Scanning (ALS) Daten. Der Fokus dieser Beiträge liegt auf Untersuchungen der systematischen und stochastischen Fehler der Methoden und den Vorteilen der Nutzung von ALS in der Glaziologie.

In einem ersten Schritt wurde die Volumenänderung des Findelengletschers im Schweizer Kanton Wallis basierenden auf ALS Höhenmodellen berechnet. Zudem wurde ein physikalisches Fehlermodell entwickelt, um eine Abschätzung der Genauigkeit der Veränderung zu geben. Die physikalische Modellierung dieser Fehler lässt deren Abschätzung an jedem Ort eines Untersuchungsgebiets zu und somit den flächenhaft integrierten Fehler quantifizieren. Gleichzeitig erlaubt es, die festgestellten Fehler ihrem Ursprung zuzuweisen.

Nach der Feststellung der Genauigkeit der Höhenmodelle wurden an diesen Referenzdatensätzen in einer zweiten Publikation verschiedene etablierte Methoden zur Berechnung der Volumenänderung von Gletschern verglichen. Daraus liessen sich skalen- und methodenabhänginge Limitationen der klassischen Methoden aufzeigen und Empfehlungen über deren Nutzen sowie involvierte Unsicherheiten abgeben. Der dritte wissenschaftliche Beitrag befasste sich mit der saisonalen Volumenbilanz, respektive der Winter-Schneeakkumulation. Die vorliegende Arbeit führte zu einer Akkumulationskarte des Findelengletschers und ermöglichte so einen Einblick in die Akkumulationsverteilung und die involvierten dynamischen Gletscherprozesse. Die so erzeugten Daten tragen somit zur Verbesserung von glaziologischen Energie- und Massenbilanzmodellen bei.

Neben dem Verständnis der Gletscherprozesse ist die Albedo der Gletscheroberfläche ein vorrangiger Faktor zur Modellierung der Massenbilanz. Bisher wurden dafür vor allem Richtwerte aus der Literatur und kaum flächenhafte Messungen verwendet. In einer vierten Studie wurde deshalb die Berechnung der flächendeckenden Gletscher-Albedo aus ALS-Intensitätsdaten untersucht. Die errechnete Albedo-Näherung kann als Startpunkt für Gletscher-Massenbilanz-Modelle dienen und neben dem Nutzen der topographischen auch die spektralen Informationen von ALS verwerten.

Die Resultate dieser Publikationen demonstrieren den positiven Nutzen und die erfolgreiche Anwendung von ALS im Dienste der Glaziologie. Des weiteren werden Limitationen besprochen und in einem generellen Ausblick Perspektiven für die Weiterentwicklung der verwendeten Daten und Ansätze aufgezeigt.

TABLE OF CONTENTS

1 INTRODUCTION

1.1 General context

Climatic changes have always influenced life on earth. In the past more than 100 years, however, the growing human population started has influencing the climatic conditions on a global scale. For example, increasing greenhouse gas emissions from burning fossil fuels have led to atmospheric CO_2-concentrations surpassing historical levels. These climatic changes pose threats to all Earth's spheres, including the anthroposphere, by, e.g., increasing global mean air temperatures and rising sea levels. To assess and mitigate the impacts of such threats and enable projections into the future, climate changes in the past must be better understood. The present dissertation generally aims at strengthening the evidence for climate change on the basis of high resolution airborne laser scanning (ALS) data in glacier research and at providing an assessment of the uncertainties involved.

First, a short introduction to glaciology, measuring glacier changes, and the study site is provided in section 1.2. Subsequently, the use of airborne laser scanning for glacier applications is explored in section 1.3, the motivations for the study described and the research questions addressed in the four scientific papers in chapters 2-5 described. In chapter 6, the main results are discussed and the possibilities for further research outlined.

1.2 Climate change induced changes in glaciers: the scientific background

1.2.1 Glaciers as climate change indicators

Glaciers are bodies of ice that form where snow accumulation exceeds ablation. After a metamorphosis process from snow to firn and ice, the ice mass starts to flow downslope, driven by gravity. As the flow leads to the ice being exposed to higher temperature at lower elevations, the ice starts to melt again. A glacier consists therefore of two distinguishable regions: the accumulation area, where snow persists over summer, and the ablation area, where the existence of glacier ice is only possible by continued dynamic flow into this area of melt (Kaser et al. 2003).

The mass change of glaciers is primarily driven by climatic changes. Small changes in the temperature and precipitation regime of a glacier have a distinct influence on its mass and shape. Therefore, observed glacier changes are widely accepted as key indicators of climate change (Haeberli et al. 2007; Lemke et al. 2007).

Since the Little Ice Age, which ended at around 1850, Alpine glaciers have generally lost mass and retreated from their former maximum extent due to global warming (Zemp et al. 2006). For many glaciers, this general trend was interrupted by a few years of glacier re-advance mainly in the 1970s and 1980s. In the past three decades, glacier retreat has accelerated, and melt rates not measured previously have been observed (Zemp et al. 2006). The loss of glacier mass and the glacier retreat have a variety of so-

cio-economic impacts, affecting natural hazards, hydropower generation, irrigation, and tourism (Beniston et al. 2011; Keiler et al. 2010). On a global scale, the contribution of glacier melt water to global sea level rise is only surpassed by the thermal expansion of the oceans, which means it is the strongest land-based cause of sea level rise (Lemke et al. 2007). Long-term monitoring of glacier changes and modeling of future expected changes is therefore essential not only for climatic change studies but also for assessing and mitigating the secondary impacts of changes in glaciers on any scale.

1.2.2 Measuring and modeling glacier changes

Basically, three approaches to glacier research have been taken: local studies of single glaciers investigating processes in-depth (typically short term), studies of large glacier ensembles on a global scale, and glacier inventories (typically long term; Haeberli et al. 2007). Monitoring glacier changes in long time series is especially important to obtain information about climate fluctuations at the studied sites as well as various impacts on local, regional and global scales (Kaser et al. 2003).

Measuring glacier changes on the different scales these research strategies require has led to the evolution of multiple methods, generally involving in-situ measurements, remote sensing data, and modeling. The traditional in-situ method, called the direct glaciological approach, calculates the annual mass balance of glaciers using data from ablation stakes in the ablation area of a glacier, snow pits with snow density measurements in the accumulation area of a glacier, and extrapolation methods to account for the entire glacier surface (Østrem and Brugmann 1991). Often, expert knowledge of the glaciers is used to enhance the mass balance result by manually introducing spatially distributed accumulation and melt patterns. These methods directly lead to the mass balance in meters water equivalent, and are therefore already corrected for different snow and ice densities. However, using the direct glaciological method as exclusive input for a mass balance series will lead to an accumulation of systematic uncertainties and must therefore be checked by an independent method, ideally by decadal volume change measurements from a geodetic method (Cogley 2009; Haug et al. 2009; Huss et al. 2009; Zemp et al. 2010).

In contrast to in-situ measurements, measurements of elevation change do not directly provide the local or distributed mass balance of a glacier for two reasons. First, in the accumulation area, snow is altered to form firn and later ice in a dynamic metamorphism process. Therefore, the elevation of the snow and firn pack is changed by densification processes, which are difficult to measure with remote sensing methods. Second, the viscous nature of ice leads to a dynamic transport of the ice body from the high accumulation area to the lower ablation area. This is not only a translational process but also leads to changing surface elevations, with decreases due to submergence in the accumulation area and increases due to emergence in the ablation area. Comparing traditional in-situ with remote sensing based measurements is therefore not a straightforward task.

In order to measure the change in volume of a glacier, distributed elevation difference data covering the entire glacier at different points in time are needed. The volume difference can then be calculated by subtracting all horizontally corresponding elevations in two digital elevation models (DEMs) and summing all the elevation differences times the area per raster cell. However, the resulting volume change is not directly transformable to a glacier-wide mass balance in meters water equivalent as the density of the vol-

ume difference is not known. In addition, the local elevation changes do not represent the local mass balance, e.g. at an ablation stake location due to the dynamic processes explained earlier. Both challenges have to be tackled to calculate mass balances (Huss 2013; Sapiano et al. 1998).

Topographic data do, however, provide an independent data source to investigate glacier processes and variations. The oldest topographic data available for Switzerland are contour lines in the Siegfried and Dufour maps, dating back more than 140 years (Oberli 1979). Such maps were produced from classical in-situ geodetic surveys and their contour line locations can be used to calculate the volumetric change in a glacier (Finsterwalder 1954; Hofmann 1958). With the advent of aerial photography, photogrammetric methods were introduced to derive distributed elevation models for glacier research (e.g. since the 1950s at Storglaciären, Sweden; Zemp et al. 2010). However, the presence of shaded and low-textured surfaces, especially in the accumulation area, can lead to large inconsistencies in the resulting DEMs. This problem has only been mitigated recently with the introduction of multi-angular near-infrared airborne cameras. These newer cameras still, however, depend on the surface texture and solar illumination of the study site and may thus still produce erroneous areas in DEMs.

In contrast, airborne laser scanning as an active emitting method has been shown to produce accurate DEMs independent of external illumination and snow textures. ALS in glaciological applications is described in more detail in section 1.3.

The methods to determine elevations discussed before are usually only available for a regional area and have to be updated by sometimes expensive flight campaigns and laborious data analysis. Fortunately, earth-observing spaceborne systems provide periodic operational measurements of the earth's surface. For example, ASTER on board the Terra satellite produces photogrammetric elevation data, which can be used in glaciological applications (Global Digital Elevation Map GDEM; Tachikawa et al. 2011), although it poses some photogrammetric challenges. The spaceborne geoscience laser altimeter system (GLAS) on ICESat provided elevation measurements that were especially useful for Arctic applications (Zwally et al. 2002). However, this sensor was less useful in Alpine regions because of its temporal resolution and spatial sampling pattern. A third type of instrument, the synthetic aperture RADAR present on some satellites, is able to measure topographic changes. A milestone of near-global digital elevation models was set in the year 2000 by the Space Shuttle RADAR Topography Mission (SRTM; Rabus et al. 2003)., but is has the major limitation that it normally provides no information on the penetration depth into snow and ice (Rignot et al. 2001).

As well as measuring glacier changes in-situ or through airborne/spaceborne earth observations, various approaches to modeling glacier changes have been developed. Most of these models use input data from glacier measurements, normally with additional meteorological/climatologic data. Rather than just producing punctual information, these models can describe the changes in glacier's mass during a year or over longer periods by incorporating process knowledge and physical glacier models (Hock 1999; Huss et al. 2008; Machguth et al. 2006b).

1.2.3 Impact of shrinking glaciers

In Switzerland, the total glacier surface has diminished by about 50% since the Little Ice Age (Zemp et al. 2006). During this 150-year period, the mean annual air tempera-

ture in Switzerland has increased by approximately 1.5°C (Begert et al. 2005). Climate reports expect a further warming of 1.5 to 6°C by the end of the century with many effects that we cannot yet envisage (Lemke et al. 2007). However, it is clear that the projected increase in air temperatures will lead to further glacier shrinkage and many glaciers will have probably disappeared by the end of the century (Lemke et al. 2007).

The massive lateral moraines and multiple terminal moraines of many Alpine glaciers are impressive indications of their previous length and volume, and of the dramatic changes that have occurred during this geologically rather short 150-year period. The retreat of glaciers since the LIA, often amounting to several kilometers, and the elevation increase at the terminus are strong evidence of climatic warming. However, this glacier retreat does not only affect the size and volume of the ice bodies themselves, but also actively alters the local and regional environments, sometimes on an even larger scale. Additionally, the warming or loss of old ice and the preserved particles it contains poses an irrecoverable loss of natural climate archives (Hoelzle et al. 2011).

The strong retreat of the glaciers in Switzerland and elsewhere has many implications and affects different stakeholders in ways that are expected to intensify in the future. Being able to see “perpetual ice” is often considered a sign of a healthy ecosystem. The ice retreats will form new alpine landscapes with new ground coming to light and many new lakes present (Frey et al. 2010). These new lakes will provide new opportunities, e.g. as new touristic destinations and as sites for new hydropower generation projects. However, many of these new lakes are (and will be) dammed by loose glacier sediment and therefore create potential natural hazards (flooding, debris flow, and ice avalanches) for down-valley settlements (Frey et al. 2010).

Annual precipitation in Switzerland has not changed much in the past 150 years of measurements, or at least no trend is apparent (Begert et al. 2005). Many glacier outflows are collected as water intakes for hydropower generation. With the retreat of the glaciers, water discharge will decrease, which will directly affect the amount of water available for energy generation in summer. Today, the still larger glaciers are melting at a fast rate, which means the discharge useable for hydropower generation is above average. However, the rapid decrease in the glacier’s surface area and volume will lead in the longer term to less water being available during summers. This development could also have a profound effect on the water availability for drinking water and irrigation for larger parts of Switzerland, and even influence the discharge far away from the European Alps (Huss et al. 2014).

On the global scale, the shrinkage of glaciers is estimated to be currently contributing approximately 0.8 (+/- 0.2) mm per year to the rise in global sea levels (total rise 1993-2003: ~3 mm/a; Lemke et al. 2007). Despite the comparably small land surface area covered by glaciers (~0.5%), the glacier contribution to sea level rise amounts to approximately 28%, about twice that of the individual contributions of the Antarctic and Greenland ice sheets combined (Lemke et al. 2007).

1.3 Airborne Laser Scanning for glacier applications

1.3.1 Introduction to airborne laser scanning

Airborne laser scanning is a method employing LIDAR (light detection and ranging) measurements (Wehr and Lohr 1999). It has been in operational use since the early 1990s for a variety of applications, principally aiming at generating accurate digital elevation models on land and in shallow waters close to shorelines. The most advantageous characteristics of this active system compared to passive imaging systems are the way it is independent of the sun as a source of illumination, and it can accurately map featureless surfaces such as snow or sand, as well as map terrain by seeing through volumetric structures such as trees while at the same time mapping them (Morsdorf et al. 2004; Nelson et al. 1984).

Laser scanning is based on a method to measure the range and direction from the instrument's known location to a reflecting target. The illuminating source is typically a narrow focused, laser pulse of short duration, although continuous wave (CW) systems exist as well (Baltsavias 1999; Mallet and Bretar 2009). In the more common first mode of operation, which was used for this research, the sensor-to-target range is calculated by multiplying half the time-of-flight of a laser pulse by the speed of light (Baltsavias 1999). Repeated emissions in different directions then lead to a distributed pattern of target returns, hence the term "scanning".

Typically, an airborne sensor's position and orientation in space are measured by combining a global navigation satellite system (GNSS) and an inertial measurement unit (IMU; Wehr and Lohr 1999). In modern laser scanners, the emitted laser beam is deflected by a rotating or oscillating mirror built into the instrument, and subsequently reflected at the target's surface before returning to the detector again via the deflecting mirror. The current angular orientation of the deflection mirror is measured as well. In combination with the measured range, the positioning and attitude measuring system, the target's coordinates on ground can then be determined (Wehr and Lohr 1999).

The laser scanners mostly used today typically operate a laser at a near-infrared wavelength to allow a higher emission power due to eye safety concerns and legal restrictions in the visible part of the electro-magnetic spectrum. A most welcome by-product of these restrictions is that the scanners are then more suitable for the near-infrared wavelengths preferred for scanning on snow and ice (Lutz et al. 2003). The laser beam emitted typically works with a beam divergence of approximately 0.25 mrad (at 1/e energy level; Glennie 2007), leading to an illuminated footprint diameter of 0.25 m at a typical flying height 1000 m above ground level. The distribution of return locations and the point density per area unit are dependent on the pulse repetition frequency, the scanning frequency, the overlap area between two flight trajectory's swaths and the type of target. For example measuring a tree can lead to multiple returns per laser emission.

The principal product of an ALS flight campaign is a collection of point coordinates from all discrete laser return locations. The interpolation and filtering of such a point cloud can then be performed to establish a rasterized digital elevation product, such as a terrain model.

1.3.2 Measuring topographic glacier changes using ALS

The principal method of determining glacier volume change is the photogrammetric evaluation of aerial or spaceborne images (cf. section 1.2.2). For more than 50 years, such datasets have been available and provide an invaluable archive of past glacier states (Zemp et al. 2010). However, generating a DEM from photogrammetric data is complex, and the quality of the results depends on many factors, such as the availability and accuracy of ground control points and high contrast image information. Consequently, DEMs of glacier areas based on photogrammetry can be rather uncertain in the information on elevation.

Digital elevation models of glaciers were first generated from airborne laser scanning in the late 1990s (Kennett and Eiken 1996), including in Switzerland (Favey et al. 1999). These pilot studies showed the principal applicability of airborne laser scanning in glaciology. A few years later, in the framework of the OMEGA project (Operational Monitoring of European Glacial Areas), multi-temporal ALS data sets were acquired for Hintereisferner (Austria) and Engabreen (Norway), showing the potential of this new method for glacier monitoring (Geist 2005). In the past few years, ALS has provided data in a more operational way, e.g. in studies of single glaciers (Geist et al. 2003) and mountain ranges (Abermann et al. 2010), and contributed to regional glacier inventories (Knoll and Kerschner 2010).

To evaluate the volume change of a glacier, the corresponding local elevations from multi-temporal DEMs are co-registered, subtracted, and summed up for the entire glacier surface (Nuth and Kääb 2011; Reinhardt and Rentsch 1986). Any uncertainties in one or several DEMs used for the calculation therefore degrade the quality of the resulting volume change estimates. This effect is greater if there has been only little topographic change, i.e. if the time period between the two DEMs is short or the mass turnover of the glacier is low. An accurate DEM is therefore essential for accurate estimates of volume change and is the basis for comparison with in-situ mass balance measurement networks.

The data acquired with ALS has proven to be highly accurate. The accuracy of such data has been assessed using reference surfaces (Favey et al. 1999; Geist 2005), ground control points (Hodgson and Bresnahan 2004b; Hopkinson and Demuth 2006) and statistical error modeling approaches (Filin 2003; Goulden and Hopkinson 2010; Huising and Gomes Pereira 1998). After assessing the data for accuracy, current information on the volume change can then be obtained.

1.3.3 Measuring snow reflectance regimes

The consequences of glacier change are described in the previous sections. This section takes a closer look at the causes of glacier change. The two principal drivers of glacier melt are air temperature and net solar radiation (Ohmura et al. 2007), which can be measured and extrapolated to unmeasured sites in a reliable manner. The efficiency of the energy uptake at the glacier's surface is, however, defined by a more challenging component: the surface albedo (Wiscombe and Warren 1980). Albedo is the ratio of reflected to incident broadband radiation and strongly influences glacier ablation (Oerlemans and Knap 1998). It is influenced by surface material properties such as the snow grain size (most influential in the near-infrared part of the electromagnetic spectrum) and impurities in snow and ice (most influential in the visible part of the

spectrum; Brock et al. 2000; Oerlemans et al. 2009). To model a glacier's surface energy and mass balance, typical values from the literature are often taken to account for larger regions of the glaciers, e.g. ranging between 0.6 and 0.9 for snow in the accumulation area, 0.3 and 0.55 for firn in the transient area, and 0.2 to 0.35 for bare ice in the ablation area (Cuffey and Paterson 2010; Greuell et al. 1997; Machguth et al. 2006b).

However, glacier albedo is very spatially variable as in-situ measurements (Sugiyama et al. 2011) and retrievals from remote sensing have shown (Knap et al. 1999a; Stroeve et al. 2005). Measuring the albedo in-situ is laborious and only possible at single locations. The distributed measurement of albedo using operational remote sensing (e.g. satellite imagery) is not easy because the spatial resolution is often low and it thus cannot reproduce the spatial heterogeneity. It also depends on having cloudless imaging conditions. In addition, because the sun is the illumination source, there are directional effects from isotropic, volumetric and geometrical-optical scattering (bi-directional reflectance distribution function (BRDF) effects; cf. Schaepman-Strub et al. 2006).

The principal task of ALS is to generate very accurate topographic models. However, as a side product, LIDAR instruments typically also register the signal intensity for each pulse, providing surface reflectance information in one narrow band (Höfle and Pfeifer 2007).

1.4 Motivation for research

A tool for assessing past and present climatic changes is provided by measuring and modeling glacier changes. Glaciers react sensitively to the prevailing climatic conditions by adapting their shape and volume. Nowadays, multiple approaches exist to measure or model such changes.

Several glacier volume change studies have considered ALS uncertainties, but have often relied on calibration information from data providers or on uncertainties from reference measurements taken at other sites. The resulting data may therefore contain considerable uncertainties and should be carefully evaluated, especially if measurements of changing topography in the field of glaciology are involved.

Not enough is known about the accuracy of existing methods to measure glacier volume changes, which limits the quality of the results and extrapolations into the future. To increase the credibility of such measurements and extrapolations, a sound assessment of methodological uncertainty independent of acquisition heterogeneities is required.

To bridge the data gap between in-situ and remote sensing campaigns to measure glacial change, glacier models are widely used. Computing the annual mass balance of glaciers involves taking snow accumulation into account. Current models typically rely on meteorological measurements and try to estimate the accumulation. However, the actual snow accumulation and its deposition pattern are normally unknown. To improve mass balance models, the winter snow accumulation must therefore be measured and associated uncertainties evaluated.

A second driver of glacier change that is rarely measured is the surface albedo, which is of utmost importance as it influences the amount of incident radiation available for glacier melt. To improve glacier mass balance models, measurements of albedo, preferably by remote sensing means, should be included.

The focus of this dissertation is on these challenges and on measuring multi-annual and seasonal glacier changes, with a thorough assessment of accompanying uncertainties. The results are used to assess (i) the uncertainty of established methods for calculating glacier volume changes and (ii) the potential of ALS for deriving distributed products of winter accumulation and albedo.

1.5 Research outline

The dissertation aims to contribute to glacier change research by investigating airborne laser scanning data in different ways, addressing the four general questions:

a) What is the overall glacier volume change and how accurate are the ALS DEMs?

b) Are there any systematic or stochastic errors in traditional annual glacier volume change methods compared to the state of the art approaches?

c) What can ALS contribute to better understanding winter accumulation patterns?

d) Can ALS intensity measurements be used to derive a distributed glacier albedo map?

These are the topics of the four peer-reviewed scientific publications contained in this dissertation. The research questions to be answered in more detail are presented below:

a) Volume change and uncertainty assessment of topographic information in glaciology

In the first paper, we developed and implemented a framework to estimate the influence of both the systematic and the stochastic uncertainties in point clouds. We also interpolated DEMs derived from ALS data based on a physical error modeling approach (chapter 2). We were then able to calculate the geodetic change in volume of the Findelengletscher with accompanying uncertainty estimates.

The following research questions are addressed in chapter 2:

- What changes in the Findelengletscher were observed in the period 2005-2010?
- How accurately can glacier topography and glacier changes be reproduced using ALS? How significant are the uncertainties involved for estimating volume change?
- What is the origin of these uncertainties?

b) Evaluation of different methods to measure glacier volume change

After assessing the accuracy of the DEMs in the first contribution, we used the available ALS DEMs to simulate, for the first time, the geodetic change in glacier volume employing different methods on various spatial scales. In this way it was possible to validate the methods and the dependence of uncertainties on different spatial scales since the methodological errors that remained in the volume change arose from the different methods. In addition, uncertainties in a synchronously acquired low point density ALS

data set, which had been economically optimized, were compared with those in the high point density ALS data sets.

The following associated research questions are addressed in chapter 3:

- How can using an economically optimized ALS flight setup influence the volume change accuracy?
- What systematic and stochastic uncertainties are introduced when using different methods to derive the geodetic volume change? On what spatial scale are systematic uncertainties of concern?

c) Evaluation of winter accumulation measurements

Most research and monitoring in glaciology assess the annual mass change in glaciers by measuring glacier changes at the end of summer. However, the annual mass change is the result of processes throughout the entire year. In addition, comparing the in-situ mass balance of a glacier with volume changes measured with remote sensing is challenging due to dynamic processes such as ice flow and the unknown density conversion. Therefore, to better understand the processes governing winter accumulation, the third paper estimates end-of-winter snow accumulation patterns and glacier dynamics with unprecedented accuracy by utilizing a combination of ALS, helicopter-borne ground penetrating RADAR, and in-situ measurements on the glacier surface.

The following research questions are addressed in chapter 4:

- How could winter accumulation measurements benefit from using ALS?
- What conditions have to be fulfilled and what are the limitations?

d) Derivation of a distributed glacier surface albedo

Albedo is a paramount input factor for glacier energy and mass balance models. The point cloud data from ALS is primarily used to develop topographic models of a study site. As a side product, most ALS systems record the reflected signal intensity providing surface reflectance information in one narrow spectral band. For this purpose, different physical effects were radiometrically corrected and a homogeneous near-infrared image of the glacier produced. At the same time, in-situ albedo measurements were performed to calibrate the corrected ALS intensity data. This additional information was then used to reproduce the spatially highly variable albedo of the glacier's surface and was compared to a broadband albedo derived from a multispectral airborne digital sensor.

The following research questions are addressed in chapter 5:

- What is the benefit of using ALS intensity information?
- What is the information value of the albedo proxy derived from ALS intensity?

1.6 Project context

1.6.1 Project framework

In the framework of the "Gletscher Laserscanning Experiment Oberwallis (GLAXPO)", this PhD project was undertaken to accurately measure glacier volume changes using digital elevation models based on multi-temporal airborne laser scanning.

Two additional studies were also conducted, one to investigate the hydrology of the study site's catchment. The past and future glacier runoff was modeled on the basis of historic data and climatic scenarios (Huss et al. 2014). The second produced dynamic, interactive visualizations of past glacier changes and predicted future changes for a permanent public exhibition.

The funding partner for this project was the Axpo Holding AG, the largest Swiss energy utility. As the majority of the energy produced by Axpo is generated from hydropower, the company is directly affected by the change in the retention capacity and runoff of glaciers feeding hydroelectric power stations. It is therefore interested in the outcomes of this research.

1.6.2 Study site and data

To consider the research questions posed in this thesis, a suitable study site had to be carefully selected. A promising glacier for further research was found in the Findelengletscher in Canton Valais, Switzerland (46°N, 7° 52' E; Fig. 1-1), as the glaciology group of the Geography Department of the University of Zurich (GIUZ) had already established an in-situ mass balance measurement network there in 2004, which could provide a synergy for both the in-situ network and the ALS project. The measurement network has been established to serve as a test area for modeling glacier changes in a different research project (Machguth 2008). These measurements were collected using the direct glaciological method (Østrem and Brugmann 1991), which involves setting up a network of stakes in the ablation area and collecting the end-of-summer snow depth distributions including snow density measurements. The point data were inter- and extrapolated for the entire glacier using a manual contouring approach and drawing on expert knowledge about ablation/accumulation distributions. The general glacier data and mass balance results obtained are given in the Fluctuations of Glaciers (WGMS 2012). Since 2012, however, the in-situ data have served as input for a mass balance model developed by Huss et al. (2008, new data unpublished).

This temperate valley glacier has an area of approximately 13 km^2 (2010, cf. Fig. 1-2) and an elevation range from 2600 to 3900 m. It is expected to undergo several decades of strong melt (Farinotti et al. 2011). The Findelengletscher has been the target of glaciological research in the past (Collins 1979; Iken and Bindschadler 1986), and glacier length measurements have been performed there since 1885 (Glaciological Reports 1881-2010). As measurements from stakes and snow pits are prone to the accumulation of systematic errors, as are the inter- and extrapolation methods, an independently derived geodetic mass balance is required to validate the in-situ measurements (Zemp et al. 2010). The GIUZ therefore decided to make use of the state of the art geodetic method of airborne laser scanning to test for systematic errors. In 2005, an ALS test data set was produced for a large area in the Mattertal region, including the Findelengletscher test site, and acquired by the GIUZ. The ALS measurements produced for this project

(fall 2009, spring 2010, fall 2010) were therefore complemented with the longer time span provided by the 2005 (fall) data set. For a complete list of the ALS acquisition parameters, please refer to Table 1 in the paper in chapter 2.

Figure 1-1 The snow-covered tongue of the Findelengletscher, looking towards Zermatt, with the prominent peak of the Matterhorn in the background (September 29, 2010, by M. Zemp).

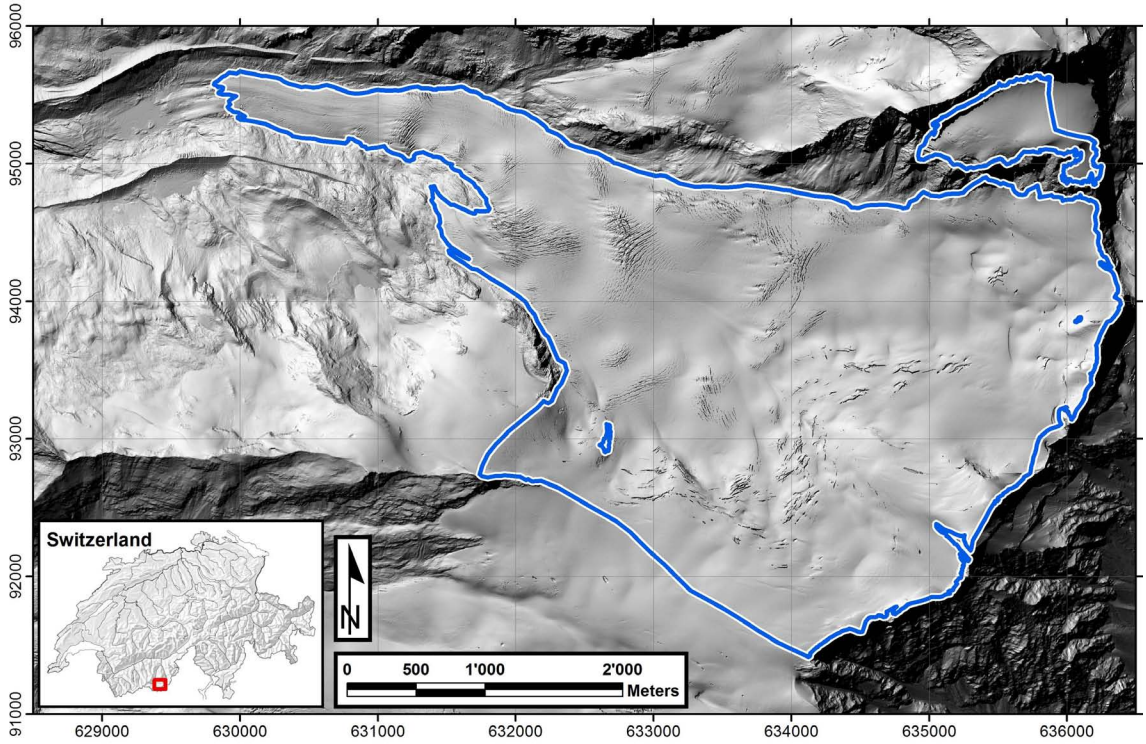

Figure 1-2 The Findelengletscher study site based on a shaded ALS relief. The blue line represents the glacier perimeter in September 2010. The coordinate system is Swiss grid CH1903, in meters.

1.7 Structure of the thesis

The thesis consists of six chapters:

Chapter 1 provides the reader with the required theoretical background to ease the understanding of the peer-reviewed scientific contributions in the following chapters. It gives an overview of glacier research and familiarizes the reader with the concept of airborne laser scanning. It also contains the research gaps to be bridged leading to the research questions and approaches addressed and discussed in the present thesis.

Chapter 2 consists of a first-authored peer-reviewed scientific publication (Joerg et al. 2012) addressing the uncertainties of ALS in glacier research in a case study. The publication is self-contained in both structure and content.

Chapter 3 consists of a first-authored peer-reviewed scientific publication (Joerg and Zemp 2014) investigating uncertainties in different methods and at different scales calculating the geodetic volume change of a glacier. The publication is self-contained in both structure and content.

Chapter 4 consists of a co-authored peer-reviewed scientific publication (Sold et al. 2013) addressing the winter snow accumulation distribution on Findelengletscher by using different methods. The publication is self-contained in both structure and content.

Chapter 5 consists of a first-authored peer-reviewed scientific publication (Joerg et al., in revision) aiming to derive a distributed albedo map using ALS intensity information. The publication is self-contained in both structure and content.

Chapter 6 summarizes and discusses the main findings from the publications presented in chapters 2-5, provides concluding remarks and a scientific outlook. In addition, an overview of the PhD candidate's professional education and additional scientific contributions is given.

2 UNCERTAINTY ASSESSMENT OF MULTI-TEMPORAL AIRBORNE LASER SCANNING DATA: A CASE STUDY ON AN ALPINE GLACIER

This chapter was published as: Joerg, P.C., Morsdorf, F., & Zemp, M. (2012). Uncertainty assessment of multi-temporal airborne laser scanning data: A case study on an Alpine glacier. *Remote Sensing of Environment*, *127*, 118-129. Reprint with permission from Elsevier.

Remote Sensing of Environment 127 (2012) 118–129

Contents lists available at SciVerse ScienceDirect

Remote Sensing of Environment

journal homepage: www.elsevier.com/locate/rse

Uncertainty assessment of multi-temporal airborne laser scanning data: A case study on an Alpine glacier

Philip Claudio Joerg *, Felix Morsdorf, Michael Zemp

Department of Geography, University of Zurich, Winterthurerstrasse 190, CH-8057, Zurich, Switzerland

ARTICLE INFO

Article history:
Received 15 March 2012
Received in revised form 5 August 2012
Accepted 11 August 2012
Available online xxxx

Keywords:
Airborne laser scanning
LiDAR
Uncertainty assessment
Error propagation
Mountain glacier
Glacier change
Multi-temporal
Digital elevation model

ABSTRACT

In glaciology, volumetric changes from multi-temporal digital elevation models (DEMs) serve to validate and calibrate glacier mass balances from traditional in situ measurements. In this study, we provide a thorough uncertainty assessment of multi-temporal airborne laser scanning DEMs based on: (a) applying a statistical error model, (b) comparing laser echoes to reference points and surfaces, and (c) developing a physical error propagation model. The latter model takes into account the measurement platform characteristics, components of the measurement process, and the surface properties. Such a model allows the estimation of systematic and stochastic uncertainties for single laser echoes, as well as for distributed surfaces in every part of the study site, independent of the reference surfaces. The full error propagation framework is applied to multi-temporal DEMs covering the highly undulating terrain in the Findelengletscher catchment in Canton Valais, Switzerland. This physical error propagation model is able to reproduce stochastic uncertainties in accordance with measurements from reference surfaces. The high laser point density in the study site reduces the stochastic uncertainties over the whole glacier area to negligibly small values. However, systematic uncertainties greatly influence the calculation of mass changes and lead to corrections of the thickness change of up to 35%.

1. Introduction

Since the 1990s, digital elevation models derived from airborne laser scanning (ALS) have been increasingly used for a wide range of applications (Shan & Toth, 2009). In the last decade, regional to nation-wide surveys have been carried out using ALS, including regions with potential relevance for glacier research, e.g. in Austria and Norway (Geist et al., 2003), and in Switzerland (Geist et al., 2003; Luethy & Stengele, 2005). As the costs associated with ALS are decreasing and the initial datasets are being updated, the prospect of multi-temporal ALS data will sustain new applications, not only in forestry (Yu et al., 2004) but also in natural hazards (Casas et al., 2011; Ventura et al., 2011). However, to make sure that these applications can be used best, new means of validation and uncertainty assessment will need to be implemented (Hopkinson et al., 2008), especially since ALS is a constantly evolving technology, and changing systems and/or survey configurations will result in different datasets with varying accuracies.

In the domain of glaciology, mass balance is traditionally measured in situ using ablation stakes and snow pits, including density measurements. Additionally, different methods are applied to inter-/extrapolate from discrete measuring locations to the entire glacier to calculate the so-called direct glaciological mass balance (cf. Østrem & Brugmann, 1991). To account for the possible accumulation of systematic errors from these seasonal or annual measurements, an independently derived geodetic mass balance at decadal intervals is required (Haug et al., 2009; Huss et al., 2009; Zemp et al., 2010). The standard geodetic method applied is digital elevation model (DEM) differencing from photogrammetric sources (e.g. Haug et al., 2009). However, photogrammetric DEM extraction is hindered by the low contrast often found in alpine environments. ALS has proved to be useful in overcoming the shortcomings of photogrammetric DEMs as it directly measures surface elevations (e.g. Geist, 2005; Kennett & Eiken, 1996).

Several studies have focused on the application of ALS to glacier surface mapping or volume changes (e.g. Abermann et al., 2009; Favey et al., 1999; Geist, 2005; Kennett & Eiken, 1996; Knoll & Kerschner, 2010). To date, ALS accuracy assessments have been conducted using reference surfaces (Favey et al., 1999; Geist, 2005), ground control points (Hodgson & Bresnahan, 2004; Hopkinson & Demuth, 2006) and theoretical or statistical error modeling approaches (Filin, 2003; Goulden & Hopkinson, 2010a; Huising & Gomes Pereira, 1998). In glaciology, stochastic uncertainties in airborne laser scanning DEMs are considered to be lower than other DEM-providing methods. In ALS, vertical accuracies are given between ±0.1 m and ±0.3 m (Abermann et al., 2010). However, estimations of uncertainties are usually based on numbers from data providers or are measured using reference surfaces or points, and may therefore not cover stochastic uncertainties present at the study site (e.g. glacier) itself. Additionally, it is not always clear

* Corresponding author. Tel.: +41 44 635 5215.
E-mail address: philip.joerg@geo.uzh.ch (P.C. Joerg).

0034-4257/$ – see front matter © 2012 Elsevier Inc. All rights reserved.
http://dx.doi.org/10.1016/j.rse.2012.08.012

which scale these stochastic uncertainties refer to, i.e. whether they refer to a single measurement (e.g. single laser return), a single raster cell or even the stochastic uncertainty of a whole study site. Furthermore, systematic uncertainties in DEMs directly influence the effects of elevation changes, but are often not considered.

In this study, we developed and implemented a three-step approach to estimate both the systematic and the stochastic uncertainties in DEMs derived from ALS data. First, we checked for co-registration and elevation-dependent errors between each pair of DEMs. In a second step, we compared the location of single laser echoes to reference points and surfaces within the study site. Following this, we used a physical error propagation model to explain the uncertainties found in the previous method and attribute them to their sources. A validation of the physical error propagation model was carried out on reference surfaces and extended to the full point cloud of each ALS survey. Finally, we applied our framework to compute changes in glacier thickness from multi-temporal DEMs and to assess the related uncertainties statistically.

2. Study area and data

2.1. Study site

The Findelengletscher is a temperate valley glacier located in the Swiss Alps (46° N, 7° 52′ E, Fig. 1) in Canton Valais, close to the village of Zermatt, Switzerland. With its area of more than 13 km^2 and a length of about 6.7 km (2010), it is one of the larger valley-type glaciers in the Alps. Since its Little Ice Age maximum extent in c. 1850, when it was 10.4 km long and 19.96 km^2 in area (Maisch et al., 2000), the glacier has retreated, interrupted by three shorter time periods of glacier re-advance (in the 1890s, 1920s, and 1980s). Furthermore, the Findelengletscher and its former tributary Adlergletscher separated in the 1990s and are now independent ice bodies.

The Findelengletscher is considered a worthwhile study site for glaciological investigations for several reasons: (1) the surface is almost completely free of debris and its slope is fairly constant, which facilitate the delineation of the glacier and in situ measurements are possible on almost every part of the glacier; (2) the glacier ranges from 2600 m a.s.l. up to 3900 m a.s.l. and is therefore assumed to sustain multiple decades of strong melt (Farinotti et al., 2011); and (3) the infrastructure of the nearby Zermatt ski resort with its cable cars and helicopter-base facilitates access to the glacier.

The Findelengletscher has been the target of glaciological research in the past (Collins, 1979; Iken & Bindschadler, 1986), and length variation measurements have been available since 1885 (Glaciological Reports, 1881–2010). These indicate that the glacier retreated by about 1900 m in total up to 2010. Huss et al. (2010) reconstructed the seasonal mass balances of the Findelengletscher from 1908 to 2008 using distributed mass balance modeling based on digital elevation models (DEMs) and driven by climate and field data. The reported cumulative specific mass balance of the Findelengletscher for the last century is approximately −26 m water equivalent (w.e.).

Direct glaciological mass balance measurements started on the Findelengletscher in 2004/05 as part of a larger research project

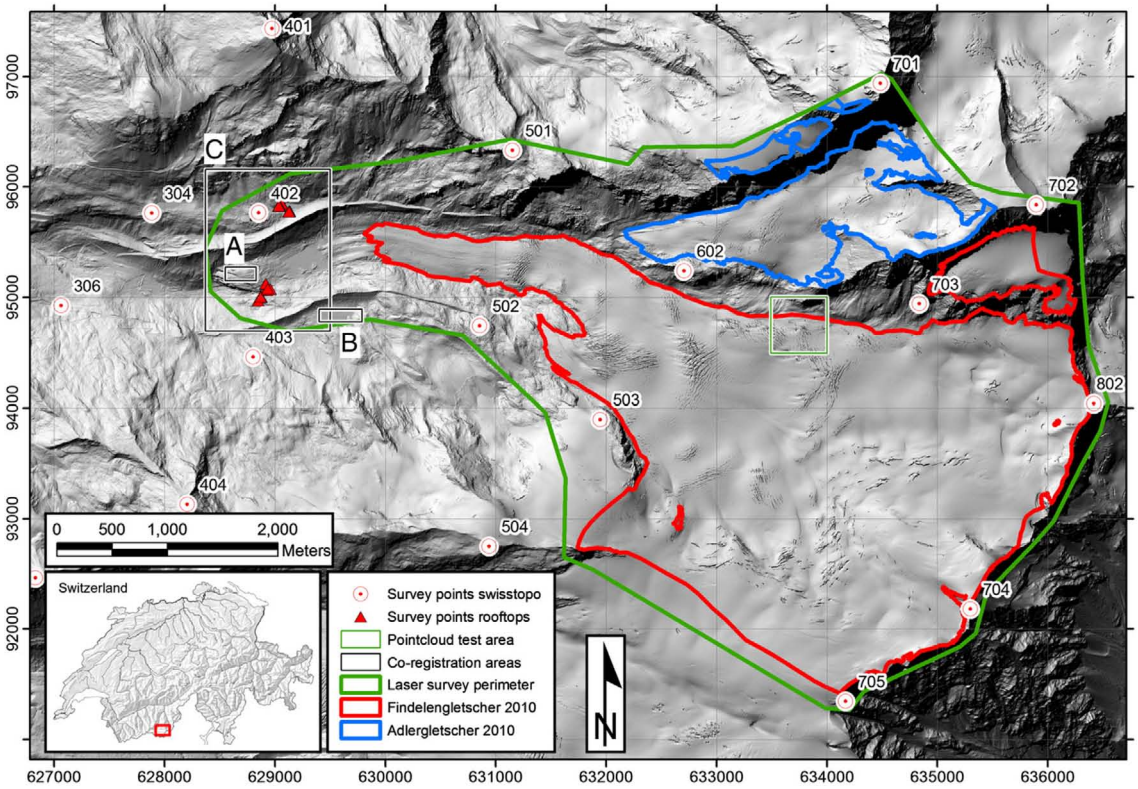

Fig. 1. Shaded relief of the Findelengletscher catchment. The ALS perimeter and glacier outlines 2010 are shown, as well as surveyed surfaces (triangles), reference fix points (circles), and co-registation evaluation areas.

(Machguth, 2008; Machguth et al., 2006), and have since been extended to a mass balance monitoring program. The resulting data (mean annual mass balances 2004/05-2009/10 of −0.38 m w.e.) are reported to the World Glacier Monitoring Service (WGMS 2011) and the Swiss Glacier Monitoring Network (Glaciological Reports, 1881–2010).

2.2. Airborne laser scanning data

Four ALS datasets were acquired by BSF-Swissphoto employing Optech ALTM 3100 (October 2005, October 2009 and April 2010) and Optech ALTM Gemini (September 2010) laser scanning systems. Detailed mission settings are presented in Table 1.

These instruments were built into Pilatus Porter fixed-wing aircrafts and work on the principle of pulsed laser emissions being deflected from an oscillating mirror in the across-track direction. Measuring the run-time from emission to detection of the laser reflection on the earth's surface provides the range to the target. Satellite-based global navigation systems (GNSS; subsequently, we use the more common term GPS, including measurements from GLONASS as well), coupled with high resolution inertial measurement units (IMU) and the current angle of the deflection mirror, supply the essential position and direction parameters of the point of origin of the laser emission (cf. Wehr & Lohr, 1999). The position of the ground point is then inferred from forward georeferencing and coordinate transformation, using the official REFRAME tool of the Swiss Federal Office of Topography (swisstopo), to the Swiss national coordinate system CH1903/LN02 (cf. Swisstopo, 2008).

These surveys resulted in average point densities between 1.1 and 14.4 points per square meter, which were interpolated into raster representations for zonal calculations (e.g. elevation differences) with 1 m x 1 m spatial resolution.

In addition to aerial photographs, ALS DEMs assisted in delineating glacier outlines by analyzing shaded reliefs, and by integrating elevation changes over the whole glacier area from multi-temporal DEMs (cf. Abermann et al., 2010).

2.3. Reference data

Differential GPS (dGPS) measurements have been carried out for two purposes in the Findelengletscher project. For the campaign in October 2005, a permanent dGPS reference station in Zermatt from the Automated GNSS Network for Switzerland (AGNES, operated by swisstopo) was used to differentially correct the ALS airplane's GPS system in post processing (maximum baseline length: 14 km, maximum elevation difference to airplane 3600 m). For the subsequent campaigns, a temporary base station was maintained on the Gornergrat (3130 m a.s.l.). The dGPS receiver used was a Trimble 5700 with a zephyr antenna on a tripod. The data were subsequently processed in Trimble Geomatics Office and Applanix POSGPS for processing the flight paths. During the ALS surveys, these baselines never exceeded 10 km horizontally and 2000 m vertically.

Reference points on rooftop edges were measured using a combination of static dGPS measurements and reflectorless tachymetry. The accuracy from the baseline report of the dGPS post-processing and the surveying of a national geodetic reference point of swisstopo resulted in accuracies<5 cm in every direction for the combined surveying system.

In addition to the rooftop reference points, former national geodetic reference points (not updated anymore) are present on exposed summits within the study area. Although these coordinates are outdated, the accuracy is still expected to be an order of magnitude higher than a single laser point. Therefore, they still provide valid reference data in regions where no other data are available, especially as they are favorably distributed around the ALS perimeter.

To avoid possible errors in the coordinate transformation from global to local coordinates (WGS 84 to the Swiss national grid), we used the same REFRAME transformation code for all ALS point datasets as well as for the ground reference survey. Therefore, a shift, rotation, or scaling effect between the two independent datasets is unlikely. However, note that if differences are present in these transformation parameters, they will lead to systematic errors.

Table 1
Data acquisition parameters and accuracy of data provider for the respective flying height of all four ALS flight campaigns.

Date of acquisition	Unit	Oct. 28–29, 2005	Oct. 4, 2009	Apr. 10, 2010	Sept. 29, 2010
Sensor employed	ALTM	3100	3100	3100	Gemini
Measuring frequency	kHz	71–100	71	71	71
Scanning angle	degrees	±23	±15	±15	±15
Scanning frequency	Hz	40–50	39	39	39
Average flying height	m	1500	1000	1000	1000
Across-track overlap	%	55	50	50	50
Average point density	Pt/m²	1.1	7.6	8.1	14.3
LASER wavelength	nm	1064	1064	1064	1064
Beam divergence	mrad (1/e)	0.30	0.30	0.30	0.25
Horizontal accuracy	m	0.75	0.50	0.50	0.18
Vertical accuracy	m (1 σ)	<0.20	<0.15	<0.15	<0.10

3. Data preparation and uncertainty assessments

3.1. Interpolation of a point cloud into a raster

A preparatory step to facilitate data analysis is to interpolate the point clouds into raster models. For this task, a multitude of methods are at hand, e.g. inverse distance weighting or kriging (cf. Cressie, 1993). We converted the point clouds into 1 m x 1 m grids and used MATLAB (The MathWorks, Inc.) to delineate all points within a single raster cell and subsequently assign the average of all elevation values to provide the cell's elevation. This proved to be a very stable approach, as statistical outliers and artifacts, e.g. cables, had been removed previously by classifying each ground point into quality classes and subsequently keeping only valid points. Note that this is a valid approach only when single returns, e.g. one return per laser shot, are present. The few raster cells that do not contain a single point (2005: approx. 25%, other years: below 1%) were interpolated using a least squares method without changing the known values. Moreover, the extrapolation behavior is linear.

3.2. Co-registration accuracy of DEMs

A first step to avoid having erroneous volume changes from systematic shifts between two DEMs is to investigate the respective co-registration. Kääb (2005) and Nuth and Kääb (2011) suggest a statistical co-registration correction between two independently generated DEMs. We applied the first two steps of this method to a stable, i.e. ice-free, portion of the DEMs. To check whether there was a systematic shift and vertical offset between two pairs of ALS elevation models, the unique differences in the raster cell elevation were divided by the tangent of the local slope and plotted against the local aspect. This resulted in scattered data, to which a cosine function was fitted by a least squares curve fit to derive the parameters magnitude (a) and direction of the horizontal shift (b), as well as a mean vertical bias ($\overline{dh}$) (Table 2). The corresponding function for F is

$$F = a \cdot \cos(b - \text{terrain aspect}) + c \quad (1)$$

where $c = \frac{\overline{dh}}{\tan\overline{\alpha}}$ (Nuth & Kääb, 2011). Subsequently, the two DEMs were iteratively shifted and the co-registration reassessed. The next step in this method reviewed the data for an altitude-dependent bias by evaluating the offset per elevation band (cf. Nuth & Kääb, 2011). Any possible bias could then be corrected by applying an elevation-dependent correction term. In our case, no such bias was found and therefore no

Table 2
Shift parameters of the co-registration correction by Nuth and Kääb (2011) for both annual mass balance ALS periods (cf. Eq. (1)). Areas A, B, and C are shown in Fig. 1. As in Table 4, the effect of snow present in 2005 explains the higher $\overline{dh}$ values in the first period.

	2005–2009			2009–2010			Comment
	A	B	C	A	B	C	Test areas
a	0.51	0.43	0.72	0.11	0.15	0.12	Magnitude of hor. shift [m]
b	27.28	1.69	47.01	351.61	5.24	283.90	Direction of shift [°]
c	0.86	01.63	1.34	0.03	0.12	0.13	Mean bias/mean slope tangent
$\overline{dh}$	0.36	0.42	0.72	0.01	0.03	0.07	Mean bias [m]

Table 3
Change in the thickness of the Findelengletscher and Adlergletscher for all periods, including uncertainties from error propagation and snow thickness measurements. *Mostly due to snow.

		Oct. 2005–Oct. 2009	Oct. 2009–Sept. 2010	Oct. 2009–Apr. 2010
Findelengletscher change in specific thickness	Uncorrected change [m]	−2.72	−0.77	1.69
	Systematic error [m]	0.51*	−0.19*	0.01
	Corrected change [m]	−2.22	−0.96	1.69
Adlergletscher change in specific thickness	Uncorrected change [m]	−1.49	−0.57	1.42
	Systematic error [m]	0.50*	−0.20*	0.01
	Corrected change [m]	−0.99	−0.77	1.42

correction was applied. The third step in the co-registration method is suitable for sensor-specific biases. We reserved this step for the modeling of the physically-based error propagation presented in Section 3.4.

3.3. Comparison with independent ground control surfaces and points

The absolute accuracy of the DEMs was assessed by using ground control points. An established standard method compares homogeneous horizontal surfaces as a reference, e.g. a football field, to the positions of laser echoes on the ground (e.g. Geist et al., 2003). However, as these reference surfaces are outside the glacier perimeter, and the accuracy of laser ground points is variable, we surveyed multiple distributed control surfaces as close as possible to the glacier to describe the relevant accuracies. The rooftops of four mountain huts and a helipad were selected as they are the most homogeneous surfaces in this high alpine environment. While the helipad was a flat horizontal platform, all the rooftops were saddle roofs, with the following characteristics: An inclined surface shows not only possible vertical offsets of the laser points, but also horizontal shifts (for the planimetric quality) by showing different vertical deviations on two rooftop surfaces with opposite slopes. This shift can be calculated using the slope of the rooftop, and in the case of a cross-gable roof (Fig. 2), the horizontal shift vector can then be fully defined. The drawback of these surfaces is that the vertical offset may not only be induced by a systematic error in the ALS system, but also by the different reflectivity of the surface types present (tin and stone rooftops), the angle of the slope of the roof, and other geometrical issues involving the range footprint-size relation and the angle of incidence (e.g. Johnson, 2009).

The ground reference points derived from dGPS and reflectorless tachymetry were converted into planes. Subsequently, objects that are not part of these surfaces like chimneys were masked out. The vertical deviation of each laser point from its corresponding reference surface intersection was then calculated and statistically assessed (Table 4).

A second dataset available contains surveyed fix points on top of ridges and summits throughout the study area. Laser returns within a 1 m horizontal radius from each reference point were used to assess any stochastic and systematic vertical uncertainties in the point cloud (Table 4).

3.4. Forward error propagation of stochastic uncertainties

Strictly speaking, accuracies from control points or surfaces are only valid at exactly these locations and may not take into account

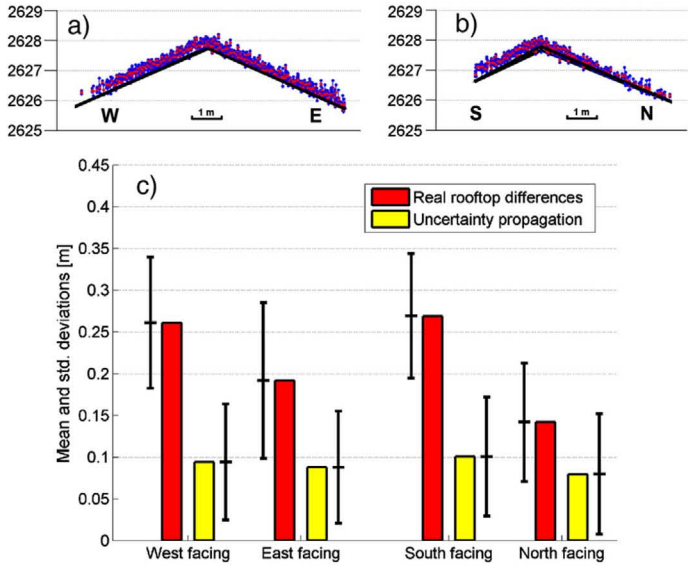

Fig. 2. ALS echoes of the 2009 campaign on a perpendicular cross-gable roof in a) and b). Actual returns are dots with vertical standard deviations from error propagation. In c), for each part of the rooftop, the mean (bar) and standard deviation (attached error bar) of the vertical difference from the laser returns to the respective rooftop surface are shown on the left. Bars and error bars on the right illustrate uncertainties from error propagation modeling for the same surfaces.

Table 4
Uncertainties from comparison with ground control surfaces and modeled uncertainty results from error propagation on the same surfaces. The third column shows differences from the fix points. Positive mean values represent laser returns above reference surfaces. Note that in October 2005 and April 2010, the reference surfaces and points were not snow-free during the ALS data acquisition, which is why the mean values and standard deviations were higher.

	Difference from reference surfaces		Uncertainty propagation		Difference from survey reference points	
Year	Mean	Std. deviation	Mean	Std. deviation	Mean	Std. deviation
2005 October	+ 0.56	0.32	+ 0.19	0.12	+0.40	0.50
2009 October	+ 0.20	0.09	+ 0.10	0.07	+0.09	0.38
2010 April	+ 0.31	0.19	+ 0.09	0.07	+0.15	0.42
2010 September	+ 0.22	0.07	+ 0.06	0.06	+0.07	0.38

the changing topographic or system-related parameters in the global study area. We therefore propose an area-wide error distribution, governed by spatially dependent factors, e.g. the topographic gradient, and system inherent parameters, e.g. the dGPS constellation.

Potential stochastic errors originate from the independent uncertainties of the airplane's position and attitude, the accuracy of the relative position and alignment of the sensor within the aircraft, as well as uncertainties in the scanning process. Multiple error sources are dependent on parameters not measured or known. We therefore partially rely on parameters defined by the mission planning and the sensor used. The overall uncertainty is subsequently calculated by employing the law of error propagation for stochastic uncertainties and by summing up systematic uncertainties.

3.4.1. Flight path accuracy

The position and attitude of the aircraft is measured with an integrated positioning and attitude indicating device. In our case, all four campaigns made use of the Applanix POS-AV 510 IMU system, which registers the position, roll, pitch, and heading angles of the aircraft's attitude as well as velocities. As an accuracy measure of the position and attitude of the airplane/scanner system, we relied on standard deviations provided by the post-processed flight path files of the smoothed best estimated trajectory (SBET) from the Applanix POSGPS software (www.applanix.com). The related uncertainties are present at a high temporal resolution in the trajectory, and include three position and three angle standard deviations, based on all accuracy-defining factors, e.g., satellite coverage and constellation, kinematic differential GPS constellation. The analysis of these deviations from all four campaigns showed a post-processed mean positional accuracy of better than 0.02 m horizontally and 0.04 m vertically, whereas the angular deviations were 0.08 mrad for both pitch and roll and 0.32 mrad for the heading. The position accuracy values are well in accordance with Glennie's (2007) rule of thumb of 2 cm + 1 PPM (part per million of the distance between the position of the aircraft and the GPS ground base station) in horizontal and vertical directions for short kinematic baselines. This stochastic position uncertainty directly degrades the accuracy of ground points by introducing the same uncertainty (Skaloud et al., 2010).

One of the largest uncertainty sources lies within the attitude precision of the inertial measurement unit of the aircraft (Glennie, 2007; Fig. 3). A small erroneous angle will, when multiplied by the distance from the airplane to the ground, lead to a positioning error of the ground point. Furthermore, it introduces an increasing vertical shift at larger scan angles by assigning the (correct) distance measurement to the wrong angle (Morin, 2002).

3.4.2. Boresight angle errors and lever-arm offset

An additional group of uncertainties we considered include the angular (so-called boresight) and positional (lever-arm) offsets between the scanner and the navigation units in the airplane. The distance offsets were determined by measurement or system calibration (Glennie, 2007). The inaccuracy is given by the uncertainty of the measurements between the two units, which are assumed to be within the range of 2 cm in every direction (Glennie, 2007). This error influences the accuracy of ground points stochastically by propagation of the same uncertainty. The boresight error is more complex to resolve, as ground points from overlapping flight strips are used to determine it. Deviations between these points are minimized by a least squares adjustment to best fit the flight strips and thus define the boresight angles. In the present case, typical residual boresight errors are used as reported in Glennie (2007). Like IMU angular uncertainties, these angular errors are projected to the ground point level via the range and add to the stochastic uncertainty of a ground point (Fig. 3).

3.4.3. Scanning system uncertainties

In the laser systems used in this study, the emitted laser beam was deflected by an oscillating mirror across the flight track. The precision of the measurement of this scanning angle is limited by the resolution of the mirror's angle encoder, which again results in positional and vertical error (Glennie, 2007). The positional error occurs only in the across-track direction and the vertical error increases with increasingly larger scanning angles (Morin, 2002).

Another influence on uncertainty is the range measurement accuracy, restricted by the system's range measuring clock, which has a limited precision (Glennie, 2007). This influence is not range dependent and

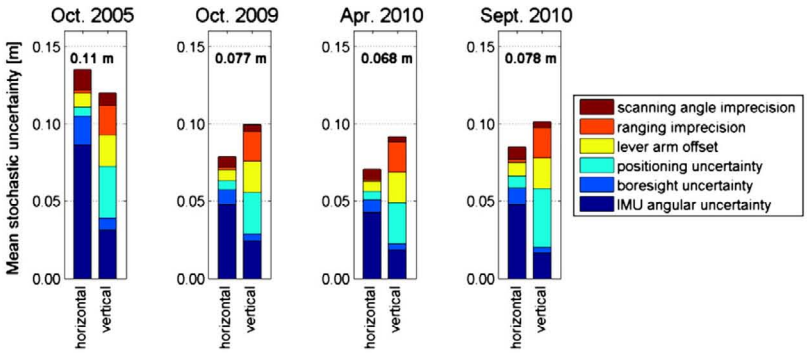

Fig. 3. Stacked mean stochastic vertical uncertainties from different sources for the point cloud. The columns on the left for each period show the contribution of horizontal stochastic uncertainties already converted to vertical uncertainties. The columns on the right show the contribution of vertical stochastic uncertainties. The resulting mean overall vertical stochastic uncertainty from error propagation is given above the bars.

adds to the stochastic uncertainty vertically, and for larger scanning angles, also horizontally (Fig. 3).

3.4.4. Overall vertical uncertainty from uncertainty propagation

The sources of errors described above introduce both horizontal and vertical uncertainties. For volume change applications, it is mainly the vertical accuracy that is of interest. We hence converted horizontal shifts to vertical shifts via the local terrain slope derived for each raster cell. The topographic gradient influences the uncertainty of the interpolated grid by leading to a vertical difference when a horizontal misregistration is present (Hodgson & Bresnahan, 2004; Kraus & Pfeifer, 1998). If a surface is level, a horizontal dislocation has no influence on the elevation. Steep regions therefore exhibit larger uncertainties in the airborne laser scanning DEMs. We used the local gradient to convert horizontal stochastic uncertainties to vertical uncertainties. All stochastic vertical uncertainties σ_i were subsequently summed to give an overall stochastic uncertainty ε for each laser ground point using

$$\varepsilon = \sqrt{\sum_{i=1}^{n} \sigma_i^2} \tag{2}$$

which describes the error propagation of uncorrelated uncertainties (cf. Burrough & McDonnell, 1998; Koblet et al., 2010; Nuth & Kääb, 2011). In a next step, the uncertainties of all laser echoes ε_i in a raster cell were combined to derive the zonal stochastic uncertainty$S_\varepsilon$by applying the standard deviation about the mean for each raster cell (Nuth & Kääb, 2011; Papula, 2003)

$$S_v = \sqrt{{S_{\varepsilon 1}}^2 + {S_{\varepsilon 2}}^2 + 2 \cdot S_{\varepsilon 1} \cdot S_{\varepsilon 2} \cdot r_{\varepsilon 1 \varepsilon 2}} \tag{3}$$

where n represents the number of laser returns per raster cell. As we are not dealing with real deviations about the mean but with multiple standard deviations, we replaced the sum of the squared differences with the sum of the squared single emission uncertainty ε_i. Using this equation, the effect of a higher point density resulted in a lower overall raster cell uncertainty. To evaluate the uncertainty of the elevation change between two DEMs in a single raster cell, the spatial autocorrelation between two elevation models should be taken into account (Burrough & McDonnell, 1998; Nuth & Kääb, 2011; Rolstad et al., 2009):

$$S_v = \sqrt{{S_{\varepsilon 1}}^2 + {S_{\varepsilon 2}}^2 + 2 \cdot S_{\varepsilon 1} \cdot S_{\varepsilon 2} \cdot r_{\varepsilon 1 \varepsilon 2}} \tag{4}$$

The uncertainty of the elevation change S_v can be calculated from the respective raster cell uncertainties S_ε and S_ε and their spatial correlation $r_{\varepsilon 1 \varepsilon 2}$ of the DEMs *s1* and *s2*. In preparation for the above equation, the local correlation coefficient r was calculated using a moving window operation leading to

$$r(s1, s2)_{x,y} = \frac{\sum_{x,y} \left(s1(x,y) - \mu(s1)_w\right) \cdot \left(s2(x,y) - \mu(s2)_w\right)}{N_w \cdot \sigma(s1) \cdot \sigma(s2)} \tag{5}$$

where r at the location x,y is calculated using the mean values μ_w, and the standard deviation values σ of the moving window area with the number of pixels N_w. This method is known from image matching algorithms (Etzelmüller, 2000; Sun et al., 2008), and based on Pearson's correlation coefficient. The moving window size we used is dependent on semi-variogram analyses of an ice-free part of the DEM differences, resulting in correlation ranges of 60 m for the periods covered in this contribution. The correlation coefficient r is close to +1 for very positively correlated raster cells (small change in local topography), zero for the absence of correlation, and negative values to −1 represent a negative correlation (Etzelmüller, 2000). Fig. 4 illustrates the local correlation for the area of the glacier tongue. Smaller moving window sizes result in spatially more accentuated correlations, while the statistical reliability decreases (Etzelmüller, 2000).

Based on the assumption of normal distribution of all uncertainties around the same average, we subsequently calculated the zonal stochastic uncertainty of a region or even the entire glacier by combining all single raster cell uncertainties S_v, using Eq. (3) once again, where n is the overall number of raster cells covered.

3.5. Systematic errors

Besides the stochastic inaccuracies mentioned earlier in this section, systematic errors play a dominant role in DEM differencing. Systematic errors potentially originate from the ALS system, from coordinate transformations, from changes in the atmosphere and from target characteristics. In this study, we assessed systematic uncertainties related to the deflection of the vertical (IMU vs. dGPS) and to reflection triggering of the ALS system, as well as to elevation changes due to snow. Systematic uncertainties in coordinate transformations were not expected since all raw data were converted using the same REFRAME tool (see Section 2.2). Potential changes in the composition of the atmosphere compared to the calibrated atmosphere, which alter the speed of light and therefore the measured range (cf. Katzenbeisser, 2003), were ignored, as were changes in the non-glacierized terrain after taking snow into consideration and other possible system calibration issues. The penetration of laser light into the snow and ice surfaces would lead to an underestimation of the surface elevation, but was assumed to be negligibly small at the accuracy level of this study (Sun et al., 2006; Thomas et al., 2006).

3.5.1. Deflection of the vertical

One possible error source could be the deflection of the vertical (DOV, cf. Goulden & Hopkinson, 2010b). With increasingly more accurate measurements of the position and attitude of the aircraft/laser scanning system, the angle between the local reference geoid normal and the ellipsoidal normal starts to account for a larger proportion of the total error budget. The direction of the emitted laser pulse is recorded by the inertial measurement unit, which uses the geoid (gravitational) as a reference, whereas the GPS system references to the ellipsoid normal (Goulden & Hopkinson, 2010b). In the relatively coarse resolution of the Earth Gravitational Model 2008 (EGM08), maximum deflections of more than 45 arc seconds exist in the European Alps (National Geospatial-Intelligence Agency NGA, 2008). In the region of the Findelengletscher and the corresponding reference surfaces, however, the magnitude of the deflection of the vertical is only about 4 arc seconds (U. Marti, swisstopo, 2011, personal communication). Therefore, even if there was a worst case with the scan angle direction parallel to the DOV direction, as mentioned in Goulden and Hopkinson (2010b), the absolute systematic uncertainty would only be approx. 0.03 m horizontally and 0.01 m vertically for 2005, and even less for 2009 and 2010 since the flying altitude above ground was lower.

These values represent the maximum error arising from the maximum scan angle. Although this error is present in a single laser point cloud, the magnitude is almost identical in all campaigns. Therefore, this systematic error is cancelled out in the volume change calculations and can thus be excluded as a source of systematic error.

3.5.2. System-induced error

In all ALS campaigns used in this study, the laser echoes were systematically located above snow-free reference surfaces. This could be a residual bias from slightly different coordinate transformation parameters or from a system-specific error. The laser's beam divergence illuminates average footprints of 0.45 m (2005), 0.30 m (2009) and 0.25 m (2010) in diameter, depending on the flying height, the beam divergence angle of the laser system and the local topography relative to the direction of the laser beam. The system records the

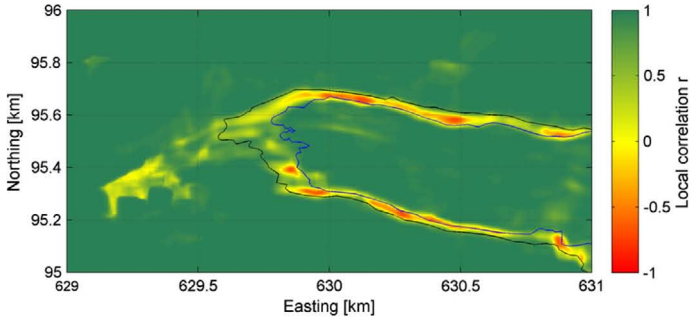

Fig. 4. Local correlation coefficient r (cf. Eq. (5)) for the Findelengletscher tongue region 2005–2009. Note the high correlations on ice-free terrain and on the center of the tongue. Low correlations were found on the borders of the tongue, where topographic parameters change substantially (black: glacier outline 2005, blue: outline 2009). (For interpretation of the references to color in this figure legend, the reader is referred to the web version of this article.)

position of the reflection at the center of the beam, although the accompanying recorded distance is only correct if the threshold exceeding reflection (triggering the distance measurement) occurred either on a surface perpendicular to the laser beam direction or the reflectivity of an inclined target is correct for the threshold of the laser distance measurement. For a homogeneously reflecting target, a distance measurement is therefore only possible at the ascending part of the Gaussian return pulse, optimally at the peak of the pulse. In every other case, the range measured might be too short due to the illumination ambiguity, leading to a positive vertical error (Morin, 2002).

Since we receive a single distance measurement for the entire footprint, the true location of the target corresponding to the recorded distance may well lie at the edge of the footprint. The factors governing this behavior are the local incidence angle, i.e. the angle between the laser beam direction and the ground surface normal, and the laser beam width. Consequently, the range may be systematically underestimated and thus the ground elevation overestimated. In addition to the subtraction of snow depths, this is the only other error we included in our systematic error propagation model (Table 3).

3.5.3. Errors induced by snow fall

This error source is important as it increases the LiDAR elevations measured on reference surfaces and has to be corrected to subsequently compare direct glaciological and geodetic mass balance measurements. In 2005 and September 2010, a snow fall event occurred some days before the ALS measurements were made. During the ALS surveys, in situ measurements of fresh snow depths were available at stake and snow pit sites on the glacier surface. We were thus able to subtract the impact of the snow depth from the involved ALS DEMs. The measured local snow heights were linearly interpolated in 100 m elevation steps and subsequently multiplied with the area covering each elevation band. Note that the evolution of snow, i.e. compaction over time and snow melt in the lower regions, was treated differently in the two cases. The event in fall 2010 was just before the ALS flight, and we therefore employed a linear snow depth trend for the whole elevation range derived from the in situ measurements. However, in 2005, the field campaign including snow depth measurements was conducted twelve days before the ALS flight took place. During that period, the temperature at a weather station close to the tongue (2500 m a.s.l.; courtesy Grande Dixence S.A.) measured a continuously positive temperature (between 0° and 15 °C). We therefore assumed that the fresh snow pack in the lower part of the glacier melted, whereas at higher elevations, elevation changes occurred mostly due to snow compaction. To account for this difference, we used a linear approximation of the measured snow depths without extrapolation to not measured higher areas, limiting the maximum snow depths to 0.50 m. This was supported by data from an automatic snow depth measuring station at 3100 m a.s.l. on the nearby Gornergrat (MeteoSwiss CLIMAP station). Dividing the summed elevation band snow volumes by the overall glacier surface area resulted in average snow height values for the Findelengletscher of 0.47 m in 2005, and 0.20 m in 2010.

4. Results

4.1. Single DEM uncertainty assessment

Fig. 2 shows a visual and statistical comparison of discrete laser ground returns of 2009 with two perpendicular sections of a cross-gable roof (black lines). The laser point cloud is plotted with vertical error bars from error propagation results appended to each laser return. This representation allows the detection of systematic shifts in every direction. In addition to the positive vertical shift present on every rooftop surface, the residual difference between two surfaces sloping in opposite directions exhibits a horizontal shift across the rooftop axis. The vertical systematic shift in the actual differences relative to the surfaces is in the range of 0.25 m and present in every DEM (cf. Table 4). The horizontal shift of the laser echoes is 0.11 m to the west and 0.18 m to the south. Examination of the shifts on other reference surfaces shows similar magnitudes but different shift directions. Consequently, no general horizontal shift correction seems to be required.

A comparison of the point clouds with survey fix points yielded similar results (Table 4), with a systematic positive elevation bias present in all of the deviations. For the three point clouds of 2009 and 2010 with higher point density, the systematic shift was lower than in 2005.

Fig. 3 describes the results of error propagation modeling on a laser ground point level. The stacked mean stochastic uncertainties for each ALS system component are shown converted to vertical uncertainties from both horizontal and vertical stochastic uncertainty parts. For computational reasons, these values stem from a point cloud test area including a steep rocky area, moraine material and glacier ice (Fig. 1). Note that the resulting stochastic uncertainty in the vertical direction of a single laser return is lower as the unique uncertainties do not sum up, but have to be treated with standard error propagation.

Due to the narrow scanning angle, a given angular uncertainty will translate to a mostly horizontal uncertainty on the ground proportional to the range. The inertial measurement unit was the source of the largest horizontal uncertainty, accounting for more than 50% of the overall horizontal stochastic uncertainty (Fig. 3). The linear shifts induced by positioning, lever-arm offset and range uncertainty were more pronounced in the vertical part of uncertainty due to the small influence of angular errors on vertical uncertainty. The overall

uncertainty in 2005 was larger (approx. 0.11 m) than in 2009 and 2010 (approx. 0.08 m) due to the higher flying altitude above ground and the larger scanning angle used. Comparison of the ALTM 3100 (2009 and April 2010) with the ALTM Gemini system (September 2010) using the same campaign setup shows stochastic uncertainties at a similar range of accuracies for both laser scanning systems (Table 4 and Fig. 3).

Maps of distributed systematic uncertainties from physical error propagation modeling are given in Fig. 5 and of stochastic uncertainties in Fig. 6. The systematic uncertainties in Fig. 5 originate from the local angle of incidence. Therefore, steep gradients clearly show a higher systematic uncertainty. Furthermore, patterns of flight strips are visible, particularly when the flight line is perpendicular to the aspect of the slope. Flat areas like most of the glacier surfaces have low systematic uncertainties. The two examples provided show the two DEMs with the most different setups: the lowest point density case in 2005 (average glacier raster cell stochastic uncertainty: 0.08 m, outside glacier area: 0.15 m) and the highest point density case in September 2010, with 0.04 m (glaciers), and 0.08 m (outside glaciers).

Stochastic uncertainties originate from different sources. In Fig. 6, one of the main apparent effects is the point density, visible in the contrast between overlapping and single flight strip regions. The color bar is scaled to the same range in both figures to allow direct comparison of the influence of different point densities (cf. Table 1) on the stochastic uncertainty. Additionally visible, but less influential, is the impact of the local gradient. The steeper the illuminated slope, the larger the ratio of the horizontal stochastic uncertainty added to the already existing vertical uncertainties. The mean raster cell stochastic uncertainty on the glacier's surface was 0.07 m in the 2005 DEM and 0.03 m in the 2010 DEM, with mean values outside the glaciers of 0.10 m (2005) and 0.03 m (Sept. 2010).

4.2. Glacier changes

The area of the Findelengletscher diminished by approx. 2% (0.27 km^2) from October 2005 to an area of 13.03 km^2 in September 2010. The corresponding change in length of the glacier tongue over this period was about −200 m. The distributed elevation difference for the whole study site is shown for all periods in Figs. 7, 8 and 9, and summarized for both glaciers in Table 3. The average thickness change from 2005 to 2010 on the Findelengletscher was −3.18 m and −1.76 m on the Adlergletscher with maximum ice losses on the glacier tongues of −35 m and −17 m, respectively. The corresponding volume changes are -42×10^6 m^3 for the Findelengletscher and -4×10^6 m^3 for the Adlergletscher. Estimates of the uncertainties for these volume differences are shown in Section 4.3. The elevation changes for the Findelengletscher are small in the accumulation area (eastern part), along the tongue (in the west) the elevation became much lower. The

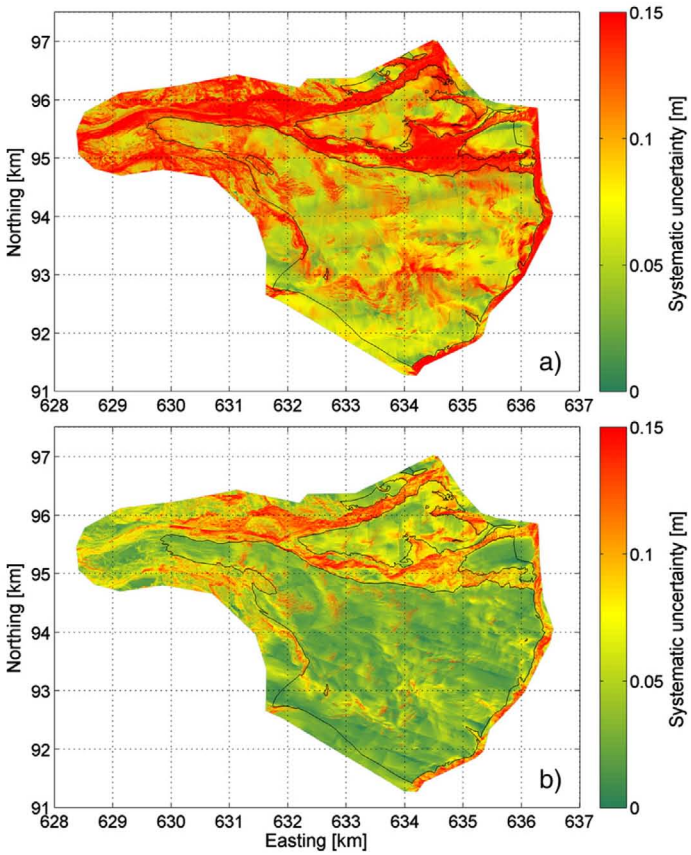

Fig. 5. Distributed systematic uncertainty of the study site of the DEM in 2005 (a) and September 2010 (b). Note that the values exceeding the color bar range are reduced to the maximum values' color, as the focus is on the glacier surfaces (within the black outlines). The mean systematic uncertainty in (a) outside the glacier's perimeters is 0.15 m. (For interpretation of the references to color in this figure legend, the reader is referred to the web version of this article.)

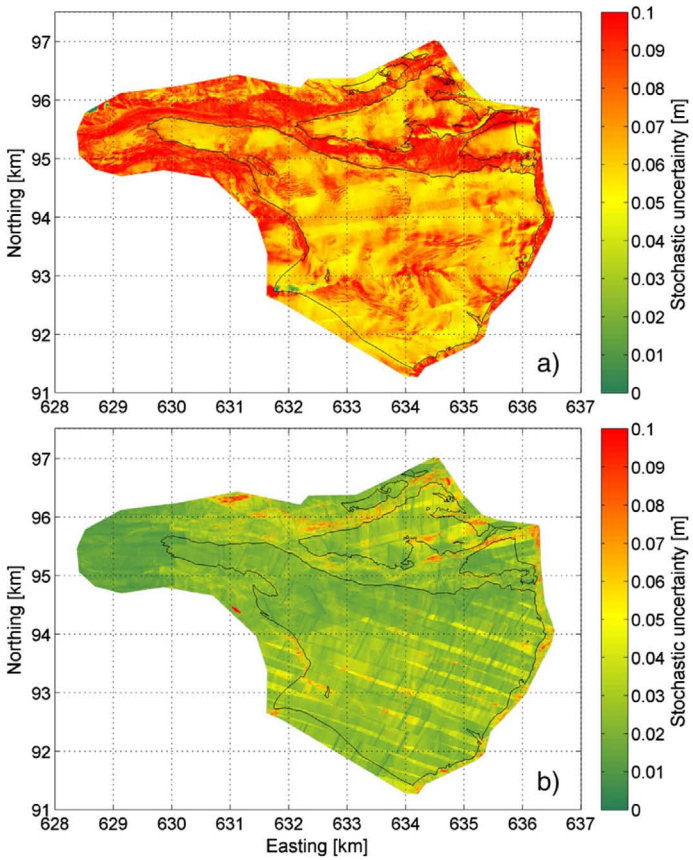

Fig. 6. Resulting distributed stochastic uncertainty of the study site of the DEM in 2005 (a) and September 2010 (b). Note that the values exceeding the color bar range are reduced to the maximum values' color, as the focus is on the glacier surfaces (within the black outlines). The mean stochastic uncertainty in (a) outside the glacier's perimeters is 0.10 m. (For interpretation of the references to color in this figure legend, the reader is referred to the web version of this article.)

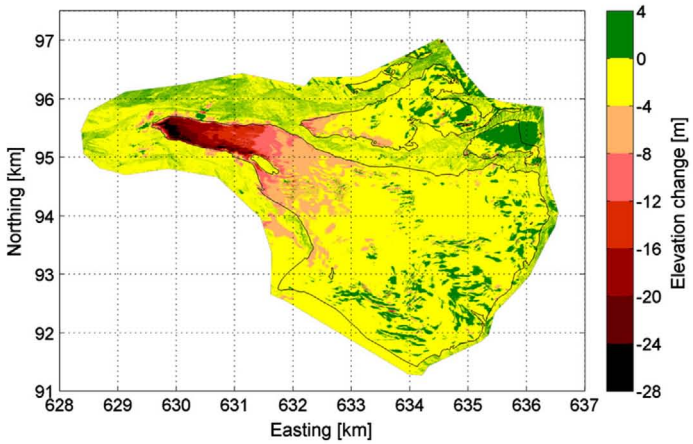

Fig. 7. Difference in elevation 2005–2009. Note that the color bar is scaled to represent 4 times the values of the 1 year period in Fig. 8, to allow a qualitative comparison between the two.

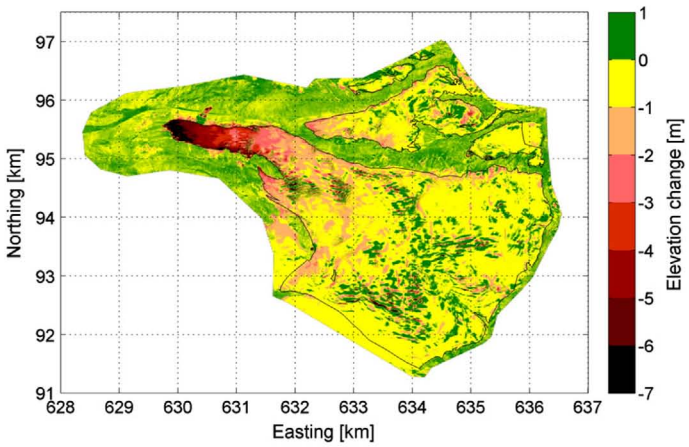

Fig. 8. Annual elevation difference 2009–2010.

same pattern was observed on the Adlergletscher, but due to the higher altitude of the terminus, to a lesser degree. The ripple features in the accumulation areas are mostly caused by a down valley propagation of crevasses. This effect was especially developed in the 1-year period (Fig. 8) as a result of the vertical resolution of the color bar range being four times higher than in Fig. 7, and thus more susceptible to smaller scale effects.

The last three surveys (October 2009, April and September 2010) comprise the hydrological year 2009/10 of the glaciers. The change in winter thickness from October 2009 to April 2010 is shown in Fig. 9. The most positive changes were found in the middle part of the glacier where snow melt and the transitional/emergence flow are balanced. Furthermore, the influence of early snow melt is visible on the south exposed sides of the moraines in the western part of the study site. Without any correction for the exact dates of the hydrological year, the change in winter volumes for the Findelengletscher was $+22\times10^6$ m^3 and $+3.2\times10^6$ m^3 for the Adlergletscher. The corresponding summer volume changes were -34.6×10^6 m^3 and -4.9×10^6 m^3, respectively, resulting in an average annual thickness loss of -0.96 m and -0.77 m.

4.3. Uncertainty assessment of glacier thickness changes

The results of the statistical co-registration approach (Table 2) reveal elevation uncertainties of several decimeters due to systematic horizontal shifts, which were lower than the 1 m pixel resolution of the DEMs. The higher vertical bias for the period 2005–2009 (between 0.36 and 0.72 m) was the result of there being 0.47 m snow present in 2005, whereas in the second period (2009–2010), the vertical bias was below 0.07 m. The horizontal shifts were smaller than the DEM's pixel resolution with no elevation-dependent bias present. We therefore opted not to perform any DEM corrections for this method. In the next step, systematic uncertainties were detected by comparing the single laser ground points to a reference surface or reference point (Table 4). Subsequent comparison of the resulting differences in the ALS point clouds show that, in our case, a common systematic positive offset in the vertical axis in the order of a few decimeters was present, i.e. all four DEMs were located above references. As these systematic offsets (after snow correction) are common to all DEMs, their effect cancels out when calculating elevation differences.

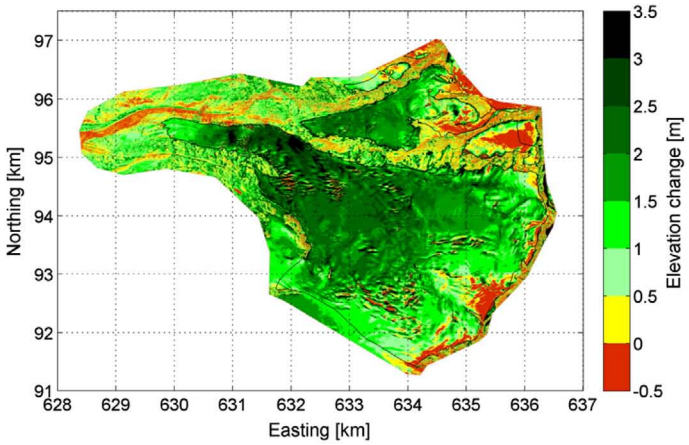

Fig. 9. Change in winter elevation October 2009–April 2010. Note the influence of the glacier flow dynamics on the distribution of the elevation changes: low or negative elevation changes in the high accumulation area are due to submergence (and wind erosion) and more positive values on the glacier surface than around the tongue due to emergence flow.

To obtain the spatially distributed uncertainties, we applied the physical error propagation modeling as described in Section 3. Overall stochastic uncertainties for single raster cells ranged mostly between 0.05 and 0.10 m on the glacier surface (cf. Fig. 6), whereas in the steep moraine zones and boulder-rich, topographically heterogeneous forefield, the stochastic uncertainties were visibly higher.

While the stochastic uncertainties of thickness change locally were more than 0.30 m, the resulting overall (zonal) stochastic uncertainty for the entire glacier area was very low due to the high number of measurements made (Table 3). The resulting values for the overall thickness changes are therefore mainly influenced by systematic errors present in the DEMs (cf. Table 3). Fresh snow cover during some of the surveys and some ALS system dependent errors resulted in corrections of glacier thickness change of up to 35% on the Adlergletscher, and 25% on the Findelengletscher. Over the entire 5-year period, simple DEM differencing indicated that the average thickness changes for the Findelengletscher were −3.49 m and for the Adlergletscher −2.06 m. In this period, average thickness change became less negative by 0.32 m for the Findelengletscher and 0.30 m for the Adlergletscher. The (corrected) winter and summer thickness changes for the period 2009/10 were +1.69 m and −2.65 m for the Findelengletscher, and for the Adlergletscher +1.42 m and −2.19 m, respectively.

5. Discussion

5.1. Uncertainties of the ALS point clouds and derived DEMs

The main contribution of this study is the development of a framework to assess systematic and stochastic uncertainties of ALS-derived DEMs in highly undulated terrain. Using reference points and surfaces from in situ surveys allowed a direct investigation of systematic as well as stochastic uncertainties. In order to explain the provenance of uncertainties, we developed a physical error propagation model for the ALS system. The results of this method show similar magnitudes of stochastic uncertainties to the stochastic uncertainties measured with laser echoes on reference surfaces. For the systematic errors ranging from a few decimeters to half a meter, our model was able to attribute about half to the ALS system. The major error sources identified were the IMU angular and dGPS positioning uncertainties (cf. Fig. 3). The remaining systematic positive bias (compared to reference surfaces) might originate from inaccuracies in the coordinate transformation parameters, atmospheric effects, or from changing characteristics or elevations of the terrain outside glaciers, which is assumed to be stable.

One main source of systematic errors is the sporadic or seasonal snow cover. In our study, estimates from in situ snow measurements on the glacier can explain a major part of the remaining systematic uncertainty in the ALS surveys in October 2005 as well as in April and September 2010 (cf. 3.5.3). In the April 2010 campaign, the vertical systematic shift was not as large because the snow was redistributed by wind and extensive melting due to the exposed location of the reference points occurred.

The most important factors for deriving the most accurate elevation model possible are: a stable differential GPS constellation and a precise IMU unit in the airplane, and the in situ surveying of reference surfaces and fresh snow thicknesses. The precision of the IMU unit is, coupled with the flying height above ground, the single most system-inherent uncertainty factor. With respect to the topography, a steep local slope and large angle of incidence of the laser beam degrade the accuracy. They introduce a systematic vertical shift and a larger stochastic uncertainty by appending a larger proportion of the horizontal uncertainty to the vertical uncertainties.

5.2. Uncertainties of DEM differencing

If direct in situ reference data is not available, Nuth and Kääb's (2011) method of co-registering DEMs using a statistical approach provides a valuable way to deal with systematic relative shifts of DEMs in horizontal and vertical directions. However, corrections for temporary snow must be applied to the DEMs in advance. Note that the values used were interpolated for the glacier surface based on in situ measurements, but the regions used for the co-registration approach are at lower altitudes where less or no snow was present, which introduces an additional uncertainty. This is visible, for example, in 2009–2010 on the bare rock area (A) (Table 2), where the mean bias was reduced to 0.01 m even though we know from snow depth measurements on the glacier, that the mean snow depth is 0.20 m. The co-registration approach is therefore not entirely suitable for our study. Furthermore, the perimeters used for co-registration are suboptimal because stable areas are small and still contain moraines prone to erosion, steep creeping slopes and ski runs that are leveled out. Therefore, the use of independent ground control surfaces is mandatory at our study site to investigate systematic uncertainties.

5.3. Changes in the glaciers and related uncertainties

The remaining glacier areas for the Findelengletscher and the Adlergletscher are 13.03 km^2 and 2.24 km^2, respectively, i.e. the glacier system has lost about 30% of its LIA extent (cf. Maisch et al., 2000). The geodetically derived frontal retreat between October 2005 and September 2010 amounts in total to 200 m, which is significantly larger than the 16 m reported from annual in situ observations (cf. Glaciological Reports, 1881–2010, updated online data). Assuming a density of 850 ± 60 kg m^{-3} for converting the observed thickness changes into the geodetic mass balance of Findelengletscher results in -2.70 ± 0.19 m w.e. for the period from October 2005 to September 2010. This is significantly more negative than the glaciological mass balance (−2.07 m w.e.) for the corresponding period reported to the WGMS (2011, updated), and shows the need for an early re-analysis of this mass balance series.

6. Conclusion

We applied ALS in high mountain topography to assess glacier change based on differencing DEMs over a time period of five years as well as over one hydrological year. The corresponding winter and summer seasons were investigated separately. The well-defined setup of the ALS surveys, optimized for the glaciological purposes, and a homogenized post-processing resulted in high-precision DEMs. Furthermore, we were able to assess the stochastic and systematic uncertainty of the DEMs and resulting changes by comparing them with reference points and areas from independent surveys, as well as by applying statistical and physical error modeling. The latter approach allowed uncertainties to be attributed to error sources (in the ALS system) and provided distributed uncertainty fields over the target.

The local (stochastic and systematic) uncertainties amounted to just of a few decimeters. This shows that ALS is well suited for analyzing glacier change in high mountain terrain and that there are no drawbacks in shadow- and snow-covered regions. For derived elevation changes, the calculation of zonal uncertainties over the glacier revealed that stochastic uncertainties are not significant for change analysis but systematic uncertainties need to be considered.

Our results indicate that significantly more ice was lost between 2005 and 2010 than earlier reports from in situ measurements suggest. The new data provides a useful basis for a thorough re-analysis of these observation series. Even with the large surface changes observed in this study, potential error sources and related uncertainties still need to be carefully assessed. This will clearly be even more necessary for applications where the change signal is smaller, either because the time between the observations is shorter or because the processes act on longer temporal scales.

Acknowledgements

We are grateful to Wilfried Haeberli and Michael Schaepman for their valuable support with this project. The authors acknowledge the hard work of the Findelengletscher field teams of the Universities of Fribourg and Zurich; without their combined effort, this project would not have been possible. We thank BSF Swissphoto for the acquisition of the ALS data and their continuous support. Many thanks to Silvia Dingwall for reviewing the language of the article. Urs Marti of swisstopo kindly provided us with an independent deflection of the vertical measurement; Grande Dixence SA provided measurements of a meteorological station. We thank an anonymous reviewer for helpful comments, which have helped improve the manuscript significantly. This project was supported by the Swiss Energy Utility Axpo.

References

Abermann, J., Fischer, A., Lambrecht, A., & Geist, T. (2010). On the potential of very high-resolution repeat DEMs in glacial and periglacial environments. *The Cryosphere, 4*, 53–65.

Abermann, J., Lambrecht, A., Fischer, A., & Kuhn, M. (2009). Quantifying changes and trends in glacier area and volume in the Austrian Ötztal Alps (1969–1997–2006). *The Cryosphere, 3*, 415–441.

Burrough, P. A., & McDonnell, R. A. (1998). *Principles of geographical information systems*. Oxford: Oxford University Press.

Casas, A., Riaño, D., Greenberg, J., & Ustin, S. (2011). Assessing levee stability with geometric parameters derived from airborne LiDAR. *Remote Sensing of Environment, 117*, 281–288.

Collins, D. N. (1979). Quantitative determination of the subglacial hydrology of two Alpine glaciers. *Journal of Glaciology, 23*, 347–362.

Cressie, N. (1993). *Statistics for Spatial Data.* : Wiley-Interscience.

Etzelmüller, B. (2000). On the quantification of surface changes using grid-based digital elevation models (DEMs). *Transactions in GIS, 4*, 129–143.

Farinotti, D., Usselmann, S., Huss, M., Bauder, A., & Funk, M. (2011). Runoff evolution in the Swiss Alps: projections for selected high-alpine catchments based on ENSEMBLES scenarios. *Hydrological Processes, 26*, 1909–1924.

Favey, E., Geiger, A., Gudmundsson, G. H., & Wehr, A. (1999). Evaluating the potential of an airborne laser-scanning system for measuring volume changes of glaciers. *Geografiska Annaler: Series A, Physical Geography, 81*, 555–561.

Filin, S. (2003). Recovery of systematic biases in laser altimetry data using natural surfaces. *Photogrammetric Engineering & Remote Sensing, 69*, 1235–1242.

Geist, T. (2005). Application of airborne laser scanner technology in glacier research. *Institute of Geography* (pp. 118). Innsbruck: University of Innsbruck.

Geist, T., Lutz, E., & Stötter, J. (2003). Airborne laser scanning technology and its potential for applications in glaciology. *International Archives of Photogrommetry, Remote Sensing and Spatial Information Science, 34*, 101–106.

Glaciological Reports (1881–2010). The Swiss Glaciers. *Yearbooks of the Cryospheric Commission of the Swiss Academy of Sciences (SCNAT) published since 1964 by the Laboratory of Hydraulics. Hydrology and Glaciology (VAW) of ETH Zürich.*

Glennie, C. (2007). Rigorous 3D error analysis of kinematic scanning LIDAR systems. *Journal of Applied Geodesy, 1*, 147–157.

Goulden, T., & Hopkinson, C. (2010a). The forward propagation of integrated system component errors within airborne lidar data. *Photogrammetric Engineering & Remote Sensing, 76*, 589–601.

Goulden, T., & Hopkinson, C. (2010b). Investigating the effect of the deflection of the vertical on lidar observations. *Canadian Journal of Remote Sensing, 36*, S365–S375.

Haug, T., Rolstad, C., Elvehøy, H., Jackson, M., & Maalen-Johansen, I. (2009). Geodetic mass balance of the western Svartisen ice cap, Norway, in the periods 1968–1985 and 1985–2002. *Annals of Glaciology, 50*, 119–125.

Hodgson, M. E., & Bresnahan, P. (2004). Accuracy of airborne lidar-derived elevation: Empirical assessment and error budget. *Photogrammetric Engineering & Remote Sensing, 70*, 331–339.

Hopkinson, C., Chasmer, L., & Hall, R. (2008). The uncertainty in conifer plantation growth prediction from multi-temporal lidar datasets. *Remote Sensing of Environment, 112*, 1168–1180.

Hopkinson, C., & Demuth, M. N. (2006). Using airborne lidar to assess the influence of glacier downwasting on water resources in the Canadian Rocky Mountains. *Canadian Journal of Remote Sensing, 32*, 212–222.

Huising, E. J., & Gomes Pereira, L. M. (1998). Errors and accuracy estimates of laser data acquired by various laser scanning systems for topographic applications. *ISPRS Journal of Photogrammetry and Remote Sensing, 53*, 245–261.

Huss, M., Bauder, A., & Funk, M. (2009). Homogenization of long-term mass-balance time series. *Annals of Glaciology, 50*, 198–206.

Huss, M., Hock, R., Bauder, A., & Funk, M. (2010). 100-year mass changes in the Swiss Alps linked to the Atlantic Multidecadal Oscillation. *Geophysical Research Letters, 37*.

Iken, A., & Bindschadler, R. A. (1986). Combined measurements of subglacial water pressure and surface velocity of Findelengletscher, Switzerland: Conclusions about drainage system and sliding mechanism. *Journal of Glaciology, 32*, 101–119.

Johnson, S. E. (2009). Effect of target surface orientation on the range precision of laser detection and ranging systems. *Journal of Applied Remote Sensing, 3*, 033564.

Kääb, A. (2005). *Remote sensing of mountain glaciers and permafrost creep*. Zurich: University of Zurich.

Katzenbeisser, R. (2003). About the calibration of lidar sensors. *ISPRS Workshop "3-D Reconstruction from Airborne Laser-Scanner and InSAR data"* (pp. 1–6). Germany: Dresden.

Kennett, M., & Eiken, T. (1996). Airborne measurement of glacier surface elevation by scanning laser altimeter. *Annals of Glaciology, 24*, 293–296.

Knoll, C., & Kerschner, H. (2010). A glacier inventory for South Tyrol, Italy, based on airborne laser-scanner data. *Annals of Glaciology, 50*, 46–52.

Koblet, T., Gärtner-Roer, I., Zemp, M., Jansson, P., Thee, P., Haeberli, W., et al. (2010). Reanalysis of multi-temporal aerial images of Storglaciären, Sweden (1959–99); Part 1: Determination of length, area, and volume changes. *The Cryosphere, 4*, 333–343.

Kraus, K., & Pfeifer, N. (1998). Determination of terrain models in wooded areas with airborne laser scanner data. *ISPRS Journal of Photogrammetry and Remote Sensing, 53*, 193–203.

Luethy, J., & Stengele, R. (2005). Mapping of Switzerland – Challenges and experiences. *ISPRS WG III/3, III/4, V/3 Workshop "Laser scanning 2005"*. The Netherlands: Enschede.

Machguth, H. (2008). On the use of RCM data and gridded climatologies for regional scale glacier mass balance modeling in high mountain topography; the example of the Swiss Alps. *Department of Geography* (pp. 176). Zurich: University of Zurich.

Machguth, H., Paul, F., Hoelzle, M., & Haeberli, W. (2006). Distributed glacier mass-balance modelling as an important component of modern multi-level glacier monitoring. *Annals of Glaciology, 43*, 335–343.

Maisch, M., Wipf, A., Denneler, B., Battaglia, J., & Benz, C. (2000). *Die Gletscher der Schweizer Alpen* Gletscherhochstand 1850, Aktuelle Vergletscherung, Gletscherschwundszenarien (2 ed.). Zurich: vdf Hochschulverlag AG an der ETH Zürich.

Morin, K. (2002). Calibration of airborne laser scanners. *Department of Geomatics Engineering* (pp. 134). Calgary: The University of Calgary.

National Geospatial-Intelligence Agency NGA (). *Earth Gravitational Model 2008*. NGA Office of GEOINT Services.

Nuth, C., & Kääb, A. (2011). Co-registration and bias corrections of satellite elevation data sets for quantifying glacier thickness change. *The Cryosphere, 5*, 271–290.

Østrem, G., & Brugmann, M. (1991). *Glacier mass-balance measurements: A manual for field and office work*. Oslo: NVE.

Papula, L. (2003). *Mathematische Formelsammlung für Ingenieure und Naturwissenschaftler* (8 ed.). Wiesbaden: Vieweg.

Rolstad, C., Haug, T., & Denby, B. (2009). Spatially integrated geodetic glacier mass balance and its uncertainty based on geostatistical analysis: Application to the western Svartisen ice cap, Norway. *Journal of Glaciology, 55*, 666–680.

Shan, J., & Toth, C. K. (2009). *Topographic laser ranging and scanning: Principles and processing*. CRC Press.

Skaloud, J., Schaer, P., Stebler, Y., & Tomé, P. (2010). Real-time registration of airborne laser data with sub-decimeter accuracy. *ISPRS Journal of Photogrammetry and Remote Sensing, 65*, 208–217.

Sun, X., Cooper, J., Hom, M., Shuman, C., & Harding, D. (2006). Measurements of snow and ice surface reflectance and penetration to short laser pulses at zero phase angles and 532 and 1064-nm wavelengths. *American Geophysical Union, Fall Meeting 2006* (pp. 1121). : American Geophysical Union.

Sun, X., Pitsianis, N. P., & Bientinesi, P. (2008). Fast computation of local correlation coefficients. In F. T. Luk (Ed.), *Advanced signal processing algorithms, architectures, and implementations XVIII (Proceedings of SPIE)*. Bellingham, USA: Society of Photo-Optical Instrumentation Engineers.

Swisstopo (2008). Formulas and constants for the calculation of the Swiss conformal cylindrical projection and for the transformation between coordinate systems. In DDPS (Ed.) (p. 18). Bern: Federal Office of Topography swisstopo.

Thomas, R., Frederick, E., Krabill, W., Manizade, S., & Martin, C. (2006). Progressive increase in ice loss from Greenland. *Geophysical Research Letters, 33*, L10503.

Ventura, G., Vilardo, G., Terranova, C., & Sessa, E. B. (2011). Tracking and evolution of complex active landslides by multi-temporal airborne LiDAR data: The Montaguto landslide (Southern Italy). *Remote Sensing of Environment, 115*, 3237–3248.

Wehr, A., & Lohr, U. (1999). Airborne laser scanning—An introduction and overview. *ISPRS Journal of Photogrammetry and Remote Sensing, 54*, 68–82.

WGMS (2011). *Glacier Mass Balance Bulletin No. 11 (2008–2009)*. M. Zemp, S. U. Nussbaumer, I. Gärtner-Roer, M. Hoelzle, F. Paul, & W. Haeberli (Eds.), (pp. 102). Zurich, Switzerland: ICSU (WDS)/IUGG (IACS)/UNEP/UNESCO/WMO, World Glacier Monitoring Service.

Yu, X., Hyyppa, J., Kaartinen, H., & Maltamo, M. (2004). Automatic detection of harvested trees and determination of forest growth using airborne laser scanning. *Remote Sensing of Environment, 90*, 451–462.

Zemp, M., Jansson, P., Holmlund, P., Gärtner-Roer, I., Koblet, T., Thee, P., et al. (2010). Reanalysis of multi-temporal aerial images of Storglaciären, Sweden (1959–99); Part 2: Comparison of glaciological and volumetric mass balances. *The Cryosphere, 4*, 345–357.

3 EVALUATING VOLUMETRIC GLACIER CHANGE METHODS USING AIRBORNE LASER SCANNING DATA

Joerg, P.C., & Zemp, M. (2014). Evaluating volumetric glacier change methods using airborne laser scanning data. *Geografiska Annaler: Series A Physical Geography*, *96*, 135-145. Reprint with permission from Wiley.

EVALUATING VOLUMETRIC GLACIER CHANGE METHODS USING AIRBORNE LASER SCANNING DATA

PHILIP CLAUDIO JOERG and MICHAEL ZEMP

Department of Geography, University of Zurich, Zurich, Switzerland

Joerg, P.C. and Zemp, M., 2014. Evaluating volumetric glacier change methods using airborne laser scanning data. *Geografiska Annaler: Series A Physical Geography*, 96, 135–145. DOI:10.1111/geoa.12036

ABSTRACT. Assessments of geodetic volume change are widely used in glaciology and have a long tradition dating back to the nineteenth century. Over time, the geodetic method and corresponding data storage have been developed further, but the resulting methodological heterogeneity can lead to errors that are difficult to separate from other survey uncertainties. In this study we used high-resolution airborne laser scanning data from the Findelengletscher in the Swiss Alps to evaluate state-of-the-art volumetric glacier change methods. For the first time we have been able to simulate errors arising from different geodetic methods and spatial resolutions. The evaluation showed that, although the digital elevation models were perfectly co-registered, systematic and random method- and scale-dependent errors still occurred. These errors have an impact on the resulting volume changes at lower spatial resolutions and may lead to exponentially larger uncertainties. Volume changes from contour methods provided reasonably accurate results, while volumetric change assessments from central profile lines were especially prone to biases at any scale.

Key words: airborne laser scanning, LiDAR, glacier change, geodetic volume change, method comparison, uncertainty analysis

Introduction

Glacier changes are considered to be among the best natural indicators of climatic changes and can have severe impacts on natural hazards, the regional water cycle, and global sea level (WGMS 2008). Geodetic methods for assessing changes in glaciers' area, thickness, and volume have a long tradition in glaciology with high-quality topographic mapping reaching back to the late nineteenth century (Finsterwalder 1897; Mercanton 1916). Such data have been compiled and published by the World Glacier Monitoring Service and its predecessor since the 1960s (PSFG 1967; WGMS 2012). The results from the geodetic assessments are used to validate and calibrate the glaciological method (Zemp *et al.* 2013) and to extrapolate from the results of the limited glaciological sample in space and time (Cogley 2009; Zemp *et al.* 2009). The geodetic method has been further developed to include new sensors (triangulation, photogrammetry, laser profiling and scanning), platforms (terrestrial, airborne, spaceborne), and data storage types (contour maps, vector and raster datasets, digital point clouds). However, it is difficult to separate errors related to these acquisition heterogeneities from other error sources and related uncertainties and have only been assessed in a few studies (e.g. Reinhardt and Rentsch 1986).

Our study site comprised a 28 km^2 catchment area containing the Findelengletscher (46° N, 7° 52′ E) in Canton Valais, Switzerland. This valley-type glacier is 13 km^2 in area (2010) with an elevation range of 2600–3900 m a.s.l. Between 2005 and 2010, the average annual thickness change of Findelengletscher was –0.7 m with mean elevation changes of up to –7 m at the tongue and –0.2 m in the accumulation area (Joerg *et al.* 2012). During these five years, the glacier retreated by approximately 200 m and lost 2% of its area.

The specific annual mass balances were, according to in-situ ablation-stake and snow-pit measurements, –7.3 m *water equivalent* (*w.e.*) at the terminus and +1 m w.e. in the accumulation area, resulting in an average annual mass balance of –0.41 m w.e. for the whole glacier (WGMS 2012). The expected annual mass turnover of the Findelengletscher is approximately 1.1 m w.e. if the winter of 2010 is assumed to be unexceptional (Sold *et al.* 2013).

We used high-resolution laser scanning data from two airborne surveys of the Findelengletscher, as a validation dataset to derive changes in glacier volume by simulating different established geodetic methods at various spatial scales. We then

DOI:10.1111/geoa.12036

evaluated any systematic and random errors due to methodological differences. In addition, we discuss the relevance of these errors for the interpretation of geodetic results.

Data and methods

Laser scanning surveys

The Findelengletscher was mapped using multitemporal *digital elevation models* (*DEMs*) from *airborne laser scanning* (*ALS*) (Joerg *et al.* 2012). The elevation models used here cover the five-year period from October 2005 to September 2010 and were available as point clouds with average point densities of 1.1 *points* (*pts*) m^{-2} in 2005 and 14.3 pts m^{-2} in 2010 (Table 1).

Additionally, two synchronous flight trajectories (September 2010) with a higher flying altitude covered a large part of the study site to investigate the effect of a lower point density on the accuracy of the subsequently derived DEM. When planning an airborne laser scanning campaign, the target number of points per square meter is required to generate a flight plan. The price of the dataset depends on the point density and the survey area. To simulate the accuracy for a much larger region, we tested the cheapest flight setup possible in addition to our high point density setups. We ended up with two flight lines covering close to 90% of Findelengletscher, with an average point density of 0.4 pts m^{-2}. The high point density flight plan (yellow lines in Fig. 1) used 35 flight trajectories with a combined length of more than 180 km to cover the area of Findelengletscher (and Adlergletscher to the north), with a total flight time of 4 h. Compared with this setup, the low point density campaign needed only about 17 km with a flight time of 12 min. Based on this information, we calculated that the low point density data would cost only about 10% of the cost of the high point density setup. Note that the fixed costs for the flight to and from the area of interest are not included in this calculation. Moreover, the covered and overlapping area are smaller in the low point density setup (see footprint in Fig. 1).

Volume change from high ALS point density

As a reference for all subsequent methods and resolutions, we used the two high point density ALS point clouds acquired in fall 2005 and 2010 to interpolate each into a 1 × 1 m DEM (Fig. 2a, b). To perform this task, the average elevation of all laser points on the ground (outliers previously removed) within a given 1 × 1 m raster cell was assigned as the elevation of that cell. Subsequently, to allow the calculation of the change in volume of the entire glacier, empty raster cells were interpolated using a least squares approach without changing the existing values (Joerg *et al.* 2012). The elevation change was then calculated by subtracting elevations at the same coordinates from each other (Fig. 2c). Subsequently, to calculate the average glacier elevation change, all elevation changes were summed up for the entire glacier area and divided by the average glacier surface area on the two dates.

To simulate the effect of scale from different raster resolutions, we repeatedly calculated the volume change while increasing the raster cell size in 1 m steps from 1 × 1 m to 250 × 250 m. In a first step, elevation values outside the glacier extent of 2005 were clipped for both DEMs in MATLAB (The MathWorks, Inc.) and set to 'no data' in the 1 × 1 m resolution grid to avoid using values outside the glacier for the change calculations. In a next step, the lower resolution raster grids were defined

Table 1. ALS data acquisition parameters and flying heights for the different dates.

Parameter		28–29 October 2005	29 September 2010	29 September 2010
Sensor employed	ALTM	3100	Gemini	Gemini
Measuring frequency	(kHz)	71–100	71	33
Scanning angle	(°)	±23	±15	±20.1
Scanning frequency	(Hz)	40–50	39	13.7
Average flying height	(m)	1500	1000	2800
Across-track overlap	(%)	55	50	35
Average point density	(pts m^{-2})	1.1	14.3	0.4
LASER Wavelength	(nm)	1064	1064	1064
Beam divergence (1/e)	(mrad)	0.30	0.25	0.25
Footprint size	(m)	0.45	0.25	0.70

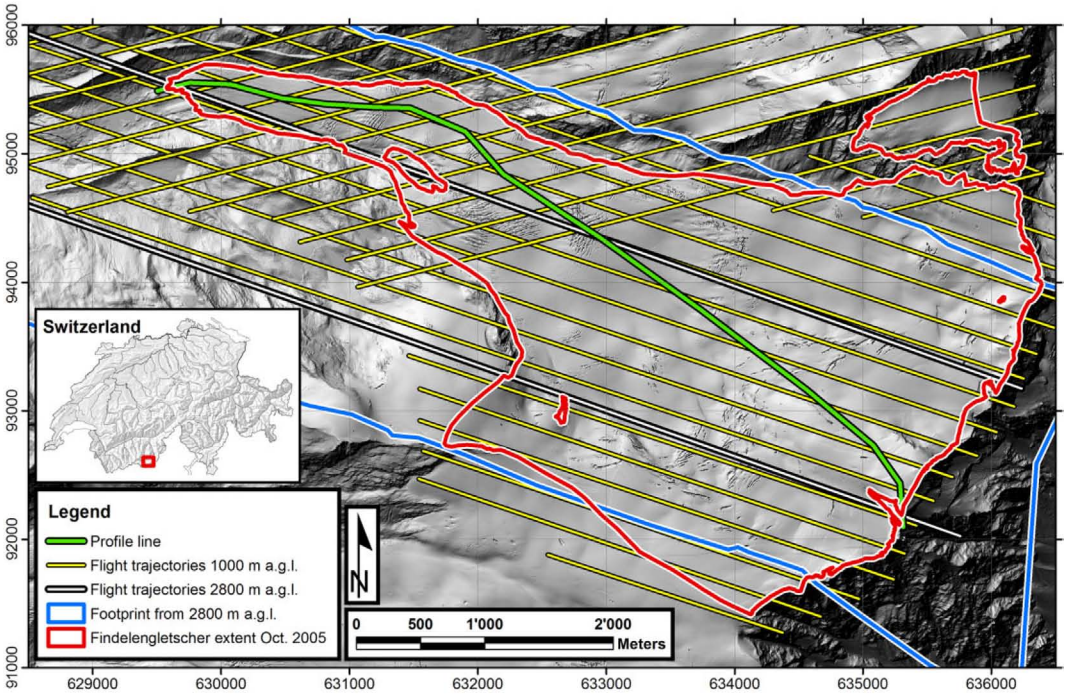

Fig. 1. Shaded relief of the Findelengletscher area. The red line shows the glacier extent in October 2005, and the green line the profile. Yellow lines indicate the flight trajectories of the high-resolution campaigns, the two white tracks (with black outlines) the two high flight trajectories, and the blue tracks the corresponding area covered on the ground. Coordinates are taken from Swiss grid CH1903, in meters.

similarly in both ALS datasets and filled with interpolated elevation values from the high-resolution raster using a bi-linear approach (the 'interp2' function in linear mode in MATLAB). The new grid intersection value is therefore the interpolation of the four nearest 1×1 m grid points. In the global grid definition process, the cell centre of the most southwesterly raster cell was kept at the same coordinates, whereas all other coordinates were generated according to the new raster resolution. Finally, both new rasters were subtracted from each other and the volume change was calculated.

Volume change from low ALS point density

On the same day the high point density dataset of September 2010 was acquired, a low point density dataset was obtained to test the most economical way to generate an ALS DEM and to investigate the effects of the lower point density on the volume change. The footprint of the two flight trajectories covered about 90% of Findelengletscher's surface (Fig. 1). We calculated the volume change per 10 m elevation band by extrapolating the measured average volume change to the unmeasured areas. The overall volume change is the sum of the volume changes of all elevation bands. As the unmeasured area was exclusively located on high elevations in the accumulation area with little volume change, the error introduced by the extrapolation is expected to be small.

Volume change from an altimetry profile

To survey a large number of glaciers, laser profiling along the centreline instead of laser scanning provides the elevation change distributed over the entire altitudinal range of a glacier (cf. Arendt *et al.* 2002). This approach was simulated by measuring elevation changes of Findelengletscher (Fig. 1) by using all DEM elevations of 2005 and 2010 of 1×1 m grid cells along the centreline. Additionally, a horizontal distance of 25 m between surveyed points was simulated to reveal the influence of scale in the horizontal sampling distance. Subsequently, we calculated

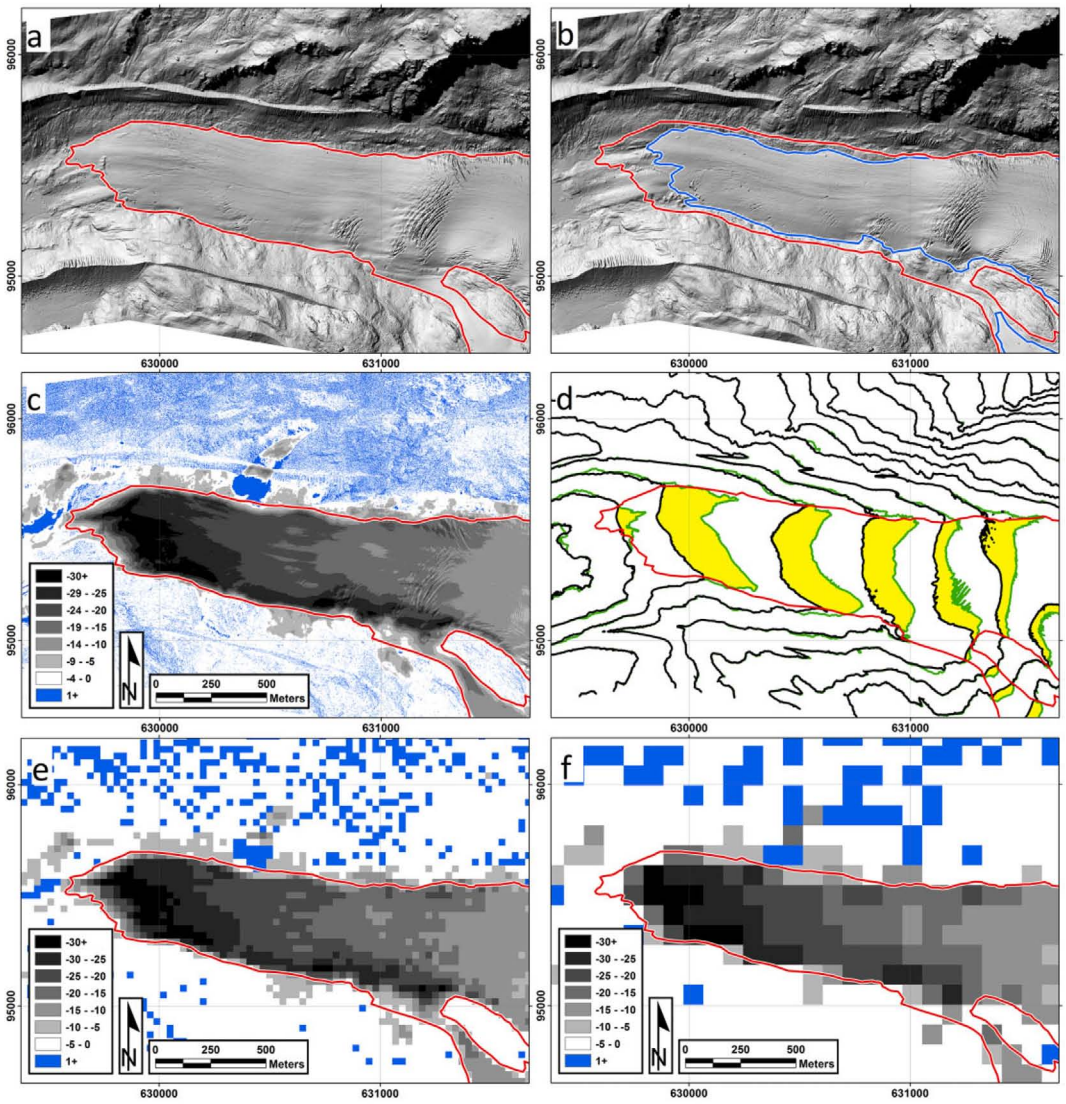

Fig. 2. Changes in the Findelengletscher tongue with the areas and hillshaded elevation models in 2005 (red; a) and 2010 (blue; b). Note the retreat of the tongue by approx. 200 m and the collapsing moraine to the north of the tongue (b). The middle row shows the elevation change in meters from the 1 × 1 m ALS DEMs (c) and an example of 50 m contour lines (d; 2005: black, 2010: green) with yellow areas showing the area differences used for the volume change calculations. The bottom row shows the elevation change of 30 m (e; similar to ASTER GDEM) and 90 m (f; similar to SRTM DEM), with resampled DEMs using the same elevation change colours as the 1 × 1 m DEM. Numbers in the legends are meters elevation change.

the average elevation change within every 10 m elevation band and multiplied that change with the mean 2005/2010 area of that corresponding elevation band. The overall volume change was then calculated by summing up all volume changes.

Volume change using elevation contours

Unlike today's DEMs, the standard elevation data 30 years ago and earlier were in the form of contour lines of the same elevation on maps (e.g. VAW/ETHZ 1967; Reinwarth 1973). Even today, contour lines from historic maps are often the only

source of data available for information on glacier elevations further back in the past, which may, in Switzerland for example, be more than 140 years old (the Siegfried and Dufour maps; Oberli 1979).

Geometrical-analytical contour approach

One approach to measuring the volumetric changes in a glacier was used by Finsterwalder (1953, 1954). This elegant method involved superimposing contour lines from two different dates and measuring the area enclosed between each horizontally displaced contour line. To calculate the volume change of an elevation band (dv_{ul}), the mean of the upper (dF_u) and lower (dF_l) difference area is multiplied by the contour interval (Δh_{ul}) between both difference areas:

$$dv_{ul} = (dF_u + dF_l)/2 \times \Delta h_{ul} \quad (1)$$

Eqn (1) therefore represents the volume of the enclosed 3-D prism (Finsterwalder 1953; Reinhardt and Rentsch 1986). Summing all volume changes per elevation band then leads to the overall volume change.

We used ArcGIS v.10.1 (ESRI, Inc.) to generate 25 m contour lines from both our ALS reference DEMs between 2525 and 3800 m a.s.l. Subsequently, the two sets of contour lines were intersected with the glacier outline of 2005 to avoid adding adjacent proglacial topographic changes, mostly from erosive processes, e.g. moraine instabilities (see Fig. 2b, northern moraine). The area differences at the 52 contour elevations (Fig. 2d) were then measured by summing all patches of each change in area, and the volume change was calculated according to Eqn (1).

To reveal the effects of scale when elevation contours were used, we used different sets of contour groups to calculate the overall volume change, i.e. we used all contour area differences (25 m elevation interval, one result), every second difference (50 m interval, two results as two alternating groups of 50 m contours exist from the 25 m dataset), every third difference (75 m, three results), and so forth, up to 200 m contour intervals (eight sets).

The same area contour difference data were also used to test a slightly different algorithm proposed by Hofmann (1958). This is similar to Eqn (1), but it geometrically approximates the frustum of a cone instead of a prism:

$$dV_{ul} = \left(dF_u + dF_l + \sqrt{dF_u \times dF_l}\right)/3 \times \Delta h_{ul} \quad (2)$$

DEM generation from contour lines

Another possibility is to use the contour lines of a survey year to directly interpolate a DEM using modern GIS techniques (e.g. Rivera and Casassa 1999; Vignon *et al.* 2003; Racoviteanu *et al.* 2007).We used the standard implementation and settings of the "topo-to-raster" method (earlier called TopoGrid) in ArcGIS v.10.1, based on the ANUDEM algorithm (Hutchinson 1989) to perform this task, and simulated the DEM generation from 25 m, 50 m, and 100 m contour intervals for each year using a 25×25 m target grid size. This method provided accurate interpolated DEM data, excelling other interpolation methods (Racoviteanu *et al.* 2007). These rasters were subsequently imported into MATLAB and bi-linearly interpolated using the built-in "interp2" function to generate a 1×1 m grid. This step then allowed the rasters to be clipped with the high-resolution glacier outline of 2005 so that edge effects could be avoided. Finally, the DEMs were subtracted and volume changes calculated.

Results

Volume change estimated with the ALS method

Deriving the high point density geodetic change in volume of the Findelengletscher from ALS DEM differencing resulted in −48.1 million m^3 volume change (−3.66 m average elevation change) between 2005 and 2010 with the 1×1 m raster resolution. All other results are presented here relative to this reference volume change, i.e. negative values indicate an overestimation of glacier thinning compared with the reference change.

Simulating DEMs with a coarser resolution up to 250 m raster cells led to results that randomly differed from the reference volume change, either underestimating or overestimating glacier mean elevation change (up to ±7%). Simulating stochastic uncertainties with the calculated values led to differences up to ±8% in volume change for 250 m raster cells (2 standard deviations, Fig. 3), increasing in an exponential manner. Note that up to a raster cell size of 25 m almost no change took place in comparison to the highest resolution raster. With a running average of 25 m in the x-axis direction (raster size) of the data, it seems the average differences never exceeded ±1.5%, although single values varied considerably.

The result with the low point density DEM showed a small bias of +1.1% (which is the same as with 25 m raster cells) compared with the high

point density DEM, i.e. a slight underestimation of glacier thinning. The accompanying stochastic uncertainties were very small as well (Tables 2 and 3). The elevation difference rasters showed no systematic, i.e. topography-dependent trend in the distribution of the elevation differences.

Volume change estimated with the altimetry profile method

The altimetry profile method resulted in an underestimation of the volume change of 18% (17%) for a 1 m (25 m) sampling distance compared with the reference DEM change. Developing the profile method fitted generally well with the reference DEM differencing method (Fig. 4), but multiple systematic effects were visible. These could, however, be attributed to physical causes. Thinning

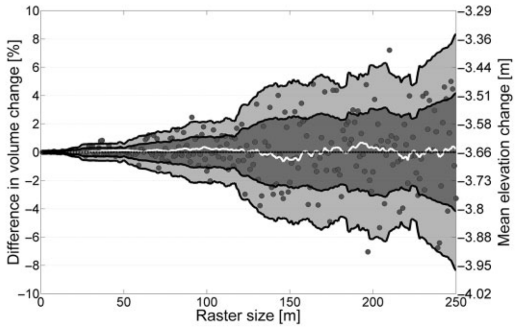

Fig. 3. Relative and absolute differences in the volume change from the ALS reference volume change due to the use of increasing raster cell sizes. Negative percentage values indicate the volume change was overestimated compared with the reference change. Each dot indicates a result that was actually calculated. The white line is the 25 m running average. The dark gray area shows a 25 m running standard deviation, and the light gray two standard deviations.

Table 2. Absolute values (val.) and variances (var.) of different thickness change methods and resolutions in the period 2005–2010.

Method	1 m		25 m		50 m		100 m		200 m	
	Val.	Var.	Val.	Var.	Val.	Var.	Val.	Var.	Val.	Var.
ALS_high	−3.7	±0.0	−3.7	±0.0	−3.7	±0.0	−3.7	±0.0	−3.7	±0.1
ALS_low	−3.6	±0.0	−3.6	±0.0						
ALS_profile	−3.0		−3.0							
CON_area			−3.8	±0.0	−3.8	±0.1	−3.7	±0.4	−3.4	±0.5
CON_dem			−3.6		−3.7		−4.3			

All numbers are in meters with the absolute values representing the average thickness change. The methods and the resolution and variance are explained in Table 4.

Table 3. Mean relative deviations (mean) and variances (var.) from the ALS reference thickness change (REF.) of different methods and resolutions in the period 2005–2010.

Method	1 m		25 m		50 m		100 m		200 m	
	Mean	Var.	Mean	Var.	Mean	Var.	Mean	Var.	Mean	Var.
ALS_high	REF.	±0.1	+0.1	±0.5	+0.2	±0.6	−1.3	±2.1	−1.4	±6.1
ALS_low	+1.1	±0.1	+1.1	±0.3						
ALS_profile	+17.6		+16.7							
CON_area			−2.7		−2.7	±2.3	−0.9	±11.5	+8.2	±14.4
CON_dem			+0.8		−0.5		−18.3			

All numbers are in percent. Negative mean values represent an overestimation of the thickness change compared with the reference change. The methods and the resolution and variance are explained in Table 4.

Table 4. Explanations for Tables 2 and 3. Note that 2 standard deviations enclose 95% of a normal distributed set of measurements.

Method	Description	Meaning of resolution	Meaning of variance
ALS_high	ALS high resolution flights	Side length of raster cell	2 standard deviations
ALS_low	ALS low resolution flights	Side length of raster cell	2 standard deviations
ALS_profile	ALS altimetry profile	Sampling distance	
CON_area	Contour area approach	Contour interval used	Max. deviation from mean
CON_dem	Contours to DEM approach	Contour interval used	

was underestimated in the upper section of the Findelengletscher, which has the largest glacier area per 10 m elevation band. There the accumulation regime is locally dependent on wind erosion and deposition, as well as on the highly inhomogeneous accumulation pattern. In contrast, the altimetry profile method overestimated the volume change at the tongue.

Volume change estimated with the contour line methods

Summing the volume changes using all contours (25 m interval) led to a difference in volume change of –2.7% for the Findelengletscher compared with the reference change (Tables 2 and 3). Note that both contour area change methods produced very similar results, which is why only the result with the Finsterwalder method (1953, 1954) is shown. Both methods overestimated thinning in the five-year period covered, with a decreasing thinning trend for increasing contour intervals (Fig. 5). Intervals smaller than 125 m showed an overestimation of glacier thinning for average values. Using 125 m and larger intervals, the deviation of the average changed its sign to underestimate thinning by up to 8.2%. The results with the 200 m interval varied greatly, with random deviations ranging between –3% and 23%.

Instead of using the area changes between multitemporal contour lines at the same elevation, we used the contours in addition to generate DEMs and subsequently subtracted these surfaces similarly to the ALS DEMs. Using 25 m (50 m, 100 m) contour intervals resulted in a relative volume change difference of 0.8% (–0.5%, –18.3%) compared with the reference change (Tables 2 and 3).

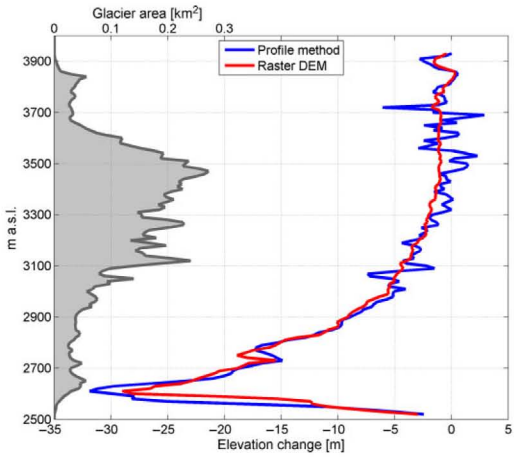

Fig. 4. Local elevation changes from the profile method and from all DEM raster cells for 10 m elevation bands. The gray area to the left is the hypsometry of the Findelengletscher, also shown in 10 m bands.

Discussion

Scaling effects in the ALS volume change

The ALS point measurements were not distributed evenly throughout the study area and hence neither in a single raster cell. Consequently, the mean elevation of a raster cell will be influenced by the irregular distribution of the enclosed points. As the influence of this effect increases with increasing raster cell sizes, we used the 1×1 m raster elevations as the reference for all subsequent

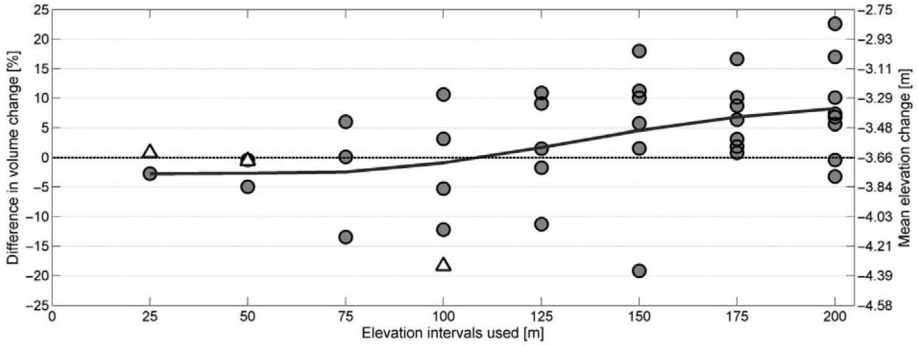

Fig. 5. Relative and absolute differences in the volume change from the ALS reference change due to the use of different contour intervals. Negative percentage values indicate the volume change was overestimated compared with the reference change. Each dot represents a result using the Finsterwalder (1954) approach; the black line is the average of all results per elevation interval. The triangles represent the differences in volume from the reference change of DEMs calculated from the contours.

calculations instead of the ALS point measurements. To fill the resampled (larger) raster cells, linear interpolations were made from the closest raster elevations in the reference raster. This approach therefore simulated high-precision data acquisition at a small location, and provided the elevation values for larger raster cells. Taking the average of all raster cell elevation values within a larger cell would better represent medium resolution DEMs from satellite sensors (i.e. ASTER, SRTM). However, it is presumed that our approach (Fig. 3) leads to larger variation, and thus should still be valid for these situations.

A raster cell size of up to of 25 m was found to be a stable size for measuring volume change in the Findelengletscher. Our results suggest that higher-resolution DEMs would not result in very much improved volume differences. Lowering the resolution to 30 m (Fig. 2e; similar to the ASTER GDEM product; Tachikawa *et al.* 2011) introduced an uncertainty of ±0.5%, while lowering it to 90 m (Fig. 2f; similar to the global SRTM product; Farr *et al.* 2007) produced an uncertainty of ±2%. These results mainly reflect the smaller sampling population as raster pixel size increases since the precision of the estimates remains the same from our resampling strategy in this experiment. Although the exponentially increasing absolute deviations are expected to be valid for different glaciers, the result depends on the geometric shape of the glacier, i.e. the size and hypsometry of the glacier, the surface roughness, the mass balance pattern, and the time interval between two geodetic campaigns. In a test comparing an additional ALS DEM from 2009 (Joerg *et al.* 2012) with the DEM from 2010, the absolute variation remained similar to the five-year study period, whereas the relative variations tripled. With little mass change, be it due to a short acquisition interval or a low annual turnover, the relative uncertainties could thus be large. The geometric shape of a glacier is another major source of uncertainty. The Findelengletscher has an average glacier tongue width of approximately 500 m, which is where the most marked elevation change took place. Here, the relative raster resolution is more important for obtaining an accurate result as edge effects show up more with larger raster sizes. In contrast, in the large accumulation area, a lower raster resolution is unlikely to impair the result much.

The standard deviation increases with raster size, depending on the location of the grid. If the centre of a raster cell is on the edge of the glacier, the elevation change for the entire raster area is represented by the centre value, even though there would be no elevation change in a large part of the cell. Depending on the number and the location of such occurrences, the calculated elevation change varies, sometimes strongly, with raster resolution. As we were using a raster increment of just 1 m per calculation step, a deviation resulting from a running average/standard deviation serves as an indicator of variability (Fig. 3); two standard deviations are regarded as a reliable boundary for more extreme values. With increasing raster sizes, a single measurement could therefore be an extreme deviation from the actual value only because of the location of the raster grid.

The underestimation of glacier thinning with systematically higher raster elevations of the lower point density data (cf. Tables 2 and 3) could be an effect of scale due to the interpolation of data voids into a 1×1 m grid, and the resulting smoothing of the glacier's surface. Another explanation could be that the extrapolation of the volume change into the unmeasured area introduced a bias. No clear spatially systematic vertical shift was detected qualitatively between the high and low point density DEMs from 2010. In addition, a systematic horizontal DEM shift would lead to a hill-shading effect, showing the topography in the DEM difference plot (Nuth and Kääb 2011), but no such effect was found either.

Assessment of the profile method

The altimetry profile method considerably underestimated glacier thinning. It can, however, map surface changes in a large number of glaciers more cheaply than the airborne laser scanning method, but the resulting extrapolated volume change differs considerably from that for the entire raster DEM. Unexpectedly, the largest part of the error does not appear to originate from the overestimation of the elevation change at the tongue (cf. Arendt *et al.* 2002; Berthier *et al.* 2010), but rather from the underestimation of the elevation change in the large accumulation area. This underestimation is probably connected with the complex accumulation patterns in the area caused by local wind erosion and deposition, as well as the movement of crevasses, which lead to variation in the local elevation changes. Overall, the reproduction of the glacier-wide change trend is quite accurate, possibly because the melt pattern of the

Findelengletscher is relatively simple. The almost debris-free westerly exposed glacier tongue has an exposition-dependent melt pattern, with stronger melting in the more southerly exposed ice and less melting to the north. The centreline therefore roughly represents the average melt on the tongue, although the influence of the restricted possible melt on the edge of the tongue is less prominent at the centreline and is expected to be relatively smaller in the five-year study period than it would be over a longer time span.

Scaling effects with the contour method

The geometrical-analytical contour approach resulted in values 2.7% more negative compared with those in the reference change when all 25 m contours were used. This is a very accurate result in comparison with that obtained with the high point density multi-temporal raster DEMs. Using contour intervals larger than 75 m resulted in our case in deviations of mean elevation change by up to ±10% compared with the reference change. The average of all groups of contours available shows a systematic decrease in glacier thinning with increasing contour intervals. This is due to the fact that the glacier's tongue is increasingly undersampled compared with the number of contours in the large accumulation area, which is changing less rapidly. The most melt took place in the lowest part of the glacier tongue. However, in our simulation and dependent on the slope of the glacier, the first 200 m contour set does not start until 200 m above the glacier's terminus, thus missing the areas where the most melt occurs and consequently underestimating the overall melt.

In historical maps, the positions of the map's contours on glacier and snow surfaces and in high mountain topography may contain large errors because of the difficulty of mapping such areas. The accumulation areas were sometimes inaccessible for surveyors on the ground, making it impossible for them to conduct high-accuracy campaigns on glacier surfaces. As a result, older volume change measurements may be very inaccurate. Later aerial images became available and were used to calculate elevations photogrammetrically. However, snow in the accumulation area often resulted in little image texture, and shadowing effects also made it difficult to position the contour lines accurately in the derived maps. Our simulation showed that the method to derive the volume change seemed in itself to be accurate nevertheless for contour lines with small elevation intervals independent of the quality of the contour line positions. With larger contour intervals, however, systematic errors could be larger.

The second approach for generating DEMs from contours resulted in volume changes similar to the ALS DEMs when using 25 m and 50 m contour intervals. The DEMs generated from two 100 m contour datasets were not able to reproduce the volume change in the Findelengletscher sufficiently well, and overestimated glacier thinning by 18%. In this case, the horizontal distance between two contour lines is too large to reproduce the smaller scale glacier changes. However, with the two shorter contour intervals, the DEM differencing method outperformed the geometrical-analytical methods not only in terms of accuracy, but also in the time needed to calculate the results. DEM differencing is therefore the method of choice.

Conclusions

We used multi-temporal high-resolution ALS data from 2005 and 2010 to evaluate standard methods for measuring volumetric change in a glacier, using the Findelengletscher as an example as it is a typical valley glacier in the Swiss Alps. Two high-resolution DEMs from ALS with an average point density of up to 14 laser returns per square meter served as the reference dataset. We compared the estimates of glacier volume change obtained with these datasets with the results from an economically optimized high-altitude ALS over-flight with reduced point density, and various datasets analyzed with different volumetric change assessment methods and on different spatial scales.

Using less expensive settings, i.e. high-altitude, large scan angles, and low pulse repetition frequency, introduced a small bias (1.1%), which can be corrected by co-registration of non-glacierized terrain. Nonetheless, it was still possible to maintain both the horizontal accuracy and the very small volume change uncertainty (<1%). The optimized ALS setup reduced the survey effort by 90%, but still provides a point density of 0.4 laser returns per square meter, which is sufficient for accurately assessing glacier volume changes.

Most current glacier volume change studies are based on DEM differencing at various spatial resolutions. Simulating the scaling effect of different raster resolutions from 1 × 1 m (reference ALS) to

250 × 250 m did not result in any volume change bias, but in an exponential increase in the random error. The corresponding uncertainty was well below 1% for a resolution of 25 × 25 m, but increased to 2% (6%) for a pixel size of 100 m (200 m).

If photogrammetric plotters or topographic maps are used, elevation contour lines have to be relied on in assessing glacier volume changes. Older analytical methods using geometric approaches can be very laborious, but results for contour line intervals up to 50 m are reasonable, with a small negative bias of 3%. However, for contour line intervals larger than 100 m, we found a positive trend in the bias (up to +8% for 200 m intervals) as it does not cover the very variable glacier tongue, and a random error of ±14%. GIS-based interpolation (based on the ANUDEM algorithm) produced similar results, with even stronger biases for contour line intervals >50 m, but it is much more efficient.

Studies based on laser altimetry typically assess the glacier elevation changes along central profile lines. We found strong local biases with opposite signs: negative on the glacier tongue, probably due to its limited lateral ice thickness, and both positive and negative in the accumulation area, probably according to whether the profile line covered deposition (positive) or erosion (negative). The overall bias was quite large (18%), and its (positive) sign depended both on the location of the profile and on the glacier hypsometry.

Overall, we can confirm that ALS DEM differencing is currently the fastest and most accurate method to derive glacier volume changes and scaling issues have a limited impact up to a spatial resolution of 50 m. Other methods, e.g. contour method with intervals larger than 50 m and profile method, can introduce systematic and random errors.

Acknowledgements

We are grateful to Wilfried Haeberli and Michael Schaepman for their valuable support with this project. Many thanks to Christopher Nuth and an anonymous reviewer for their constructive comments which helped to improve the manuscript considerably, and to Silvia Dingwall for polishing the English. We thank BSF Swissphoto for the acquisition of the ALS data and their continuous support. This project was supported by the Swiss energy utility Axpo.

Philip Claudio Joerg and Michael Zemp, Department of Geography, University of Zurich, Winterthurerstrasse 190, CH-8057 Zurich, Switzerland
E-mail: philip.joerg@geo.uzh.ch;
michael.zemp@geo.uzh.ch

References

Arendt, A.A., Echelmeyer, K.A., Harrison, W.D., Lingle, C.S. and Valentine, V.B., 2002. Rapid wastage of Alaska glaciers and their contribution to rising sea level. *Science*, 297, 382–386. doi: 10.1126/science.1072497

Berthier, E., Schiefer, E., Clarke, G.K.C., Menounos, B. and Rémy, F., 2010. Contribution of Alaskan glaciers to sea-level rise derived from satellite imagery. *Nature Geoscience*, 3, 92–95. doi: 10.1038/ngeo737

Cogley, J.G., 2009. Geodetic and direct mass-balance measurements: Comparison and joint analysis. *Annals of Glaciology*, 50, 96–100. doi: 10.3189/172756409787769744

Farr, T.G., Rosen, P.A., Caro, E., Crippen, R., Duren, R., Hensley, S., Kobrick, M., Paller, M., Rodriguez, E., Roth, L., Seal, D., Shaffer, S., Shimada, J., Umland, J., Werner, M., Oskin, M., Burbank, D. and Alsdorf, D.E., 2007. The shuttle radar topography mission. *Reviews of Geophysics*, 45. doi: 10.1029/2005RG000183

Finsterwalder, R., 1953. Die zahlenmässige Erfassung des Gletscherrückgangs an Ostalpengletschern. *Zeitschrift für Gletscherkunde und Glazialgeologie*, 2, 189–239.

Finsterwalder, R., 1954. Photogrammetry and glacier research with special reference to glacier retreat in the Eastern Alps. *Journal of Glaciology*, 2, 306–315.

Finsterwalder, S., 1897. Der Vernagtferner. *Wissenschaftliche Ergänzungshefte zur Zeitschrift des Deutschen und Österreichischen Alpenvereins*, 1, 1–96.

Hofmann, W., 1958. Der Vorstoss des Nisqually-Gletschers am Mt. Rainier, U.S.A., von 1952 bis 1956. *Zeitschrift für Gletscherkunde und Glazialgeologie*, 4, 47–60.

Hutchinson, M.F., 1989. A new procedure for gridding elevation and stream line data with automatic removal of spurious pits. *Journal of Hydrology*, 106, 211–232.

Joerg, P.C., Morsdorf, F. and Zemp, M., 2012. Uncertainty assessment of multi-temporal airborne laser scanning data: A case study on an Alpine glacier. *Remote Sensing of Environment*, 127, 118–129. doi: 10.1016/j.rse.2012.08.012

Mercanton, P.L., 1916. Vermessungen am Rhonegletscher/ Mensuration au glacier du Rhone: 1874–1915. *Neue Denkschrift der Schweizerischen Naturforschenden Gesellschaft*, 52, 189.

Nuth, C. and Kääb, A., 2011. Co-registration and bias corrections of satellite elevation data sets for quantifying glacier thickness change. *The Cryosphere*, 5, 271–290. doi: 10.5194/tc-5-271-2011

Oberli, A., 1979. Dufour-Karte und Siegfried-Atlas. In: *Unsere Landeskarten*. Schweizerischer Alpen-Club in cooperation with the Federal Office of Topography, Berne. 72 p.

PSFG, 1967. *Fluctuations of Glaciers 1959–65*. Permanent Service on Fluctuations of Glaciers, Zurich, Switzerland.

Racoviteanu, A.E., Manley, W.F., Arnaud, Y. and Williams, M.W., 2007. Evaluating digital elevation models for glaciologic applications: an example from Nevado Coro-

puna, Peruvian Andes. *Global and Planetary Change*, 59, 110–125. doi: 10.1016/j.gloplacha.2006.11.036

Reinhardt, W. and Rentsch, H., 1986. Determination of changes in volume and elevation of glaciers using digital elevation models for the Vernagtferner, Ötztal Alps, Austria. *Annals of Glaciology*, 8, 151–155.

Reinwarth, O., 1973. *Maps of Vernagtferner 1889–1969 (3 sheets)*. Permanent Service on Fluctuations of Glaciers, Zurich, Switzerland.

Rivera, A. and Casassa, G., 1999. Volume changes on Pio XI glacier, Patagonia: 1975–1995. *Global and Planetary Change*, 22, 233–244. doi: 10.1016/S0921-8181(99)00040-5

Sold, L., Huss, M., Hoelzle, M., Andereggen, H., Joerg, P.C. and Zemp, M., 2013. Methodological approaches to infer end-of-winter snow distribution on alpine glaciers. *Journal of Glaciology*, 59, 1047–1059. doi: 10.3189/2013JoG13J015

Tachikawa, T., Hato, M., Kaku, M. and Iwasaki, A., 2011. Characteristics of ASTER GDEM version 2. Vancouver, BC. 3657–3660 .

VAW/ETHZ, 1967. *Map of Aletsch Glacier (Aletschgletscher)*. Permanent Service on Fluctuations of Glaciers, Zurich, Switzerland.

Vignon, F., Arnaud, Y. and Kaser, G., 2003. Quantification of glacier volume change using topographic and ASTER DEMs: a case study in the Cordillera Blanca. 2003 IGARSS: Learning From Earth's Shapes and Colours, Toulouse, France. 2605–2607.

WGMS, 2008. *Global Glacier Changes: Facts and Figures*. UNEP, World Glacier Monitoring Service, Zurich, Switzerland.

WGMS, 2012. *Fluctuations of Glaciers 2005–2010*. ICSU(WDS)/IUGG(IACS)/UNEP/UNESCO/WMO, World Glacier Monitoring Service, Zurich, Switzerland. Publication based on database version: doi: 10.5904/wgms-fog-2012-11

Zemp, M., Hoelzle, M. and Haeberli, W., 2009. Six decades of glacier mass-balance observations: A review of the worldwide monitoring network. *Annals of Glaciology*, 50, 101–111. doi: 10.3189/172756409787769591

Zemp, M., Thibert, E., Huss, M., Stumm, D., Rolstad Denby, C., Nuth, C., Nussbaumer, S.U., Moholdt, G., Mercer, A., Mayer, C., Joerg, P.C., Jansson, P., Hynek, B., Fischer, A., Escher-Vetter, H., Elvehøy, H. and Andreassen, L.M., 2013. Reanalysing glacier mass balance measurement series. *The Cryosphere*, 7, 1227–1245. doi: 10.5194/tc-7-1227-2013

Manuscript received 5 Jul., 2013; revised and accepted 5 Dec., 2013

4 METHODOLOGICAL APPROACHES TO INFER END-OF-WINTER SNOW DISTRIBUTION ON ALPINE GLACIERS

This chapter was published as: Sold, L., Huss, M., Hoelzle, M., Joerg, P.C., & Zemp, M. (2013). Methodological approaches to inferring end-of-winter snow distribution on alpine glaciers. *Journal of Glaciology*, *59*, 1047-1059. Reprint with permission of the International Glaciological Society.

The contribution of P. Joerg to this article was the airborne laser scanning data preparation and analysis, as well as contributions to the manuscript, tables and figures by discussions and revisions.

Methodological approaches to infer end-of-winter snow distribution on alpine glaciers

Leo SOLD,[1*] Matthias HUSS,[1] Martin HOELZLE,[1] Hubert ANDEREGGEN,[2] Philip C. JOERG,[3] Michael ZEMP[3]

[1]*Department of Geosciences, University of Fribourg, Fribourg, Switzerland*
E-mail: leo.sold@unifr.ch
[2]*Airborne Scan AG, Visp, Switzerland*
[3]*Department of Geography, University of Zürich, Zürich, Switzerland*

ABSTRACT. Snow accumulation is an important component of the mass balance of alpine glaciers. To improve our understanding of the processes related to accumulation and their representation in state-of-the-art mass-balance models, extensive field measurements are required. We present measurements of snow accumulation distribution on Findelengletscher, Switzerland, for April 2010 using (1) in situ snow probings, (2) airborne ground-penetrating radar (GPR) and (3) differencing of two airborne light detection and ranging (lidar) digital elevation models (DEMs). Calculating high-resolution snow depth from DEM-differencing requires careful correction for vertical ice-flow velocity and densification in the accumulation area. All three methods reveal a general increase in snow depth with elevation, but also a significant small-scale spatial variability. Lidar-differencing and in situ snow probings show good agreement for the mean specific winter balance (0.72 and 0.78 m w.e., respectively). The lidar-derived distributed snow depth reveals significant zonal correlations with elevation, slope and curvature in a multiple linear regression model. Unlike lidar-differencing, GPR-derived snow depth is not affected by glacier dynamics or firn compaction, but to a smaller degree by snow density and liquid water content. It is thus a valuable independent data source for validation. The simultaneous availability of the three datasets facilitates the comparison of the methods and contributes to a better understanding of processes that govern winter accumulation distribution on alpine glaciers.

INTRODUCTION

Temporal changes in glacier mass balance are known to be an excellent indicator for changing climatic conditions (Haeberli and Beniston, 1998; Kaser and others, 2006; Solomon and others, 2007). The impacts of future changes in climate forcing on mass balance and runoff from glacierized catchments are the subject of intense research (e.g. Huss, 2011; Farinotti and others, 2012; Salzmann and others, 2012). Models are used to assess these impacts and provide general conclusions from a small subset of monitored glaciers (Zemp and others, 2009).

Presently, there is a wide range of mass-balance models available that cover ablation processes to all degrees of complexity (Hock, 2005, and references therein). To compute annual glacier mass balance all models need, aside from the ablation processes, to account for the amount and spatial distribution of snow accumulation. Typically, accumulation is estimated from precipitation measurements at nearby weather stations, gridded precipitation climatologies or climate model outputs that are tuned to site characteristics, usually by applying an elevation gradient and temperature threshold for snowfall (Hock, 1999; Machguth and others, 2006a, 2009). However, this is a weak representation of the actual snow accumulation pattern. Aside from avalanches, the interplay of topography and wind leads to strong variations in the spatial distribution of snow depth (Liston and Sturm, 1998; Winstral and Marks, 2002; Machguth and others, 2006b; Lehning and others, 2008; Dadic and others, 2010a). Due to the complexity of the physical modelling of preferential snow deposition and redistribution processes, and due to the difficulties inherent in the measurement of solid precipitation in high-alpine terrain, the accumulation part of state-of-the-art mass-balance models is much less developed than the description of melting processes (e.g. Dadic and others, 2010a). Improving the level of understanding with regard to the accumulation of snow on alpine glaciers is a prerequisite for strengthening the physical justification of the accumulation modules of mass-balance models (Machguth and others, 2006b). To date, only a few studies have tackled this issue by providing the necessary extensive end-of-winter snow depth distribution measurements (Machguth and others, 2006b; Dadic and others, 2010a,b). However, evaluating the accuracy of the estimated spatial distribution requires separate reference data to be available.

The spatial distribution of snow depth is commonly measured by time-consuming in situ probings that provide point values and can have large uncertainties in accumulation zones where locating the previous summer surface can be challenging. Other possible approaches are ground-penetrating radar (GPR) and differencing of digital elevation models (DEMs). GPR provides a non-destructive method for various purposes in glaciology. This is supported by the low conductivity and, hence, the deep penetration of the signal into snow and ice at MHz frequencies. The signal is reflected from boundaries with a contrast in dielectric permittivity that can be related to a change in material properties (e.g. from ice to bedrock, variations in density, impurities such as dust

*Present address: Department of Geosciences, Geography Unit, University of Fribourg, Fribourg, Switzerland.

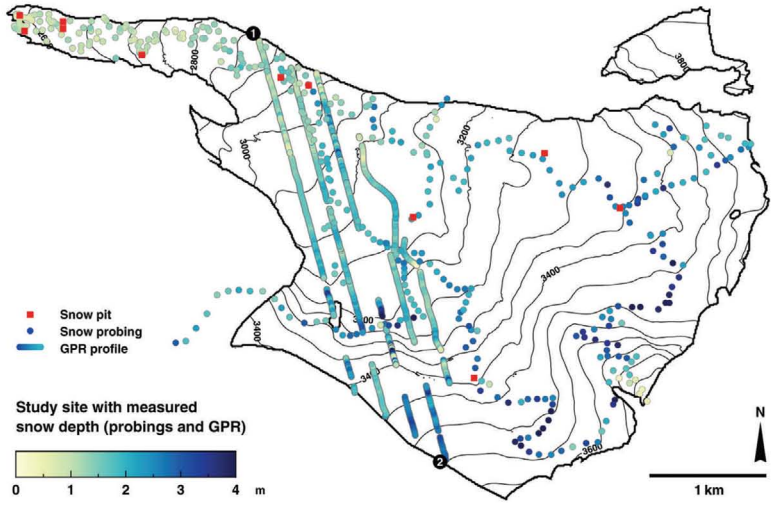

Fig. 1. Map of the study site: Findelengletscher, Valais, Switzerland. Dots show manual snow probings, lines represent GPR profiles, the colour code shows measured snow depth in April 2010.

or ash, or water content (Ulriksen, 1982; Plewes and Hubbard, 2001)). Since the 1960s this has been used for ground-based or airborne detection of ice thickness (Robin and others, 1969; Bauder and others, 2003; Damm, 2004; Lalumiere and Prinsenberg, 2009) or internal layers within snow and firn (Kohler and others, 1997; Kanagaratnam and others, 2004; Dunse and others, 2009; Heilig and others, 2010). Radar-based surveys of snow accumulation distribution have focused on ice sheets (Helm and others, 2007; Dunse and others, 2008; Eisen and others, 2008; Kruetzmann and others, 2011) and snow on the ground (Marchand and others, 2003; Yankielun and others, 2004; Marshall and Koh, 2008). For mapping snow accumulation on alpine glaciers, however, the airborne application of GPR has only been addressed by Machguth and others (2006b), although results show that it can be a highly effective tool, especially in remote and inaccessible areas.

More attention has been paid to the use of DEM-differencing to assess changes in glacier mass balance (Arendt and others, 2002; Bamber and Rivera, 2007; Abermann and others, 2010; Kääb and others, 2012). Light detection and ranging (lidar) scanning systems offer a high-precision tool for range measurements, that has been applied for ~20 years. The travel time of a laser pulse from emission until reflection from a target and return to a detector, coupled with the speed of light in the air conditions, provides a measure for the distance between the sensor and the illuminated spot. In airborne applications, the exact position and orientation of the aircraft are necessary to locate the ground points, which are then interpolated to the regular grid of a DEM (Ackermann, 1999; Wehr and Lohr, 1999). In our study, repeated lidar DEMs of Findelengletscher, Switzerland (Joerg and others, 2012), provide spatially distributed elevation changes between autumn and spring. To obtain distributed snow depth over glaciated surfaces, this requires corrections of the vertical ice velocity and firn compaction in the surface differencing scheme. Such corrections have not been realized so far, although studies indicate their need (Dadic and others, 2010a,b; Helfricht and others, 2012, 2013).

In this study we discuss simultaneous measurements of snow accumulation distribution on an alpine valley glacier, using the traditional glaciological approach of in situ snow probings and snow density pits, helicopter-borne GPR measurements of the snow depth and surface elevation changes given by differencing of two lidar DEMs. Snow probings and DEM-differencing provide the winter mass balance of Findelengletscher. Furthermore, we show how the geodetically derived snow depth distribution can be corrected for the vertical ice velocity and firn compaction, based on the in situ probings and long-term mass-balance and geometry changes. The result is a fully distributed dataset that is validated with the GPR measurements and correlated against elevation, surface slope and curvature. Analysis of the three datasets provides new insights into the ability of the utilized methods to correctly represent snow depth, and contributes to a better understanding of processes that govern winter accumulation of alpine glaciers.

STUDY SITE AND FIELD DATA

Findelengletscher is a large temperate valley glacier (13.0 km^2) in Valais, Switzerland. It is northwesterly exposed and covers an elevation range from 2600 to 3900 m a.s.l. (Fig. 1). Situated directly below the main ridge, local precipitation largely depends on the wind direction. The accumulation area strongly benefits from south- and south-easterly conditions. A glacier mass-balance monitoring programme was started in 2004 (Machguth, 2008). Annual mass balance is determined with a network of 13 ablation stakes and two snow density pits. On average, the measurements indicate a negative mass balance (Joerg and others, 2012), leading to a continued retreat of the glacier snout (Glaciological Reports, 2011). Glaciological measurements of seasonal mass balance from snow probings and density profiles combined with repeated terrestrial snowline photographs are available from 2009 (Huss and others, 2013).

The conventional method of vertically probing the underlying ice (or last summer) surface through the snowpack provides a direct measurement of snow depth as a

point value (Østrem and Brugman, 1991). The probe measurements were carried out on 10–11 April 2010. For practical reasons, they were taken along the walking paths leading from the upper accumulation area to the tongue of Findelengletscher (Fig. 1). In its accumulation area the boundary between snow and firn is typically made up of a clearly defined ice lens of variable thickness, that often can be unambiguously detected with a probe. However, careful probing is necessary to avoid misinterpretation of internal ice layers within the snow cover. The entire glacier elevation range was covered by 403 probings (Fig. 2), each of which was made up of two to five averaged probings to account for outliers (crevasses) and small-scale variability. Mean snow depth from all probings was 1.86 m, and the standard deviation within multiple measurements at a given location was 0.13 m. The measured snow depth was elevation-dependent but highly variable (Fig. 2).

Additionally, the bulk density of a snow column was measured in 11 snow pits across the glacier. Values ranged from 223 to 294 kg m^{-3} on the glacier tongue to 407 kg m^{-3} at the centre of the glacier (3130 m a.s.l.). This probably represents (1) different process regimes in snowpack evolution, involving wind effects on initial deposition, erosion and redeposition of snow and/or (2) differences in the prevalent processes of snow metamorphism. While the internal vertical variability of the snow density was not covered by the sampling scheme, multiple bulk measurements were taken at ten of the snow pits. Standard deviation within measurements at these locations was 21 kg m^{-3}. Density was averaged over 100 m elevation bands. For bands that were not covered by at least one measurement, the average of neighbouring bands was used. Weighting density according to the area of the respective elevation bands revealed a spatial mean snow density of 362 kg m^{-3}. To follow the ongoing monitoring programme of seasonal mass balance of Findelengletscher we applied an enhanced traditional extrapolation scheme to the snow probings, to obtain snow depth on a 25 m × 25 m resolution grid. It is based on a distance-weighted average of probings within a radius of 400 m around each gridpoint. If fewer than three measurements were available, the search radius was increased. Additionally, we superimposed small-scale snow depth variability due to local effects that might not be captured by the spatially discontinuous probings. According to a procedure described by Huss and others (2008), snow depths were decreased over steep slopes (>40°) and convex terrain shapes, whereas they were increased for concave surfaces. These corrections are relatively small for the central parts of the glacier, but are important to yield realistic snow depths for regions prone to avalanching and wind erosion.

The GPR system was a Noggin 500 (Sensors & Software Inc., Canada) that operated a shielded antenna with a centre frequency of 500 MHz. It was directly mounted on the bottom of a helicopter. Traces were recorded with a constant time increment of 0.1 s at a waveform sampling interval of 0.2 ns. Their position was provided by a synchronized GPS with a horizontal accuracy of 1–5 m. On 10–11 April, ~12 000 traces were recorded with the helicopter flying at ~10 m s^{-1} and 5–10 m above ground. The angle of beam spread is 45° and 60° perpendicular and along the flight direction, respectively. Hence, the footprint size at the snow surface is less than 8 m × 12 m. The survey covered 12.7 km of linear tracks in ten profiles between 2900 and 3550 m a.s.l. across the glacier (Fig. 1). In an airborne

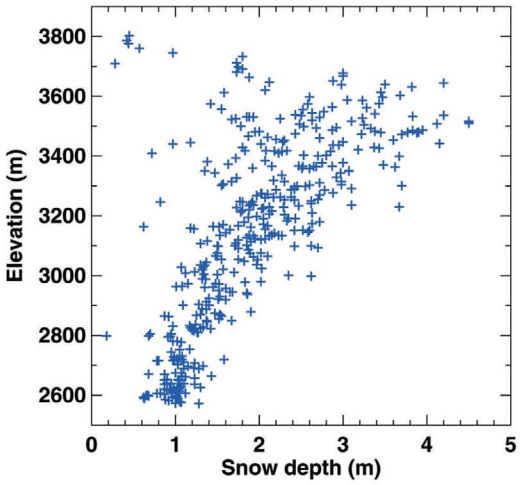

Fig. 2. Measured snow depth from 403 probings in April 2010.

application of the GPR system the risk of interference with other essential and safety-of-life radio services is high. A special licence for the campaign was granted by the Swiss telecommunication regulator (OFCOM).

Lidar surveys were carried out on 4 October 2009, while the ablation area of Findelengletscher (<3200 m a.s.l.) was snow-free, and on 10 April 2010 at the end of the accumulation season. The Optech ALTM 3100 scanning system was mounted to a Pilatus Porter fixed-wing aircraft equipped with differential GPS and an inertial measurement unit to derive its position and orientation. Average point density was 7.6 and 8.1 m^{-2}, respectively. Joerg and others (2012) describe the geo-referencing, point cloud interpolation and generation of the grid (1 m × 1 m cell size) in further detail and provide an extensive uncertainty assessment. Standard deviation on reference surfaces was 0.09 m (October 2009) and 0.19 m (April 2010, reference surfaces snow-covered). Additionally, longer-term geometry change is given by two lidar DEMs from similar surveys on 28–29 October 2005 and 29 September 2010.

METHODS

Processing of GPR data

Many processing techniques for GPR data have been adopted from seismic reflection surveys that have a similar principle (Davis and Annan, 1989; Fisher and others, 1996). Since the selection of processing steps and their parameter settings depend strongly on field conditions, survey design and intention, no universal procedure is available (Ulriksen, 1982; Fisher and others, 1996; Annan, 1999). In the given order, the following processing steps were found to sufficiently improve the helicopter-borne GPR data quality:

1. Spatial interpolation; correction for variations in the helicopter's velocity. Traces were interpolated linearly to an equidistant spacing of 1 m.
2. Frequency bandpass 300–1000 MHz; the high-pass filter removed bending and constant offset of the signal while the low-pass filter removed high-frequency speckle and noise (Jol, 2009).

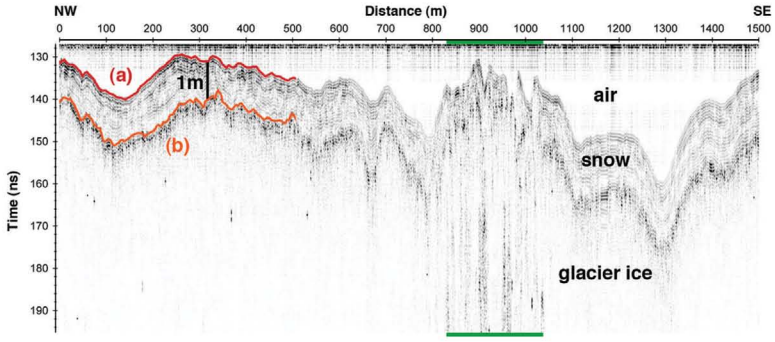

Fig. 3. First 1500 m of GPR profile 1 which lie in the ablation area (Fig. 1) after processing. (a) The reflection of the interface between air and snow. (b) The reflection of the interface between snow and glacier ice. The green markers indicate a crevassed area in the centre of the glacier.

3. Background removal; subtracting the average over the distance domain from all traces in the profile reduced the effects of signal ringing and the airwave.
4. Gain function, linear and exponential; to account for signal attenuation with depth.

Migration did not improve the data quality and was not applied. For all measured radar profiles these processing steps allowed the the air/snow interface and the snow/firn or snow/ice interface to be distinguished without the help of separate snow depth data (Fig. 3). The reflectors were marked in the processing software (Reflexw, Sandmeier Scientific Software) either manually or semi-automatically with a built-in phase-following tool. To convert the difference in two-way travel time between the two marked reflectors from the time to the depth domain, an assumption for the radar wave velocity is required. Density and liquid water content strongly affect the dielectric properties of snow and several empirical formulas exist to compute the permittivity (Kovacs and others, 1993; Frolov and Macheret, 1999). According to Frolov and Macheret (1999), we obtained the relative permittivity, $\varepsilon'_{\mathrm{d}}$, of dry snow from the mean measured density, $\rho = 362\,\mathrm{kg\,m^{-3}}$, as

$$\varepsilon'_{\mathrm{d}} = (1 + 0.857\rho)^2. \quad (1)$$

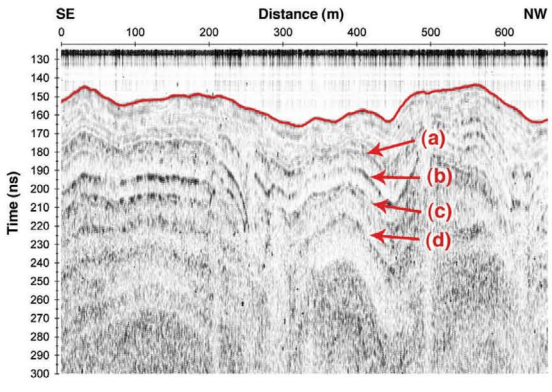

Fig. 4. GPR profile 2 which lies in the accumulation area (Fig. 1), after processing with reflectors of the snow surface (marked) and (a–d) annual summer surfaces.

The mean radar wave velocity, u, was then computed as $u = c \cdot (\varepsilon'_{\mathrm{d}})^{-0.5} = 0.229\,\mathrm{m\,ns^{-1}}$. This constant value was used to derive snow depth from the reflectors in the GPR profiles. However, uncertainties and variations in snow density directly affect u and, therefore, the conversion from travel time to snow depth. Further, we assume that the snowpack was dry. This is in line with observations during fieldwork, except for the glacier tongue that was not covered by GPR profiles. An analysis of the related errors is given in the Discussion.

The 500 MHz antenna also resolved some internal layering of the snowpack. In the accumulation area of Findelengletscher, several firn layers from previous years could be distinguished (Fig. 4). While the 2009 surface could still be determined consistently, the successive dating of the earlier summer surfaces remained speculative. The penetration depth of the GPR signal depends on the height of the helicopter above ground and the physical properties of the subsurface. In the accumulation area we found reflections from down to 20 m below the snow surface.

Geodetic elevation change from lidar DEMs

In a first-order approach, the elevation change of each gridcell was interpreted as snow accumulation (Grünewald and others, 2010; Egli and others, 2012; Helfricht and others, 2012). The resulting pattern of maximal snow depths on the glacier tongue and small snow depths in the accumulation area (Fig. 5) was, however, inconsistent with in situ snow probings that revealed increasing snow depth with elevation (Fig. 2). The principle of comparing two DEMs of different dates makes this approach sensitive to secondary processes that alter the glacier surface elevation. This involves (1) the vertical displacement of the ice surface as part of the glacier flow, hereafter referred to as the emergence velocity, which is positive (emergence) in the ablation area and negative (submergence) in the accumulation area, (2) surface lowering due to firn compaction in the accumulation area and (3) surface lowering from melt after the acquisition of the October 2009 DEM. The formation of superimposed ice on the summer surface is assumed to be negligible in our case, due to the temperate nature of Findelengletscher.

The ice emergence velocity affects the measured surface elevation change as the glacier moves during the time-span between the two generated DEMs (Helfricht and others,

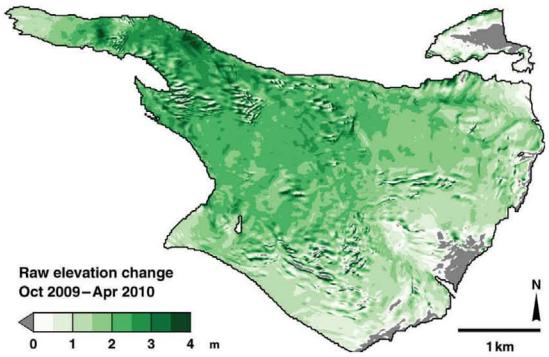

Fig. 5. Raw lidar-derived elevation change from October 2009 to April 2010. Grey shading indicates negative values.

2012, 2013). For a glacier that is in balance with climatological and all other forcings, this vertical component of glacier flow is equal to the reversed local annual mass-balance rate, $-b_a$, divided by the density of ice, ρ_{ice}. In the accumulation area, the compaction of firn, v_{firn}, adds to the glacier surface elevation change. A potential imbalance of mass balance and ice flow can be accounted for with the observed annual geometry changes, Δz. The annual vertical displacement, v_z, of the last summer surface is derived for fixed points, (x, y), on the glacier surface. Thus, it is not affected by horizontal flow and slope (Cuffey and Paterson, 2010) and can be written as

$$v_z = v_z(x, y) = \Delta z - \frac{b_a}{\rho_{ice}} + v_{firn}, \quad (2)$$

where positive values point upwards (emergence), and negative values indicate a lowering of the surface (submergence). Over the cycle of one hydrological year and integrated over the whole firn column, one annual accumulation layer is transformed from snow to ice. At the top of the firn column this results in a surface lowering of

$$v_{firn} = b_a \cdot (\rho_0^{-1} - \rho_{ice}^{-1}), \quad (3)$$

with ρ_0 as the initial firn density. Equations (2) and (3) can be combined to give

$$v_z = \Delta z - \frac{b_a}{\rho}, \quad (4)$$

with $\rho = \rho_{ice}$ in the ablation area and $\rho = \rho_0$ in the accumulation area. For the initial firn density we set $\rho_0 = 550\,\mathrm{kg\,m^{-3}}$ as an average from repeated measurements in previous years. Density of glacier ice was set to $\rho_{ice} = 900\,\mathrm{kg\,m^{-3}}$.

The annual mass balance of every cell of a 25 m × 25 m resolution grid for the hydrological years 2005/06 to 2009/10 was evaluated using a distributed accumulation and melt model (Huss and others, 2009), that was tuned to the in situ mass-balance measurements of each year individually. In this model, the spatial variations in annual mass balance for unmeasured regions of the glacier are given by a description of physical processes (Fig. 6a). The geodetic geometry change was available for the same period from differencing of two lidar DEMs. By annually averaging the mass balance and geometry changes for all years of the geodetic survey, $\overline{b_a}$ and $\overline{\Delta z}$ were obtained. The spatially integrated estimation of the emergence velocity is equal to

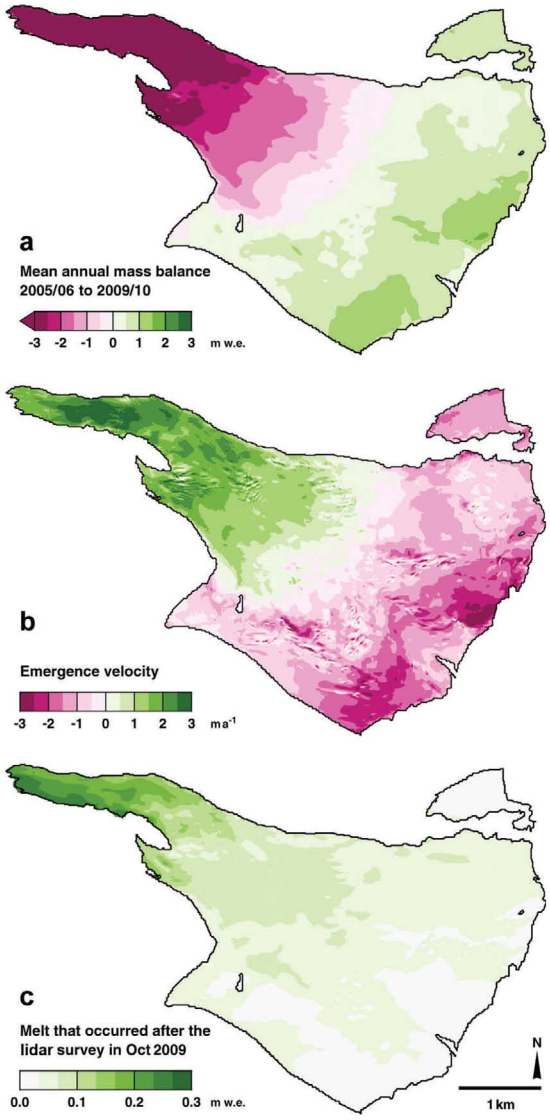

Fig. 6. (a) Mean annual mass balance 2005/06 to 2009/10. (b) Vertical component of ice flow (emergence velocity), derived from the mean annual mass balance and observed geometry changes. A positive velocity is directed upwards (emergence). (c) Modelled melt that occurred after the lidar DEM was generated in October 2009.

zero when the effect from firn compaction is omitted (Fig. 6b). This is a result of the cumulative annual mass balance, b_a, corresponding to the geodetic mass change, Δz, in Eqn (2). This estimation refers to the displacement of the summer surface, so a spatial average different from zero would imply a glacier volume change due to ice flow.

Because the time-step from October 2009 to April 2010 corresponds to a fraction rather than a full year, the annual average emergence velocity must be scaled to fit this time-span. However, the choice of this scaling must integrate temporal variations of the respective processes. Changes in the glacial drainage system affect ice-flow characteristics and are known to show seasonality (Iken and Truffer, 1997).

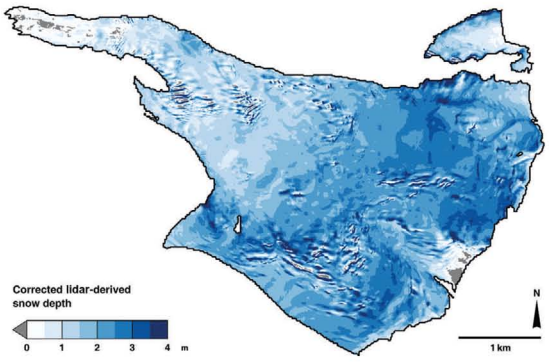

Fig. 7. Snow depth derived from lidar DEMs corrected for emergence velocity, firn compaction and autumn melt (Eqn (5)). Grey shading indicates negative values.

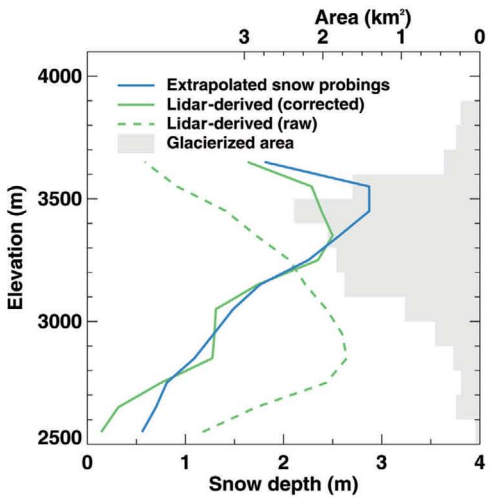

Fig. 8. Vertical distribution of mean snow depth in 100 m elevation bands derived from extrapolated snow probings, raw lidar-differencing and lidar-differencing corrected for emergence velocity, firn compaction and autumn melt (Eqn (5)). The distribution of the glaciated area is shown in grey.

Furthermore, the densification of firn depends on its temperature and the accumulation in subsequent years. Thus, we introduced a tuning factor, $f = 0.795$, to account for seasonal and annual variations in ice-flow velocity and firn compaction rates. This factor f was derived by minimizing the square error of the resulting snow depth to the in situ snow probings (see Discussion).

The melt occurring after the lidar survey in October 2009 was estimated using a distributed temperature-index model (Hock, 1999; Huss and others, 2009). The model was driven by daily temperature and precipitation obtained from a weather station at Zermatt (6 km distance from the glacier tongue, 1638 m a.s.l.). The resulting cumulative melt, m (m ice eq.), was added to the difference, Δh, of the two lidar DEMs in October and April. On the glacier tongue it had the highest impact of up to 0.3 m (Fig. 6c). Together with the scaled correction for emergence velocity and firn compaction, v_z, this provides a corrected snow depth, d, (Fig. 7) as

$$d = \Delta h + m - f \cdot v_z. \quad (5)$$

The elevation-dependent distribution of snow depth derived from the extrapolated snow probings and lidar-differencing underlines the need for this correction (Fig. 8). The uncorrected lidar-derived snow depth is strongly affected by emergence velocity and firn compaction. After application of the correction the two methods show good agreement in most of the elevation bands.

The presented method to derive the snow accumulation distribution from lidar-differencing requires, in addition to the two DEMs, long-term annual mass-balance and geometry changes and in situ measurements of snow depth. This expense can be reduced if the geometry changes can be omitted, implying that the glacier is in equilibrium. Furthermore, information about the vertical displacement of the glacier surface could be derived, for example, from GPS measurements or triangulation of the positions of the commonly used mass-balance stakes. If the vertical displacement of the last summer surface during the winter is known, at least for a few points, the scaling of the correction and its calibration with in situ snow probings are redundant. Otherwise, an estimation of snow depth is necessary to scale the correction to fit the time-span between the generation of the two DEMs. To provide a stable fit, these estimations should preferably exist for areas where the annual emergence velocity is high, i.e. on the glacier tongue and in the upper accumulation area, but are not required to cover the glacier representatively.

RESULTS

The three datasets differ in the type of spatial information they present. GPR profiles provide snow depth in linear transects and do not cover the entire glacier representatively. To compare GPR with in situ probings and lidar-derived snow depth, the probings must be extrapolated to achieve a least common spatial coverage of all three datasets. None of them is considered to be the ground reference, to allow full advantage to be taken of their simultaneous availability.

All three methods reveal the increase in snow depth with elevation. They disagree in crevassed areas, where the determination of a meaningful snow depth value is hampered by its large variability within the GPR footprint and movement of the crevasses with time that affects the local lidar-derived snow depth (Fig. 9). Both lidar and GPR are able to resolve the small-scale variability of snow depth, to a certain degree, due to their spatial resolution. Obviously, this is not the case for the spatially extrapolated snow probings (Fig. 9). Along the GPR profiles, with a constant spacing of 1 m between measurements, the root-mean-square error (rmse) and bias in the datasets is calculated using the closest gridpoints of the snow depth maps from lidar and extrapolated probings. In this comparison, the extrapolated snow probings reveal a higher, and lidar-differencing a lower, snow depth than GPR (Table 1). The generally high rmse of 0.39–0.62 m between the methods can partly be explained by the extrapolation scheme for the snow probings and the mass balance underlying the correction of lidar snow depth. Further, due to the high resolution of the lidar DEMs, the horizontal ice flow adds a local stochastic uncertainty by shifting small-scale surface features, including crevasses, to neighbouring gridcells. The smallest rmse was found to be 0.39 m between

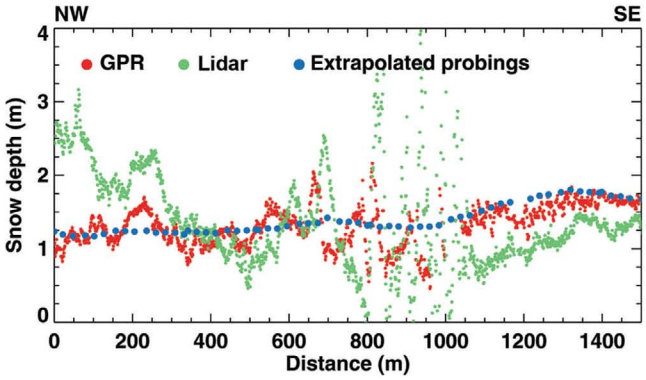

Fig. 9. Snow depth obtained from GPR and at the nearest gridcells of the extrapolated snow probings and corrected lidar DEM-differencing along the first 1500 m of GPR profile 1, ranging from 2880 to 3080 m a.s.l. (Fig. 1).

the extrapolated probings and lidar-derived snow depth. This is probably because of the fitting of the correction to the snow probings. Differences of the in situ snow probings (not extrapolated) to GPR and lidar will be highlighted in the Discussion (Figs 12 and 13).

The traditional glaciological approach, using extrapolated snow probings and snow density in the elevation bands, provides a winter mass balance of Findelengletscher of 0.78 m w.e. The lidar-differencing yields a similar result of 0.72 m w.e. Although the point snow probings were used for the extrapolation and the scaling of the correction for ice emergence velocity, the good agreement in winter mass balance underlines the high potential of deriving snow depth by lidar DEM-differencing.

The extrapolated snow probings allow a spatial comparison with the lidar-derived snow depth distribution to be made. Because the in situ snow probings were used to find the optimal scaling factor, f, of the lidar correction, the two datasets are not fully independent. However, the linear scaling of the correction (Eqn (5)), which has a strong altitudinal gradient (Fig. 6b), affects the distribution of snow between the ablation and accumulation areas and, only to a lesser extent, its variability at a smaller scale. Furthermore, a similar value of f would have been found using the GPR snow depth instead of the in situ probings (see Discussion). Thus, the dependence of the two datasets plays a minor role when comparing the spatial snow accumulation distribution. The two methods show good agreement for large parts of the glacier (Fig. 10). They disagree on snow depth for marginal regions of the glacier, especially in areas that were not covered by snow probings or mass-balance measurements and, thus, were not adequately represented in the respective spatial extrapolation. Particularly, this involves parts of the accumulation area and the uppermost part of the glacier, where wind erosion of snow is most pronounced.

The availability of distributed snow depth data and high-resolution DEMs allowed us to investigate snow depth distribution with surface topography, such as elevation, slope and curvature. While elevation affects the amount of precipitation, slope and curvature were taken as proxies for local variations in snow depth due to preferential deposition and redistribution (Huss and others, 2008; Lehning and others, 2008). We followed previous studies that used multiple linear regression (Schmidt and others, 2009; Farinotti and others, 2010) in the form

$$d = \beta_0 + \beta_1 x_1 + \beta_2 x_2 + \beta_3 x_3 \quad (6)$$

to estimate snow depth, d. All grids were upscaled to a 10 m × 10 m cell size to reduce computation time. The October 2009 lidar DEM provided elevation, x_1, and allowed computation of slope, x_2, and curvature, x_3, (Zevenbergen and Thorne, 1987). The coefficients β_i were found by least-squares estimation from the lidar-derived distributed snow depth (Fig. 7). Curvature was derived within a radius of 70 m around each gridcell. Although not supported by any physical process, this radius provided the highest correlation with snow depth. A positive sign indicates a convex surface. Crevassed areas were masked because the lidar-derived snow depth gives unreliable results in these regions.

Over the entire glacier, correlation of snow depth with elevation is $r = 0.40$, while slope (95% central range: 3–31°) has little influence ($r = 0.20$). Higher snow depths are found in areas with a concave curvature ($r = -0.27$). This multiple linear regression model can only partially explain snow depth variability ($r = 0.51$, $p < 0.001$ for all given correlations). This is in line with the findings of Farinotti and others (2010). They point out that this cannot be interpreted as absence of an influence of these factors on snow depth, as it can be nonlinear or masked by other factors, such as variations in wind speed and its prevailing direction (Purves and others, 1998; Plattner and others, 2006).

From previous studies it is known that deposition and redistribution of snow is largely determined by the interplay

Table 1. Root-mean-square error (rmse) and bias of extrapolated snow probings (ESP), lidar and GPR-derived snow depth along the GPR profile lines (crevassed areas masked, profile lines shown in Fig. 1)

A	B	rmse	Bias $A - B$
		m	m
GPR	lidar	0.623	0.107
ESP	lidar	0.385	0.164
GPR	ESP	0.565	–0.057

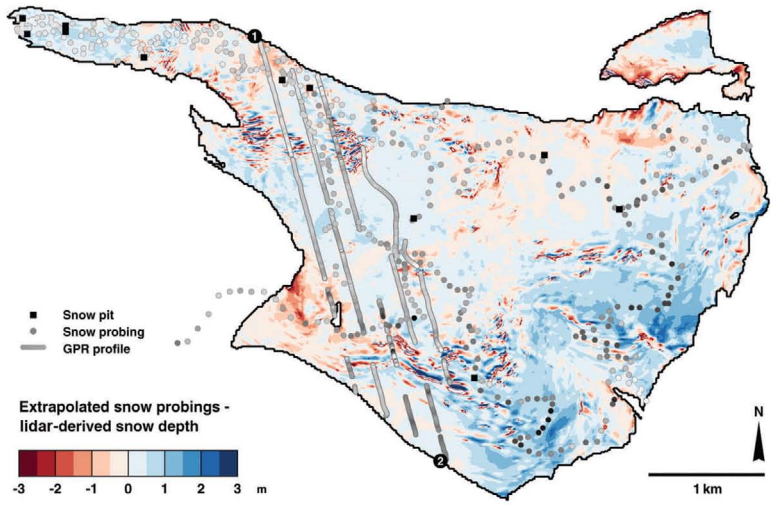

Fig. 10. Difference of corrected lidar-derived to extrapolated snow depth from probings. Blue indicates an underestimation, and red an overestimation, of lidar-derived snow depth compared with the extrapolated probings.

of wind and surrounding topography (Liston and Sturm, 1998; Winstral and Marks, 2002; Lehning and others, 2008; Dadic and others, 2010a). In the regression this was incorporated as curvature on the small scale of a 70 m radius. Obviously, this approach does not respect actual local wind fields that are also formed by surface features on larger scales. To account for spatial variations in the influence of the selected variables, we introduced a zonal regression using the same variables but restricted to a 2 km × 2 km moving box around each gridcell of the lidar-derived snow depth map. By running a separate regression for the surroundings of each gridcell, we derived a smoothed map of the strength of the linear dependence of snow depth on the selected variables (Fig. 11).

The zonal regression shows a better performance than the regression for the entire glacier and allows a more detailed interpretation. The multiple linear correlation coefficient ranges from $r = 0.22$ on the upper glacier tongue (2900 m a.s.l.) and in the lower accumulation area (3250–3350 m a.s.l.) to $r = 0.83$ in the upper ablation area (3100–3200 m a.s.l.) and upper accumulation area (>3450 m a.s.l.) (Fig. 11c). If instead the same number of gridcells is randomly chosen from across the glacier, the multiple linear correlation coefficient is $r = 0.45 \pm 0.01$. The size of the moving box determines the smoothness and the data range of the correlation coefficient maps in the expected way (e.g. $0.18 \leq r \leq 0.94$ for 1 km × 1 km, $0.30 \leq r \leq 0.83$ for 3 km × 3 km). Thus, the variable correlation coefficients for the zonal regression can be attributed to spatial variations in the relation of snow depth to the examined topographic variables. While the upper glacier tongue might show overestimation of lidar-derived snow depth, as indicated by GPR and snow probings (Figs 9 and 10), the weak performance in the lower accumulation area is related to the changing sign in the correlation with elevation. Zonal correlation with elevation (Fig. 11a) highlights that a linear elevation gradient is not representative for the entire glacier. Instead, the correlation of elevation and snow depth changes sign at high altitudes. For slope, the correlation is less than $|r| = 0.38$ for 75% of the glaciated area and also changes to a negative sign at high altitudes ($p < 0.001$ for all correlations). At the same time, a regression over the whole of this area of negative zonal correlation with slope gives $r = -0.03$. Curvature yields strictly negative correlations that are generally stronger at higher altitudes (Fig. 11b). However, the effect of curvature on snow depth is not restricted to the 70 m scale that is used here and can thus be underestimated by the regression.

For elevation, slope and curvature, the effect on snow depth is not constant over the entire glacier. This is likely to be linked to variations in wind speed and exposure that are controlled by the surrounding topography. Therefore, elevation, slope and fixed-scale curvature alone cannot sufficiently explain snow depth distribution in a linear regression model for the entire glacier, but can within subregions of similar influence of wind fields.

DISCUSSION

Systematic bias in the snow probings dataset

In contrast to the snow probings, GPR provides snow depth as continuous profiles, instead of discrete point values. Thus, we evaluated a potential difference of the snow probings from the GPR data as a function of distance between the measurements. Therefore, all possible pairs of one measurement from each method were identified. Mean and standard deviation of the difference between every two measurements were obtained for all pairs with less than a critical distance, increased in 10 m steps. This allows a comparison of the two datasets to be made, despite the variable distance between the snow probings and the GPR profiles.

A good agreement between the two datasets is found where the distance between snow probings and GPR profiles is small (Fig. 12), and variability is of the same order within multiple probings as at individual locations (0.13 m). However, variability not only increases with distance, but the snow probings exceed the GPR-derived snow depth. This becomes important at distances >30 m and indicates that the analysed subsets of the two methods cover different

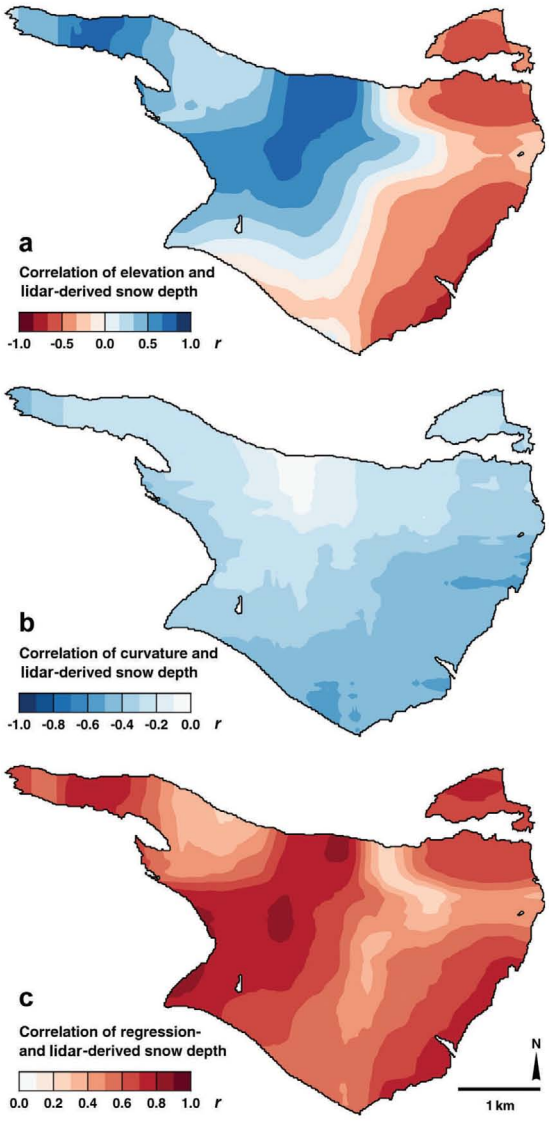

Fig. 11. Correlation of lidar-derived snow depth with (a) elevation, (b) curvature (70 m scale) and (c) regression-derived snow depth for the surrounding 2 km × 2 km box of each gridcell.

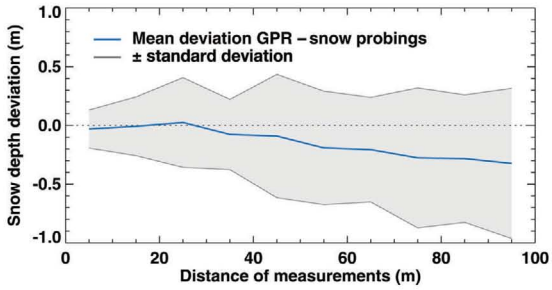

Fig. 12. Distance-dependent deviation of GPR-derived snow depth for probings, shown as mean and standard deviation of all measured deviations within each 10 m class. Each class contains all possible measurement pairs of the two datasets with a distance shorter than the upper class limit.

regions of snow accumulation. We interpret this distance-dependent deviation between the datasets as a systematic bias in the in situ measurements that might be explained by either one or both of these processes: (1) the GPR profiles cover parts of the glacier surface that are inaccessible and are therefore not represented in the snow probings and/or (2) the walking path corresponding to the snow probings inadvertently avoided ridges and steeper parts of the glacier that are prone to wind erosion and thus shallower snow depth, and rather was attracted by depressions, shallow troughs or flat areas in which snow tends to be deposited.

Uncertainties in GPR-derived snow depth

GPR provides estimates of snow depth that are not affected by glacier dynamics, such as firn compaction or ice flow. Nevertheless, uncertainties that arise from the choice of radio-wave velocity and the practical vertical resolution of the radargrams need to be taken into account. Also, it should be noted that the accuracy of the observer when digitizing the reflectors could play a role that cannot be exactly quantified.

The resolution of the GPR data limits the accuracy of recognized reflector travel times. It depends on the signal bandwidth, that can be approximated by the centre frequency for most GPR systems. It is typically estimated to be about half the wavelength, λ, but depends on the signal-to-noise ratio (Jol, 2009). Thus, in the given case with a frequency of 500 MHz and a velocity of 0.229 m ns^{-1}, the vertical resolution is $\sim \lambda/2 = 0.23$ m.

As shown above, the velocity of the radar pulse depends on the characteristics of the snowpack. For snow density, the standard deviation of 21 kg m^{-3} from snow pits where more than one density profile is available is used as an estimate of the measurement accuracy. The total standard deviation of measured density from the area-weighted mean (68 kg m^{-3}) accounts for uncertainties in the density extrapolation method and the use of a constant density. Using Eqn (1), the related total standard error in radio-wave velocity is $\pm$0.011 m ns^{-1}. By linearity, the effect on the resulting snow depth then is $\pm$4.7%.

For the computation of radio-wave velocity we assumed the snowpack to be dry along the GPR profiles. Although this was in line with observations during fieldwork, from guideline values (e.g. Fierz and others, 2009) a water content of <3% vol. cannot be ruled out. Due to the high permittivity of water, this could have a considerable influence on the radio-wave velocity in the snowpack. Based on numerous sets of measurements, Frolov and Macheret (1999) compute the increase in dielectric permittivity, $\Delta\varepsilon'$, due to the relative water content, θ, as

$$\Delta\varepsilon' = 16.7\,\theta + 42.5\,\theta^2. \quad (7)$$

Thus, liquid water content of up to 3% could reduce the radio-wave velocity from 0.229 m ns^{-1} to 0.199 m ns^{-1} by causing a higher dielectric permittivity of the snowpack. For the resulting snow depth this relative change of up to −13.1% could make a significant difference but cannot be determined exactly. Furthermore, the water content varies not only with depth in the snowpack but also spatially (Techel and Pielmeier, 2011). This makes it difficult to

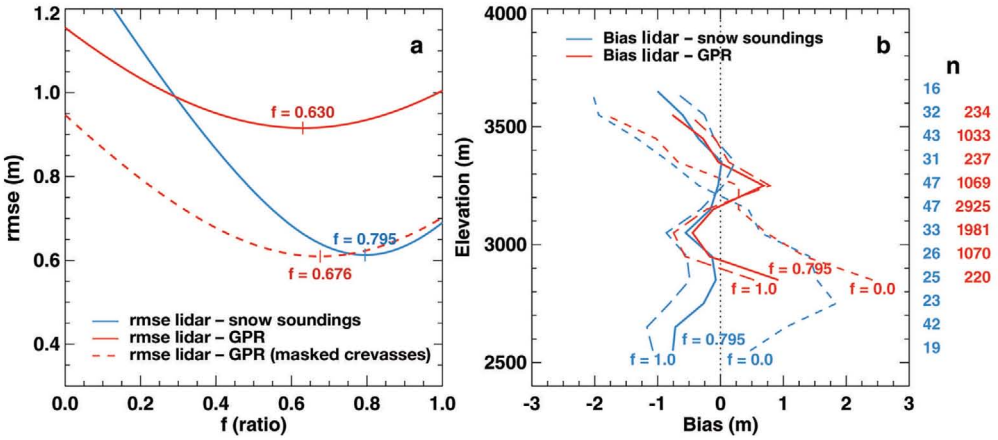

Fig. 13. (a) Determination of the optimal scaling factor, f, of the annual vertical surface velocity by minimizing the rmse of lidar-derived snow depth to GPR and in situ probings. (b) Elevation-dependent bias in lidar- to GPR-derived snow depth (red) and probings (blue) for different choices of the scaling factor, f, shown as mean deviation from n measurements within 100 m elevation bands.

incorporate this factor in the analysis. During fieldwork, the snowpack in the lower parts of the glacier (i.e. the tongue) showed evidence of some liquid water content, whereas the snow pits in the elevation range covered by GPR profiles were dry, due to lower temperatures. Furthermore, the velocity of 0.229 m ns^{-1} which is used in this study indicates good agreement with the in situ snow probings (Fig. 12). A reduced velocity would even increase the already negative deviation from the extrapolated snow probings (Table 1). Thus, the effect is likely to be small.

Ice-flow dynamics affect lidar-derived snow depth

From the vertical distribution of mean snow depth (Fig. 8) it is obvious that the correction for emergence velocity and firn compaction is necessary when evaluating snow depth distribution from repeated lidar DEMs. As described, the resulting vertical velocity of the autumn glacier surface was estimated as an annual average from long-term mass-balance and geometry changes. Since the temporal difference of the DEMs did not correspond to a full year and to account for interannual variations, the correction was scaled by a factor f (Eqn (5)).

Earlier studies interpreted seasonal variations in the ice-flow dynamics of Findelengletscher to be a result of changes in the subglacial drainage system (Iken and Bindschadler, 1986; Iken and Truffer, 1997). The horizontal ice-flow velocity was measured by triangulation at several points on the glacier tongue and revealed a counter-intuitive behaviour. Peak velocity in May and June was followed by a rapid decrease. Starting in October and over the whole winter, horizontal velocity increased (Iken and Truffer, 1997). Although these results cannot be directly transferred to the current situation or individual years, using the half-year fraction $f = 0.5$ of v_z to cover the time-span from October 2009 to April 2010 is inappropriate. Instead, the optimal fraction of $f = 0.795$ is found iteratively by minimizing the rmse of snow depth, d, to the available in situ data from snow probings. The GPR data were not chosen as a reference here because they do not cover the glacier representatively. Nonetheless, the optimal f would correspond well if it were instead obtained with the GPR-derived snow depth ($f = 0.676$; Fig. 13a).

Comparison of lidar-derived snow depth with GPR and probings for different values of f shows the strong elevation-dependent bias in the uncorrected data ($f = 0$; Fig. 13b). With the correction scaled by $f = 0.795$ to best fit the snow probings, the imbalance of snow depth overestimation in the ablation area and underestimation in the accumulation area is compensated. Underestimation of snow depth on the lower glacier tongue and in the upper accumulation area might be explained by a local overestimation in the correction for the vertical surface velocity.

The high value of f compared with the expected half-year fraction cannot be explained by seasonal variations in ice-flow velocity alone. Since the correction is based on average mass-balance and geometry changes from a 5 year period, short-term fluctuations are not adequately represented. These can be due to changes in ice-flow velocity but also to variations in the mass balance in recent years that affect firn compaction rates in the accumulation area. The glaciological time series shows a mass balance of +0.83 m w.e. for the accumulation area of Findelengletscher in 2009. For the other years that were used for the calculation of the correction (2005–10), values range from +0.58 to +0.65 m w.e. Thus, firn compaction played a larger role in the period October 2009 to April 2010 than is estimated in the correction, leading to a higher value of f when the correction is fitted to the snow probings.

By calibrating the scaling factor, f, with the snow depth from probings, the correction of the lidar-derived snow depth takes the interannual and seasonal variations in emergence velocity and firn compaction into account. However, the two processes are independent of each other, do not affect the same area and probably do not vary synchronously. Therefore, the scaling factor, f, represents a tuning parameter that integrates all influential processes and allows reconciling the correction of raw lidar-derived snow depth with the individual conditions during the time-span from October 2009 to April 2010.

CONCLUSIONS

We have discussed measurements of snow accumulation distribution in April 2010 on Findelengletscher from

403 snow probings, 12.7 km of GPR profiles and differencing of two lidar DEMs. The lidar-derived elevation change must be corrected for the glacier emergence velocity and firn compaction. We successfully obtained this correction from long-term mass-balance and geometry changes. All three datasets reveal the general increase in snow depth with elevation. In contrast to the snow probings, GPR and lidar-differencing are able to capture its small-scale variability. Over the entire glacier, snow depth can only partially be explained by elevation, slope and curvature, since deposition and redistribution of snow is strongly determined by local wind fields. We have shown that the explanatory power of these topographic variables is significant within subregions on the glacier. Comparison between snow probings and GPR-derived snow depth indicates a bias in the dataset of snow probings that probably originates from a non-representative distribution of sampling sites.

Single-offset GPR is an effective tool for snow depth measurements that is not affected by glacier dynamics and firn compaction in the accumulation area. It is prone to few uncertainties if estimates for snow density and liquid water content exist. However, the GPR profiles should cover the glacier representatively (e.g. on a grid). Airborne data acquisition is efficient and flexible, but the Swiss telecommunication regulator (OFCOM) allows airborne use of the GPR system only under strict conditions and in uninhabited regions, such as on alpine glaciers. Thus, further technical and regulatory development is needed to fulfil the requirements of national and international authorities for future studies. Lidar provides a fully distributed set of snow depth data with very high spatial resolution, which is not achievable by the application of GPR or conventional glaciological measurements. When corrected for glacier dynamics, lidar-differencing is a powerful tool to assess snow depth distribution on alpine glaciers, but it is expensive in terms of external data requirements. In the presented comparison, the traditional approach of using snow probings remains the only method that is independent of separate input data. However, snow probings typically do not reproduce the small-scale variability of snow depth. We conclude that the choice between the presented methods should depend on the availability of in situ measurements and the desired balance between accuracy and spatially distributed data. GPR provides a compromise in both respects. It requires snow density and wetness estimations that need not necessarily be gained from in situ measurements but that determine the main uncertainties. At the same time, because it provides snow depth along linear profiles, its ability to reproduce the spatial variability lies between the probings and the fully distributed lidar-differencing scheme.

The time-matched availability of the three datasets accounts for the need to have separate data sources as a basis to evaluate the performance of individual methods. Their comparison and combination illustrates a detailed image of winter snow accumulation that benefits from each method's advantages and will provide a valuable dataset in the future to validate accumulation models of varying complexities.

ACKNOWLEDGEMENTS

We thank N. Salzmann, A. Linsbauer, H. Machguth and other members of the field team for the repeated campaigns and ongoing mass-balance measurements. Constructive comments of two anonymous reviewers helped to improve and clarify the manuscript. This study is supported by the Swiss National Science Foundation (SNSF), grant 200021_134768.

REFERENCES

Abermann J, Fischer A, Lambrecht A and Geist T (2010) On the potential of very high-resolution repeat DEMs in glacial and periglacial environments. *Cryosphere*, **4**(1), 53–65 (doi: 10.5194/tc-4-53-2010, 2010)

Ackermann F (1999) Airborne laser scanning – present status and future expectations. *ISPRS J. Photogramm. Rem. Sens*, **54**(2–3), 64–67 (doi: 10.1016/S0924-2716(99)00009-X)

Annan AP (1999) *Practical processing of GPR data*. Sensors & Software Inc., Mississauga, Ont. http://www.ees.nmt.edu/outside/courses/Geop446/Docs/GPR_data_process.pdf

Arendt AA, Echelmeyer KA, Harrison WD, Lingle CS and Valentine VB (2002) Rapid wastage of Alaska glaciers and their contribution to rising sea level. *Science*, **297**(5580), 382–386 (doi: 10.1126/science.1072497)

Bamber JL and Rivera A (2007) A review of remote sensing methods for glacier mass balance determination. *Global Planet. Change*, **59**(1–4), 138–148 (doi: 10.1016/j.gloplacha.2006.11.031)

Bauder A, Funk M and Gudmundsson GH (2003) The ice-thickness distribution of Unteraargletscher, Switzerland. *Ann. Glaciol.*, **37**, 331–336 (doi: 10.3189/172756403781815852)

Cuffey KM and Paterson WSB (2010) *The physics of glaciers*, 4th edn. Butterworth-Heinemann, Oxford

Dadic R, Mott R, Lehning M and Burlando P (2010a) Wind influence on snow depth distribution and accumulation over glaciers. *J. Geophys. Res.*, **115**(F1), F01012 (doi: 10.1029/2009JF001261)

Dadic R, Mott R, Lehning M and Burlando P (2010b) Parameterization for wind-induced preferential deposition of snow. *Hydrol. Process.*, **24**(14), 1994–2006 (doi: 10.1002/hyp.7776)

Damm V (2004) Ice thickness and bedrock map of Matusevich Glacier drainage system (Oates Coast). *Terra Antart.*, **11**(1), 85–90

Davis JL and Annan AP (1989) Ground-penetrating radar for high-resolution mapping of soil and rock stratigraphy. *Geophys. Prospect.*, **37**(5), 531–551 (doi: 10.1111/j.1365-2478.1989.02221.x)

Dunse T, Eisen O, Helm V, Rack W, Steinhage D and Parry V (2008) Characteristics and small-scale variability of GPR signals and their relation to snow accumulation in Greenland's percolation zone. *J. Glaciol.*, **54**(185), 333–342 (doi: 10.3189/002214308784886207)

Dunse T, Schuler TV, Hagen JO, Eiken T, Brandt O and Høgda KA (2009) Recent fluctuations in the extent of the firn area of Austfonna, Svalbard, inferred from GPR. *Ann. Glaciol.*, **50**, 155–162 (doi: 10.3189/172756409787769780)

Egli L, Jonas T, Grünewald T, Schirmer M and Burlando P (2012) Dynamics of snow ablation in a small Alpine catchment observed by repeated terrestrial laser scans. *Hydrol. Process.*, **26**(10), 1574–1585 (doi: 10.1002/hyp.8244)

Eisen O and 15 others (2008) Ground-based measurements of spatial and temporal variability of snow accumulation in East Antarctica. *Rev. Geophys.*, **46**(RG2), RG2001 (doi: 10.1029/2006RG000218)

Farinotti D, Magnusson J, Huss M and Bauder A (2010) Snow accumulation distribution inferred from time-lapse photography and simple modelling. *Hydrol. Process.*, **24**(15), 2087–2097 (doi: 10.1002/hyp.7629)

Farinotti D, Usselmann S, Huss M, Bauder A and Funk M (2012) Runoff evolution in the Swiss Alps: projections for selected high-alpine catchments based on ENSEMBLES scenarios. *Hydrol. Process.*, **26**(13), 1909–1924 (doi: 10.1002/hyp.8276)

Fierz C and 8 others (2009) *The international classification for seasonal snow on the ground*. (IHP Technical Documents in Hydrology 83) UNESCO–International Hydrological Programme, Paris

Fisher SC, Stewart RR and Jol HM (1996) Ground penetrating radar (GPR) data enhancement using seismic techniques. *J. Environ. Eng. Geophys.*, **1**(2), 89–96 (doi: 10.4133/JEEG1.2.89)

Frolov AD and Macheret YuYa (1999) On dielectric properties of dry and wet snow. *Hydrol. Process.*, **13**(12–13), 1755–1760 (doi: 10.1002/(SICI)1099-1085(199909)13:12/13<1755::AID-HYP854>3.0.CO;2-T)

Glaciological Reports (2011) The Swiss glaciers, 2005/06–2006/07. *Yearbooks of the Cryospheric Commission of the Swiss Academy of Sciences (SCNAT)*, **127–128**. VAW-ETHZ, Zürich

Grünewald T, Schirmer M, Mott R and Lehning M (2010) Spatial and temporal variability of snow depth and ablation rates in a small mountain catchment. *Cryosphere*, **4**(2), 215–225 (doi: 10.5194/tc-4-215-2010)

Haeberli W and Beniston M (1998) Climate change and its impacts on glaciers and permafrost in the Alps. *Ambio*, **27**(4), 258–265

Heilig A, Eisen O and Schneebeli M (2010) Temporal observations of a seasonal snowpack using upward-looking GPR. *Hydrol. Process.*, **24**(22), 3133–3145 (doi: 10.1002/hyp.7749)

Helfricht K, Schöber J, Seiser B, Fischer A, Stötter J and Kuhn M (2012) Snow accumulation of a high alpine catchment derived from LiDAR measurements. *Adv. Geosci.*, **32**, 31–39 (doi: 10.5194/adgeo-32-31-2012)

Helfricht K, Kuhn M, Keuschnig M and Heilig A (2013) LiDAR snow cover studies on glacier surface: significance of snow- and ice dynamical processes. *Cryosphere Discuss.*, **7**(2), 1787–1832 (doi: 10.5194/tcd-7-1787-2013)

Helm V and 6 others (2007) Winter accumulation in the percolation zone of Greenland measured by airborne radar altimeter. *Geophys. Res. Lett.*, **34**(6), L06501 (doi: 10.1029/2006GL029185)

Hock R (1999) A distributed temperature-index ice- and snowmelt model including potential direct solar radiation. *J. Glaciol.*, **45**(149), 101–111

Hock R (2005) Glacier melt: a review on processes and their modelling. *Progr. Phys. Geogr.*, **29**(3), 362–391 (doi: 10.1191/0309133305pp453ra)

Huss M (2011) Present and future contribution of glacier storage change to runoff from macroscale drainage basins in Europe. *Water Resour. Res.*, **47**(W7), W07511 (doi: 10.1029/2010WR010299)

Huss M, Bauder A, Funk M and Hock R (2008) Determination of the seasonal mass balance of four Alpine glaciers since 1865. *J. Geophys. Res.*, **113**(F1), F01015 (doi: 10.1029/2007JF000803)

Huss M, Bauder A and Funk M (2009) Homogenization of long-term mass-balance time series. *Ann. Glaciol.*, **50**(50), 198–206 (doi: 10.3189/172756409787769627)

Huss M and 6 others (2013) Towards remote monitoring of sub-seasonal glacier mass balance. *Ann. Glaciol.*, **54**(63 Pt 1), 75–83 (doi: 10.3189/2013AoG63A427)

Iken A and Bindschadler RA (1986) Combined measurements of subglacial water pressure and surface velocity of Findelengletscher, Switzerland: conclusions about drainage system and sliding mechanism. *J. Glaciol.*, **32**(110), 101–119

Iken A and Truffer M (1997) The relationship between subglacial water pressure and velocity of Findelengletscher, Switzerland, during its advance and retreat. *J. Glaciol.*, **43**(144), 328–338

Joerg P, Morsdorf F and Zemp M (2012) Uncertainty assessment of multi-temporal airborne laser scanning data: a case study at an Alpine glacier. *Remote Sens. Environ.*, **127**, 118–129 (doi: 10.1016/j.rse.2012.08.012)

Jol HM (2009) *Ground penetrating radar theory and applications*. Elsevier Science, Amsterdam

Kääb A, Berthier E, Nuth C, Gardelle J and Arnaud Y (2012) Contrasting patterns of early twenty-first-century glacier mass change in the Himalayas. *Nature*, **488**(7412), 495–498 (doi: 10.1038/nature11324)

Kanagaratnam P, Gogineni SP, Ramasami V and Braaten D (2004) A wideband radar for high-resolution mapping of near-surface internal layers in glacial ice. *IEEE Trans. Geosci. Remote Sens.*, **42**(3), 483–490 (doi: 10.1109/TGRS.2004.823451)

Kaser G, Cogley JG, Dyurgerov MB, Meier MF and Ohmura A (2006) Mass balance of glaciers and ice caps: consensus estimates for 1961–2004. *Geophys. Res. Lett.*, **33**(19), L19501 (doi: 10.1029/2006GL027511)

Kohler J, Moore J, Kennett M, Engeset R and Elvehøy H (1997) Using ground-penetrating radar to image previous years' summer surfaces for mass-balance measurements. *Ann. Glaciol.*, **24**, 355–360

Kovacs A, Gow AJ and Morey RM (1993) A reassessment of the in-situ dielectric constant of polar firn. *CRREL Rep.* 93-26

Kruetzmann NC, Rack W, McDonald AJ and George SE (2011) Snow accumulation and compaction derived from GPR data near Ross Island, Antarctica. *Cryosphere*, **5**(2), 391–404 (doi: 10.5194/tc-5-391-2011)

Lalumiere L and Prinsenberg S (2009) Integration of a helicopter-based ground penetrating radar (GPR) with a laser, video and GPS system. In Chung JS, Prinsenberg S, Hong SW and Nagata S eds. *Proceedings of the 19th International Offshore and Polar Engineering Conference, 21–26 June 2009, Osaka, Japan, Vol. 1*. International Society of Offshore and Polar Engineers, Cupertino, CA, 658–665

Lehning M, Löwe H, Ryser M and Radeschall N (2008) Inhomogeneous precipitation distribution and snow transport in steep terrain. *Water Resour. Res.*, **44**(W7), W07404 (doi: 10.1029/2007WR006545)

Liston GE and Sturm M (1998) A snow-transport model for complex terrain. *J. Glaciol.*, **44**(148), 498–516

Machguth H (2008) On the use of RCM data and gridded climatologies for regional scale glacier mass balance modeling in high mountain topography: the example of the Swiss Alps. (PhD thesis, University of Zürich)

Machguth H, Paul F, Hoelzle M and Haeberli W (2006a) Distributed glacier mass-balance modelling as an important component of modern multi-level glacier monitoring. *Ann. Glaciol.*, **43**, 335–343 (doi: 10.3189/172756406781812285)

Machguth H, Eisen O, Paul F and Hoelzle M (2006b) Strong spatial variability of snow accumulation observed with helicopter-borne GPR on two adjacent Alpine glaciers. *Geophys. Res. Lett.*, **33**(13), L13503 (doi: 10.1029/2006GL026576)

Machguth H, Paul F, Kotlarski S and Hoelzle M (2009) Calculating distributed glacier mass balance for the Swiss Alps from regional climate model output: a methodical description and interpretation of the results. *J. Geophys. Res.*, **114**(D19), D19106 (doi: 10.1029/2009JD011775)

Marchand W-D, Killingtveit Å, Wilén P and Wikström P (2003) Comparison of ground-based and airborne snow depth measurements with georadar systems, case study. *Nord. Hydrol.*, **34**(5), 427–448 (doi: 10.2166/nh.2003.025)

Marshall H-P and Koh G (2008) FMCW radars for snow research. *Cold Reg. Sci. Technol.*, **52**(2), 118–131 (doi: 10.1016/j.coldregions.2007.04.008)

Østrem G and Brugman M (1991) *Glacier mass-balance measurements: a manual for field and office work*. (NHRI Science Report 4) Environment Canada. National Hydrology Research Institute, Saskatoon, Sask

Plattner Ch, Braun LN and Brenning A (2006) Spatial variability of snow accumulation on Vernagtferner, Austrian Alps, in winter 2003/04. *Z. Gletscherkd. Glazialgeol.*, **39**, 43–58

Plewes LA and Hubbard B (2001) A review of the use of radio-echo sounding in glaciology. *Progr. Phys. Geogr.*, **25**(2), 203–236 (doi: 10.1177/030913330102500203)

Purves RS, Barton JS, Mackaness WA and Sugden DE (1998) The development of a rule-based spatial model of wind transport and deposition of snow. *Ann. Glaciol.*, **26**, 197–202

Robin GdeQ, Evans S and Bailey JT (1969) Interpretation of radio echo sounding in polar ice sheets. *Philos. Trans. R. Soc. London, Ser. A*, **265**(1166), 437–505 (doi: 10.1098/rsta.1969.0063)

Salzmann N, Machguth H and Linsbauer A (2012) The Swiss Alpine glaciers' response to the global '2°C air temperature target'. *Environ. Res. Lett.*, **7**(4), 044001 (doi: 10.1088/1748-9326/7/4/044001)

Schmidt S, Weber B and Winiger M (2009) Analyses of seasonal snow disappearance in an alpine valley from micro- to meso-scale (Loetschental, Switzerland). *Hydrol. Process.*, **23**(7), 1041–1051 (doi: 10.1002/hyp.7205)

Solomon S and 7 others eds. (2007) *Climate change 2007: the physical science basis. Contribution of Working Group I to the Fourth Assessment Report of the Intergovernmental Panel on Climate Change*. Cambridge University Press, Cambridge

Techel F and Pielmeier C (2011) Point observations of liquid water content in wet snow – investigating methodical, spatial and temporal aspects. *Cryosphere*, **5**(2), 405–418 (doi: 10.5194/tc-5-405-2011)

Ulriksen P (1982) Application of impulse radar to civil engineering. (PhD thesis, Lund University of Technology)

Wehr A and Lohr U (1999) Airborne laser scanning – an introduction and overview. *ISPRS J. Photogramm. Rem. Sens*, **54**(2), 68–82 (doi: 10.1016/S0924-2716(99)00011-8)

Winstral A and Marks D (2002) Simulating wind fields and snow redistribution using terrain-based parameters to model snow accumulation and melt over a semi-arid mountain catchment. *Hydrol. Process.*, **16**(18), 3585–3603 (doi: 10.1002/hyp.1238)

Yankielun N, Rosenthal W and Davis RE (2004) Alpine snow depth measurements from aerial FMCW radar. *Cold Reg. Sci. Technol.*, **40**(1–2), 123–134 (doi: 10.1016/j.coldregions.2004.06.005)

Zemp M, Hoelzle M and Haeberli W (2009) Six decades of glacier mass-balance observations: a review of the worldwide monitoring network. *Ann. Glaciol.*, **50**(50), 101–111 (doi: 10.3189/172756409787769591)

Zevenbergen LW and Thorne CR (1987) Quantitative analysis of land surface topography. *Earth Surf. Process. Landf.*, **12**(1), 47–56 (doi: 10.1002/esp.3290120107)

MS received 22 January 2013 and accepted in revised form 2 September 2013

5 COMPUTATION OF A DISTRIBUTED GLACIER SURFACE ALBEDO PROXY USING AIRBORNE LASER SCANNING INTENSITY DATA AND IN-SITU SPECTRO-RADIOMETRIC MEASUREMENTS

This chapter has been re-submitted after revisions as: Joerg, P.C., Weyermann, J., Morsdorf, F., Zemp, M., & Schaepman, M.E.: Computation of a distributed glacier surface albedo proxy using airborne laser scanning intensity data and in-situ spectro-radiometric measurements. *Remote Sensing of Environment.*

Abstract

In recent years, multi-temporal topographic measurements from airborne laser scanning (ALS) have been increasingly used as a source of spatially explicit and accurate information to calculate geodetic glacier mass balances. Simultaneously to collecting topographic data, most ALS instruments record the backscattered intensity for each laser emission and therefore provide additional information on the reflectance characteristics of the surveyed surface. Along with air temperature, the surface albedo of snow and ice was identified as a major driving factor of glacier melt. Consequently, better knowledge on the spatial distribution of the glacier albedo could substantially improve energy balance based glacier melt modeling. In this study, we collected on-glacier spectro-radiometric and albedometer measurements to serve as ground reference to radiometrically calibrate high resolution ALS intensity data into a distributed albedo proxy map. This method resulted in an albedo proxy with values between 0.6 on the glacier tongue and 0.9 on fresh snow in high altitudes. 99.6% of all values fell within the albedo boundary conditions, i.e. values between 0 and 1. Corrected near-infrared ALS intensity data provided a distributed product that allows simulating albedo in glacier energy and mass balance models more realistically. Remaining challenges are (i) a different surface albedo response in the visual part of the electro-magnetic spectrum, (ii) the low radiometric resolution of the ALS system for higher intensity values, and (iii) an insufficient correction of the snow bi-directional reflectance distribution function (BRDF).

5.1 Introduction

Glacier ablation is primarily driven by air temperature and net solar radiation (e.g. Ohmura et al. 2007). The glacier surface energy balance describes the amount of energy available for melt and depends not only on the incident radiation, but also on the energy uptake efficiency (cf. Wiscombe and Warren 1980). This important factor is the surface bi-hemispherical reflectance, further on called albedo, defined as the ratio of reflected to incident radiation, and strongly influencing ablation (Oerlemans et al. 2009; Schaepman-Strub et al. 2006). Snow albedo is inversely correlated with snow grain size and the concentration of impurities in the snow pack whereas ice albedo is mostly de-

pendent on the content of debris and smaller sized mineral and biogenic cover (Brock et al. 2000; Oerlemans et al. 2009). Typical value ranges for snow (firn, ice) albedo from measurements and used for glacier energy and mass balance modeling range between 0.6 and 0.9 (0.3-0.55, 0.2-0.35) (e.g. Cuffey and Paterson 2010; Greuell et al. 1997; Klok and Oerlemans 2004; Machguth et al. 2006b).

Current glacier energy and mass balance models rely on single or multiple albedo values which are usually estimated from literature or modeled, e.g. by simulating albedo as a function of aging snow or snow depth, and often assumed to be spatially homogeneous on a larger part on the glacier surface (Klok and Oerlemans 2004; Machguth et al. 2006b). To improve these assumptions, the albedo can either be measured directly on the glacier (Brock et al. 2000; Sugiyama et al. 2011) or derived from remote sensing data (Knap et al. 1999a; Stroeve et al. 2005). However, the spatial distribution of albedo on a glacier can be highly variable (Sugiyama et al. 2011) and the spatial resolution of a satellite instrument might not be satisfactory for the application on smaller valley type or mountain glaciers. In addition, passive optical measurements depend on the sun as illumination source and contain directional effects as a result from isotropic, volumetric and geometrical-optical scattering (summarized as bi-directional reflectance distribution function (BRDF) effects, for terminology see Schaepman-Strub et al. (2006)).

In the past decade, measurements of the geodetic elevation change of glaciers using airborne laser scanning (ALS) provided operational data (e.g. Abermann et al. 2009; Geist 2005; Joerg et al. 2012). As a side product to topographic information, most airborne laser scanning systems record the backscattered intensity providing surface reflectance information in one narrow spectral band (e.g. 1 nm sampling width). For glacier laser scanning applications, typically the near-infrared part of the electro-magnetic spectrum is used. Lutz and others (2003) showed that a near-infrared wavelength is particularly well suited to derive information on snow and ice characteristics. However, to make use of this information, the data has to be radiometrically corrected for different physical effects (Höfle and Pfeifer 2007; Kaasalainen et al. 2011; Vain et al. 2009). Finally, ALS measures in a monostatic configuration, having the same illumination and observation geometries.

In this study, we derive a spatially distributed glacier surface albedo derived from radiometrically calibrated ALS intensity data. However, as only one single narrow band in the near-infrared part of the electro-magnetic spectrum is provided by our ALS system, the resulting product is seen as an albedo proxy. To provide suitable reference data, we synchronously collected in-situ spectral reflectance and albedo values at different altitudes on the Alpine glacier. We use the on-glacier reference data from spectro-radiometric measurements at four different locations to derive the broadband albedo. Additionally, we correct all-day albedometer measurements at a single location for topographic effects of the inclined glacier surface and perform a sky view correction to eliminate the influence of the surrounding higher regions on the broadband albedo. Furthermore, we physically pre-process ALS intensities to derive a homogenous data set, including an assessment of two types of bi-directional reflectance distribution functions (BRDF) of snow. Subsequently, we correlate the corrected ALS intensities with the reference in-situ albedo to generate an albedo proxy map. Finally, we assess and discuss the derived albedo map for its validity and some persistent uncertainties, including a comparison with a broadband albedo map derived from a synchronous multi-spectral aerial camera data set.

5.2 Study site and data

5.2.1 Study site

Our study site encloses the Findelengletscher (46° N, 7° 52’ E) located in the Canton Valais, Switzerland. This valley-type glacier is one of the larger ones in the Alps with an area of more than 13 km^2 (in 2010). As it covers an elevation range from 2600 m up to 3900 m a.s.l., it is expected to sustain multiple decades from now on, despite the strong retreat in the last decades (cf. Glaciological Reports, 1881-2010). Since 2004/05, glaciological mass balance measurements were available (Machguth 2008; Machguth et al. 2006b) serving as baseline within a long-term mass balance monitoring program.

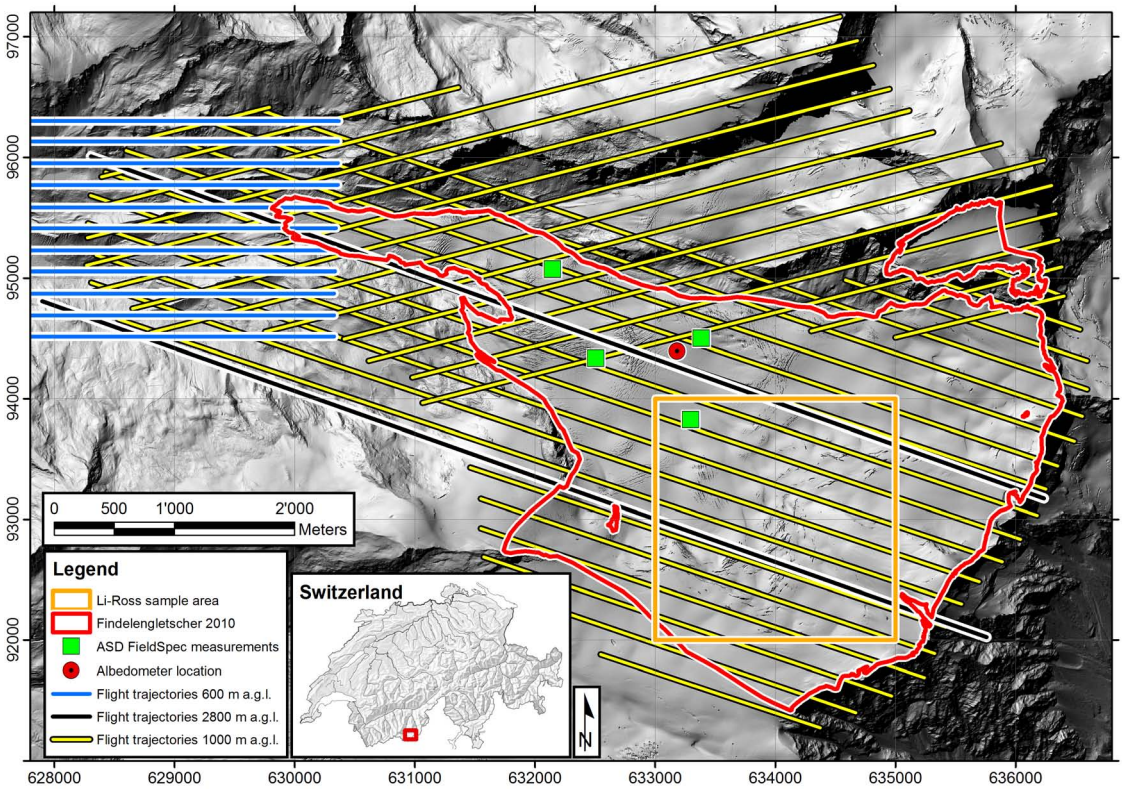

Figure 5-1 Shaded relief of the study site with flight trajectories and in-situ reference locations. Coordinates used are in meters in the Swiss national grid (CH1903).

Four days before the in-situ and ALS measurements in September 2010, a snowfall event covered the entire Findelengletscher with a layer of fresh snow. The typically present end-of-summer differentiation between snow, firn, and ice including transition zones in between these facies types became consequently indistinct. Snow depth measurements at ablation stakes revealed that at the day of the campaign, about 0.05-0.10 m of snow was still present on the tongue (2600 m a.s.l.), though melting fast. In higher altitudes, the snow depth generally increased with high spatial variability, to a maximum measured snow depth of 0.28 m at 3413 m a.s.l.

5.2.2 ALS data

On September 29, 2010, ALS (Optech Inc., ALTM Gemini) was used on board a Pilatus Porter fixed-wing aircraft to retrieve topographic information in order to support the in-situ glaciological mass balance measurements. The weather during data acquisition was cloud-free with an excellent visibility. The built-in surveying system consisted of a pulsed laser, whose emissions were deflected across the flight track using an oscillating mirror. The range distance of each laser emission is calculated by the two way time-of-flight between the ground and the emitter/detector, under the assumption of a constant speed of light. A global positioning system (GPS) coupled with an inertial navigation system (INS) provided position and attitude of the aircraft. These data, together with the range measurement and instantaneous angle of the deflecting mirror, allowed allocating a coordinate in a given reference system for each ground projected field of view (Wehr and Lohr 1999).

The entire glacier area was surveyed from a nominal flight altitude of 1000 m above ground (cf. Table 5-1 and Fig. 5-1). A second acquisition at a lower nominal flying altitude of 600 m above ground and a higher pulse repetition frequency (PRF) and higher resolution was performed as well, but only covered the lower parts of the glacier. Additionally, two flight trajectories at a higher altitude of 2800 m above ground were acquired for a large portion of the glacier area to investigate effects on the accuracy of this lower point density digital elevation model (DEM) and the behavior of the recorded intensity compared to the standard setup flown at 1000 m above ground.

Table 5-1 Data acquisition parameters for the respective flying height.

Date of acquisition	Sept. 29, 2010			
Sensor employed	Optech ALTM Gemini			
Average flying altitude	[m a.g.l.]	600	1000	2800
Pulse repetition frequency (PRF)	[kHz]	100	71	33
Scanning angle	[degrees]	± 15	± 15	± 20.1
Line scanning frequency	[Hz]	39	39	13.7
Across-track overlap	[%]	40	50	35
Average point density	[Pt/m^2]	14.4	8.2	0.4
laser wavelength	[nm]	1064	1064	1064
Beam divergence (1/e)	[mrad]	0.25	0.25	0.25

Point cloud data were available in binary LAS format including intensity values represented as digital numbers (DN) and the flight path data was available as smoothed best estimated trajectory (SBET) data set with a 250 Hz position and attitude recording rate. The emitted laser power was calculated from sensor calibration reports provided by the manufacturer of the scanning system (Optech Inc., data not shown) and the power was assumed to be stable for each respective pulse repetition frequency setting during the entire flight.

5.2.3 ADS 80 data

At the same day as the ALS data was acquired, an independent flight campaign with an Airborne Digital Sensor (Leica Geosystems AG, ADS 80) was performed by the Federal Office of Topography (swisstopo). The camera collected data in the blue (420-492 nm), green (533-587 nm), red (604-664 nm), and near-infrared (833-920 nm) part of the electro-magnetic spectrum. Although the camera would provide multi-angular data for photogrammetry purposes, we limited processing to the nadir multispectral data. Data collection took place on 11:14 UTC at an altitude of 7600 m a.s.l. on an east-west oriented flight trajectory. The flight strip covered most of the Findelengletscher; about 12% in the southernmost part were not covered.

5.2.4 Ground reference data

To investigate and calibrate the ALS intensity and ADS reflectance measurements, we used a twofold approach. To monitor changes in the snow surface and solar irradiance during the flight campaigns, we installed an albedometer (Kipp & Zonen CM 7B) at 3118 m a.s.l. on a part of the glacier with a gentle slope of approx. 3° to the west. The albedometer consisted of two oppositely mounted zenith and nadir facing pyranometers measuring the broadband radiation between 305 and 2800 nm over each hemisphere. Combining both measurements provides the bi-hemispherical reflectance (BHR), also called the (blue sky) broadband albedo (Schaepman-Strub et al. 2006). The area of the albedometer's location was covered by laser returns from three different flight trajectories at different times of the day allowing for a comparison of changes in the measured broadband albedo with changes in the ALS intensity.

In order to expand the reference data set to different locations and surface types at different altitudes, we additionally performed measurements using a spectro-radiometer (Analytical Spectral Devices, Inc., FieldSpec 3 Pro), covering the spectral range between 350 and 2500 nm. We measured at four locations while collecting nadir measurements with a 25° field of view fore optics. Consequently, the applicable scattering concept was hemispherical-conical reflectance factor (HCRF). These HCRFs were then transformed to broadband albedo (cf. Section 3.1.2).

5.3 Methods

5.3.1 Ground reference data processing

Albedometer measurements

The albedometer recorded the incident and reflected hemispherical radiation in W/m^2. The ratio between these two hemispherical radiation measurements is the broadband albedo, describing the integrated surface reflectance ranging between 0 (i.e. no reflectance) and 1 (i.e. 100% reflectance).

Although the albedo was directly deducible from the albedometer measurements, the recorded result was influenced by the local topography and the portion of terrain visible in the upward-looking pyranometer (sky-view factor). The downward-looking pyranometer's FOV was completely looking at terrain. To be able to relate these albedo

measurements with the small field of view of the ALS measurements (BCRF), we had to minimize both effects in the albedometer measurements.

In this highly undulated terrain, with nearby peaks towering more than 1000 m over the albedometer position, the sky view correction was of high relevance. Mountains higher than the albedometer elevation on the one hand obstructed diffuse skylight and on the other reflected a portion of the solar radiation back into the upward-looking pyranometer. The area of the hemisphere covered by terrain was calculated with a viewshed analysis based on the position of the albedometer and the surrounding ALS DEM. Bare rock and snow covered different proportions of the visible surface and featured different reflectance characteristics. We adapted the sky view correction factors described in detail by Corripio (2004) by calculating the fraction of direct and diffuse radiation from the sun and the fraction of reflected diffuse radiation from the ground and multiple scattering between the ground and the sky. While the calculation of the radiation from the sun without terrain interaction was straightforward, the terrain reflected radiation depended on the surface properties. We used photos of the surrounding terrain taken at the albedometer location to estimate the fraction of the terrain covered by snow (0.65) and bare rock (0.35), and derived their average albedo from literature: 0.80 for snow (clean fresh and dry snow at high elevations, e.g. Dozier et al. 2009; Warren 1982) and 0.15 for rock (Paul et al. 2005). Additionally, the model contained a factor that was influenced by the fraction of the sunlit and visible ground. We therefore simulated shadowing in our study site over the entire measuring period of the albedometer in 0.1 h steps and calculated the fraction of shaded raster cells in respect to sunlit cells in the area overlapping the albedometer viewshed.

The sum of these four factors (available for each 0.1 h time interval) was subsequently multiplied with the measurement of incoming radiation leading to a correction of incoming radiation and albedo values.

Secondly, we corrected the albedo for the topographic effect of the non-horizontal measuring site by using a Lambertian correction (Law and Nichol 2004).

$$\alpha_H = \alpha_I \cdot \cos(z) / \cos(i) \qquad (1)$$

Equation (1) uses the solar zenith angle *z* and the angle of incidence *i* (the angle between the surface normal and the incident sun vector) to correct the measured albedo on inclined terrain α_I into the horizontal albedo α_H. The angles used were calculated based on the ALS DEM at the location of the albedometer and using the sun trajectory for this day of the year.

ASD FieldSpec transects

During the ALS survey and albedometer data acquisition, we measured four glacier surface plots with a spectro-radiometer at different locations (Fig. 5-1). Each plot of approx. 15 x 20 m consisted of three parallel transects, separated by 10 m and oriented parallel to the solar principal plane. Before and after each surface measurement, we calibrated the instrument for changes in the solar irradiance using a white reference Spectralon panel (Labsphere, Inc.).

We then transformed the narrowband reflectance (expressed as HCRF) $r(\lambda)$ into broadband albedo α_{ASD} by weighting the reflectance with the incident spectral irradiance $L_{\downarrow}(\lambda)$ (Liu et al. 2010; Negi and Kokhanovsky 2011; Warren 1982).

$$\alpha_{ASD} = \frac{\int r(\lambda) \cdot F_{\downarrow}(\lambda) d\lambda}{\int F_{\downarrow}(\lambda) d\lambda} \qquad (2)$$

Subsequently, we corrected the broadband albedo values for the influence of the local topography using the solar angles at the time of each plot measurement and the local surface normal as described in equation (1). As the spectro-radiometer provided HCRF instead of BHR, and a different spectral range compared to the albedometer's broadband albedo, we decided to account for these effects by introducing a correction factor. The in-situ spectro-radiometer measurements were chosen to be only 200 m away from the albedometer location at a similar altitude. Similar environmental variables (altitude, location, exposition, slope, snow cover) present at these two nearby locations allowed assumption of similar albedo and subsequent calculation of an albedo offset from the corrected albedometer values and the corresponding spectro-radiometer broadband albedo measurements. The correction factor was then applied to all four measurements.

5.3.2 ALS intensity data pre-processing

ALS intensity information is usually defined as the total energy per return and is either provided as single unit-less digital numbers for multiple-return (also discrete return) systems or as discrete series of DNs containing the whole return waveform for each emitted pulse for full-waveform systems (e.g. Mallet and Bretar 2009; Wagner 2010). The instrument type we used was a discrete digitizing system. In discrete return systems, the term intensity is sometimes not clearly defined and a waveform analysis to derive a well-defined intensity is not possible. Therefore, we performed tests correcting the discrete return intensity data: once under the assumption of a true intensity value (i.e. return energy), and once under the assumption that the recorded intensity is the maximum amplitude of the signal power. These tests have revealed that we are provided with the peak power and not the return energy.

The entire returned pulse energy was assumed to be reflected from a single scatterer larger than the laser footprint (the so called extended target), i.e. we excluded multiple echoes. In addition, we assumed a stable laser emission level per PRF and a constant system transmission factor for the entire flight campaign (Höfle and Pfeifer 2007). Spatially distributed point observations were mapped into a regular grid with 1 x 1 m cell size by averaging all enclosed intensity values with a local angle of incidence smaller than 40°.

Range correction

An important factor influencing the returned signal strength is the range distance between scanner and target. The range distance is influenced by topography, by the flight altitude and by different scanning angles across the flight track (Luzum et al. 2004). The reduction of the intensity is based on the LiDAR equation and is inversely proportional to the 2nd power of the range (Baltsavias 1999). The intensity correction for a scatterer larger than the laser footprint size at a given range R is R^2/R_{ref}^2 , with R_{ref} being an

arbitrary reference range to normalize the output values (Höfle and Pfeifer 2007; Luzum et al. 2004; Vain et al. 2011).

Pulse power correction

ALS intensity values are not only affected by processes occurring after the pulse was emitted, but as well directly by the emitted signal power. The signal power for a given laser source is a function of the pulse repetition frequency, i.e. the more pulses per second, the weaker the emitted pulse. The intensity values of discrete returns from a full-waveform system can be calculated by Gaussian decomposition methods and integration of the full width at half maximum (FWHM) or standard deviation of each derived Gaussian (Heinzel and Koch 2011; Mallet and Bretar 2009). In that case, the term intensity is equivalent to the power of the return pulse. To correct for different power levels, two parameters of the scanner have to be known: the width of the emitted pulses and the pulse energy, the latter varies with PRF. This information is available from calibration reports of the scanner manufacturer and only valid for the particular scanner used (pers. comm. Optech Inc.). Knowing these values, one can calculate the peak power of the emitted laser pulse for each PRF by dividing the pulse energy by the pulse width. Finally, the chosen reference PRF power P_{ref} is divided by the actual PRF power P_{PRF} (similar to Vain and others (2009) but using power instead of energy).

Topographic correction

A secondary effect of the intensity being proportional to the peak power is the dependence of the angle of incidence at the target. An inclined target surface relative to the emitted laser pulse vector leads to receiving an elongated version of the sent pulse with reduced peak amplitude. If the scattering behavior of the target's surface is assumed to be Lambertian, the peak power is reduced by $1/\cos(i)$ with i as the local angle of incidence. However, the scattering of snow is known to be non-Lambertian, i.e. has a distinctive directional scattering behavior (e.g. Li et al. 2007; Lyapustin et al. 2010). Due to the monostatic measurement setup, an ALS system always measures in the hot spot region of the BRDF, generating its own "solar" principle plane. The geometrical-optical scattering concept of ALS can therefore be described by the bi-conical reflectance function (BCRF) using a single wavelength at 1064 nm. Snow reflectance measurements are thus characterized by high backscatter and a large single (direct) scattering component. We employed a kernel-based approach for normalization of the anisotropic reflectance behavior of snow. Li-Ross kernels (Roujean et al. 1992; Wanner et al. 1995) model the individual influence of volume- and geometric-optical scattering effects on the angular reflectance behavior of surfaces. Initially designed for vegetation, these functions were shown to be applicable to a multitude of natural surface types, including snow (e.g. Stroeve et al. 2005). Derived from physical principles, such an approach dramatically reduces the degrees of freedom over purely statistical-empirical approaches (Wanner et al. 1995). The present work shows the applicability also in the case of ALS measurements.

We used a patch of 2 x 2 km of snow on the higher part of the Findelengletscher to train a Li-Ross based correction method dependent on the intensities with their respective angle of incidences (also Fig. 5-1). A combination of the Li-sparse geometric-optical kernel and the Ross-thick volumetric kernel provided a good fit to the measured ALS intensities in the used range of local incidence angles from 0 to 40 degrees. The local

incidence angle was employed as angular offset between illumination and observation direction, assuming observation in the forward scatter direction and solar principle plane.

Atmospheric correction

Atmospheric effects like scattering and absorption further reduce the received signal strength (Höfle and Pfeifer 2007). We calculated atmospheric attenuation values at the laser's wavelength using MODTRAN (Berk et al. 2006). Settings in MODTRAN were set to 50 km visibility, dry air and rural aerosol content to match the clear high Alpine conditions present at the day of the campaign. As we were working with three different ALS mission settings (Table 5-1) with different elevations above sea level and above ground, we calculated three different attenuation coefficients *a*: for the 600 m range *R* (1000 m; 2800 m) of the campaign, we assumed a mean flight altitude of 2600 m (4200 m; 6000 m) above sea level and a mean target elevation of 2000 m (3200 m; 3200 m). The resulting attenuation coefficients used for the atmospheric correction were 0.12, 0.11, and 0.06 dB/km, respectively. These values were considerably lower than those reported for similar ranges by Höfle and Pfeifer (2007), due to the better visibility at the high elevation above sea level of our signal paths. The resulting atmospheric condition η_{atm} used is (Höfle and Pfeifer 2007):

$$\eta_{atm} = 10^{-2 \cdot R \cdot a/10000} \qquad (3)$$

5.3.3 From intensity values to an albedo proxy

The resulting correction equation for the Lambertian case of the ALS intensities used is

$$I_{cor} = I_{ori} \cdot \frac{R^2}{R_{ref}^2} \cdot 10^{-2 \cdot R \cdot a/10000} \cdot \frac{P_{ref}}{P_{PRF}} \cdot \frac{1}{\cos(i)} \qquad (4)$$

where I_{cor} and I_{ori} are corrected and originally recorded DNs of intensity for each laser return. In the case of the Li-Ross method, the cosine part of the equation is substituted by a correction factor taken from a lookup table for the respective angle of incidence.

In the next step, the corrected intensity data were linked to the corrected spectro-radiometric and albedometer measurements. For the spectro-radiometric measurements, we clipped the ALS intensity point cloud to the same area as the patch defined by in-situ GPS measurements. To minimize the temporal influence of changes of the snow surface between ground and aerial measurements, we used only those ALS intensity values that were closest in time to the in-situ measurements. In the albedometer case, three ALS intensities from different times were available to compare with the synchronous broadband albedo. To homogenize the ALS intensities, we used averaged data from a 10 x 10 m patch around the albedometer position.

To finally link the ALS intensities with albedo data, we used the seven available reference albedo values to derive slope and offset values based on a linear regression (Fig. 5-2). Subsequently, these values were used to correct all ALS intensities in order to produce a glacier-wide albedo map.

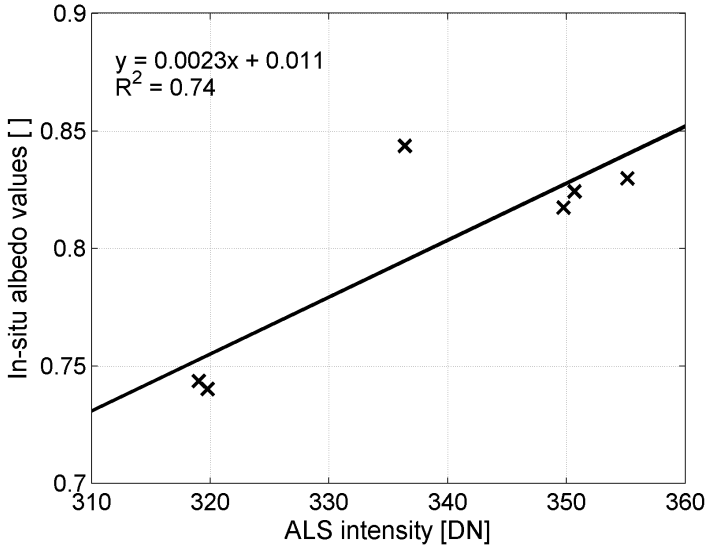

Figure 5-2 Corrected ALS intensity and in-situ broadband albedo measured at transect locations and albedometer position (see Fig. 5-1). The linear regression was used for converting all ALS intensities (Fig. 5-4b) to a distributed albedo map (Fig. 5-6a).

5.3.4 ADS 80 data processing

The digital image strip from ADS 80 was orthorectified using ERDAS LPS 2013 (Intergraph Corp.) and the ALS DEM from the same day. Subsequently, the data were processed to atmospherically corrected reflectance using the ATCOR-4 software (Richter and Schläpfer 2002) and a rural standard aerosol model. Then, the data were corrected for BRDF effects by utilizing data from goniometer measurements on snow from different locations than our field measurements, taken from the spectral data base Specchio (Hueni et al. 2009). Due to the north-south viewing direction of the ADS 80 sensor and the current solar azimuth angle of 175°, we extracted only goniometer measurements in the solar principal plane. The measurements were available in 15° sensor zenith angle steps from 75° in the backscatter to 75° in the forward scattering region of the solar principal plane and for solar zenith angles between 56° and 78°. The spectroradiometric measurements were convolved for the spectral response functions of the four ADS 80 bands and subsequently, a lookup table with the bidirectional reflectance factors (BRF) was generated. To account for solar zenith angles not covered in the BRF lookup table, we extrapolated all measurements from the same sensor zenith angle using a linear model. Subsequently, the solar and sensor geometry for each surface pixel was calculated using the ALS DEM and corrected for BRDF effects using to the BRF lookup table factors. Finally, a multiple linear regression was performed using the in-situ albedo data and the four BRDF corrected band reflectance values in an area of 10 m around the measurement positions. Then, a narrowband to broadband albedo conversion was performed using these factors according to equation (5).

$$\alpha_{broad} = 2.41 \cdot \alpha_{blue} - 0.66 \cdot \alpha_{green} - 0.93 \cdot \alpha_{red} + 0.09 \cdot \alpha_{nir} \quad (5)$$

The conversion to broadband albedo α_{broad} contains the four ADS 80 band reflectances (e.g. α_{blue} for the blue band) and weighting factors derived in the regression. Note that

our conversion is optimized for snow and has not been tested on other surface types. A similar method was applied e.g. for Landsat TM (Knap et al. 1999b) and other instruments (Liang 2001).

5.4 Results

5.4.1 Correcting in-situ data for geometric-optical effects

Using the uncorrected radiance values provided by the albedometer to directly calculate the broadband albedo resulted in a strongly changing albedo over time, starting at a value of 0.65 at 9:30 a.m. local time and ending with an albedo of 0.80 at 4:00 p.m. (Fig. 5-3). Although the snow reflectance was expected to change slightly, i.e. decrease, over the course of the measuring period due to suspected melt and increasing snow grain size (e.g. Wiscombe and Warren 1980), the calculated diurnal albedo values were far off the anticipated range and demanded correction (Jonsell et al. 2003; Mannstein 1985).

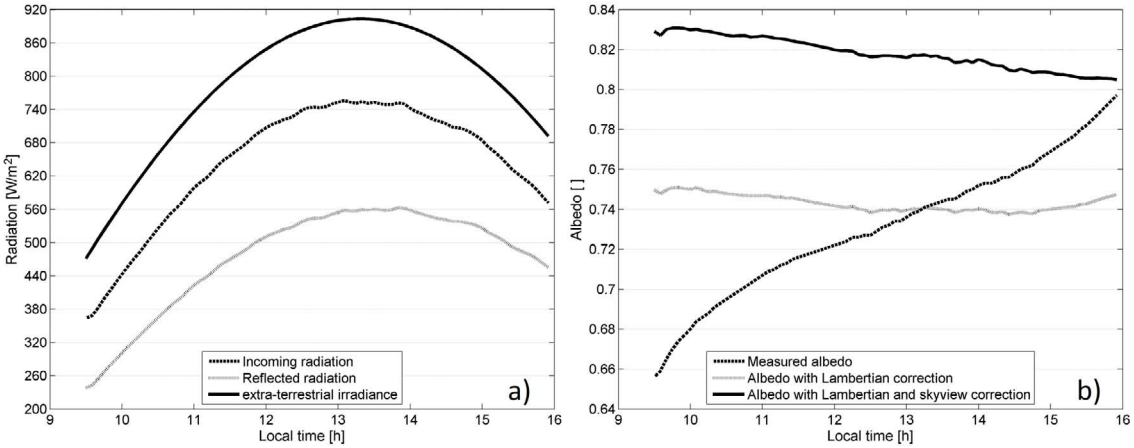

Figure 5-3 Measured incoming and reflected radiation from albedometer measurements as well as modeled extra-terrestrial irradiance at top of atmosphere for that day (a). The smooth shape of the measured curves, similar to the extra-terrestrial one, demonstrates the clear atmospheric conditions during the day of the survey. The derived albedo values from these measurements (b) show the need to correct for topographic effects using a Lambertian and a sky view correction.

The horizontal albedo with the Lambertian correction applied already exhibited a much improved shape, although in the afternoon, the values still increased to unrealistic values (Fig. 5-3). We then applied the sky view correction with a measured terrain covered fraction of 0.20 of the upward-looking pyranometer's hemisphere. Consequently, one fifth of the "sky" was obstructed by terrain consisting of bare rock and snow. The resulting sky view correction factors ranged between 1.11 for the earliest measurement and 1.07 for the last one in the afternoon. This results in generally higher albedo values decreasing over the course of the entire day in a linear way. The corrected albedo values finally ranged between 0.83 in the morning and 0.81 in the afternoon.

The derived broadband albedo from the FieldSpec's first plot was adjusted to match the albedometer measurement at the time of the FieldSpec measurements. The derived offset of 0.08 was subsequently applied to all FieldSpec measurements. The adjusted spectro-radiometric broadband albedo then ranged between 0.73 and 0.83, increasing with altitude.

5.4.2 Physical correction of ALS intensity data

We used four pre-processing steps on the ALS intensity data to reduce physical and sensor-dependent effects before converting the intensity data into albedo proxy values. Additionally, to qualitatively check the influence of each correction step on the generated intensity maps (Fig. 5-4), we calculated the standard deviation of all intensity values within a raster cell. As the correction steps in the processing chain also changed the mean value in a raster cell, we normalized the standard deviations with the mean of the raster cell and therefore present the standard deviations as a percentage of the mean value. The changes from raw, uncorrected intensity values to a fully corrected, more homogeneous intensity raster can be seen in Figure 5-4.

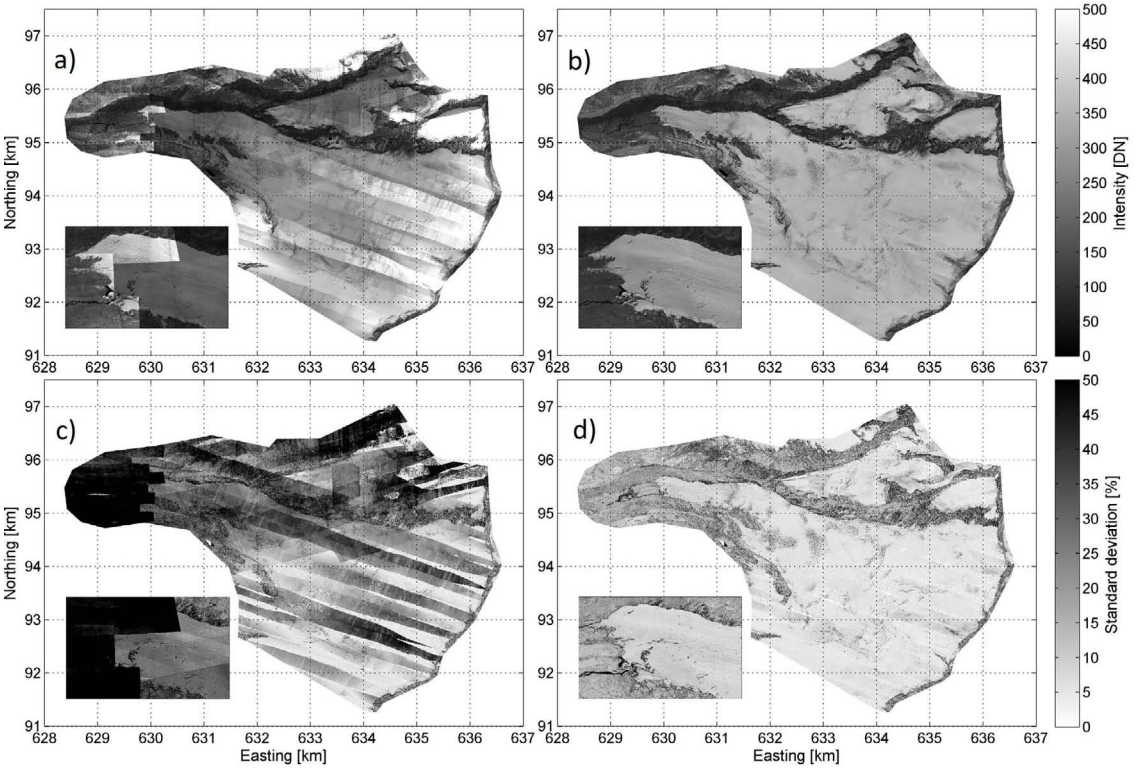

Figure 5-4 Raw (a) and physically corrected ALS intensity data (b, topography correction: Li-Ross) show the need for intensity corrections. The corrected intensity (b) presents an albedo proxy where different surface characteristics and features (e.g. crevasses, see insets of the tongue) are visible. The relative change in the per raster cell standard deviations is visualized before (c) and after (d) the intensity corrections. Note that the lowest standard deviations in the corrected raster (d) are areas where only data from one flight strip are present. Values exceeding the color bar range are reduced to the maximum values' color to preserve a high contrast in the image.

In the corresponding Table 5-2, we present the changes in average per raster cell standard deviations for snow-free terrain, the area of the glacier tongue and the glacier area excluding the tongue for a number of corrections applied. For example, after range normalization, the relative standard deviation at the glacier tongue was reduced to 59% of the initial standard deviation, meaning that the influence of the range accounts for 41% of the originally present variability. Further corrections for different PRFs, atmospheric influences and two types of topographic corrections showed an additional decrease of the relative standard deviations in most cases. The lowest variability of inten-

sity values for the glacier tongue and snow-free area was achieved when applying all correction steps, including the Lambertian topographic correction. On the other hand, for the higher glacier area only, the topographic corrections did not further decrease the standard deviations.

Table 5-2 Standard deviations of raw ALS intensity values with a combination of corrections applied. The relative variation with respect to the uncorrected intensity standard deviations is shown for snow-free terrain, snow at the lower glacier tongue as well as higher elevation snow.

Corrections applied					Terrain only	Glacier snow (tongue)	Glacier snow
Range normalization	PRF	Atmospheric	Topographic (Lambertian)	Topographic (Li-Ross)	Standard deviation [%]	Standard deviation [%]	Standard deviation [%]
					100.00	100.00	100.00
X					63.31	59.16	75.59
X	X				36.84	29.04	30.23
X	X	X			36.20	28.14	29.89
X	X	X	X		34.52	28.00	29.96
X	X	X		X	36.94	28.16	30.49

Figure 5-5 shows the influence of variations of the angle of incidence on the recorded intensity of snow, after being corrected for range, PRF, and atmospheric effects for a 2 x 2 km snow area (Li-Ross sample area in Fig. 5-1). As expected, with increasing angles of incidence, the values of the return intensity were decreasing. After a perfect topographic correction, the new average was expected to be a horizontal line. However, after the Lambertian correction was applied, the resulting average values per degree angle of incidence exhibited an increasing trend, showing an overcorrection of the data. Having trained Li-Ross kernels on the same test area provided a better correction of the mean values, i.e. produced an almost horizontal line.

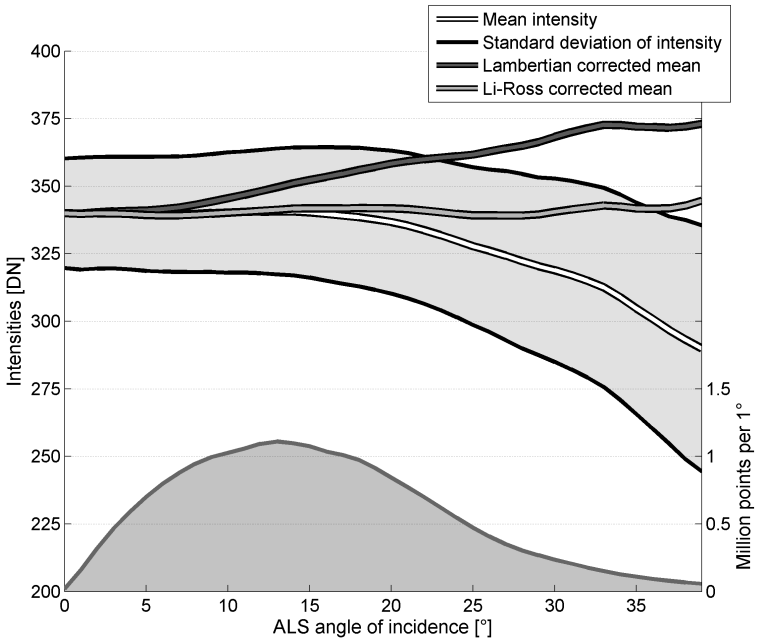

Figure 5-5 Effects of the topographic correction for a 2 x 2 km sample patch of snow (cf. Fig. 5-1). The mean intensity and standard deviation show the decline of intensity with larger angles of incidence before the topographic correction was applied. Correcting for the topography using the Lambertian approach shows an overcorrection, while the Li-Ross correction was able to shift the average intensities to a similar value independent of the angle of incidence. The number of points per degree (angle of incidence) is shown below.

5.4.3 Spatially distributed albedo proxy derived from intensity values

A linear regression was used to correlate the normalized ALS intensity values with the corrected in-situ measurements of the albedo (Fig. 5-2). The seven value pairs showed a good agreement, with a resulting coefficient of determination (R^2) of 0.74. The linear model was then used to generate a distributed albedo proxy map. In the resulting converted raster, 80% of all values on the glacier were in between 0.7 and 0.9, 50% of all albedo values were within the range of the ground reference albedo measurements (0.74 to 0.84). The empirical model fulfilled the physical boundary conditions of the albedo definition, i.e. values ranging between 0 and 1, for 99.6 % of all values. The derived glacier albedo proxy map (Fig. 5-6a) revealed a mean of 0.79 for the entire Findelengletscher, with average values at the tongue of 0.66 (0.05-0.10 m of snow) and 0.8 in higher areas (up to 0.28 m of snow). These results are in good agreement with measurements of snow depths and corresponding albedo values from an automated weather station on the Morteratschgletscher (Oerlemans and Knap 1998).

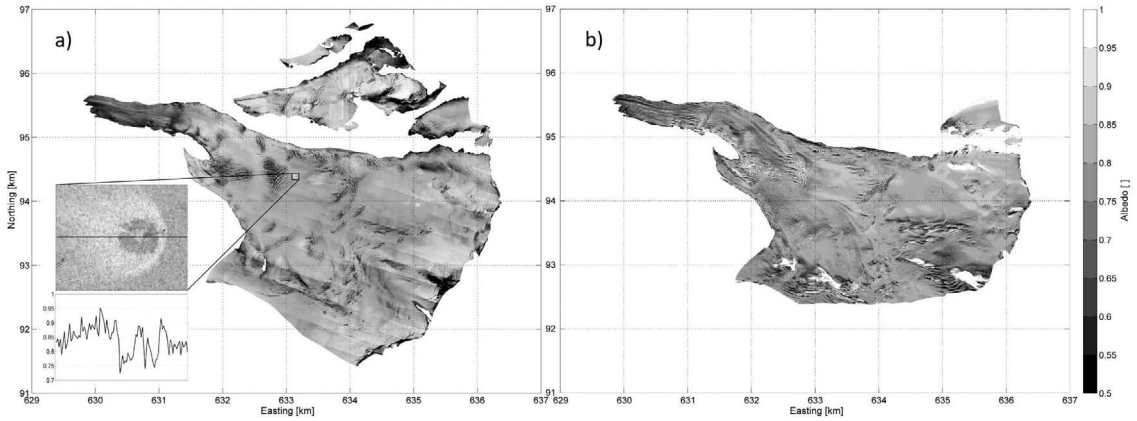

Figure 5-6 Distributed albedo proxy map derived from ALS intensity values and ground reference measurements (a; topographic correction: Li-Ross) of Findelengletscher (south) and a contributing glacier (Adlergletscher, north). The inset shows a detail of the halo pattern where the helicopter landed (approaching from the west). Below are the albedo proxy values of the transect across the landing site. Note the areas of the deposition of fine grained snow (high albedo), the dark circular area where the fine grained snow was blown away, and the center part showing a higher albedo again, possibly due to the protected zone directly below the helicopter's fuselage. The ADS 80 reference albedo of Findelengletscher (b) is shown for comparison. Shadow areas were excluded and are therefore visible as gaps in the map, as is an area to the south, which was not covered by the sensor.

The high sensitivity of the ALS wavelength concerning different snow grain sizes (Dozier and Painter 2004) is nicely shown in the halo pattern of helicopter landing sites (inset in Fig. 5-6a), showing the redistribution of fine snow grains (high albedo halo) and residual larger grains (center). Redistributed snow grain sizes are also visible in the glacier's accumulation area, where areas downwind from small crests were filled with redistributed small diameter snow grains. Crevasses are visible as dark linear features, as the fresh snow cover was not sufficient to cover the bare ice surface beneath.

Where only ALS measurements from flight transects from one direction were present (mostly in the southwest of the Findelengletscher), a linear artifact persisted in the map (cf. section 5.5.2).

5.4.4 Spatially distributed albedo derived from ADS 80

ADS 80 multispectral imagery has served to derive broadband albedo (Fig. 5-6b) as a reference to the ALS albedo proxy map (Fig. 5-6a). Comparing the statistics for the entire glacier, the mean albedo values differ by only 0.01, with the ALS derived values being slightly higher. The standard deviations are 0.09 in the ADS 80 case and 0.13 in the case of ALS. Differencing the ALS and ADS 80 albedo maps led to a high agreement for large regions for albedo values within ±0.1, with larger differences at the tongue. For that region, the statistical agreement is again high with the ADS 80 measuring a mean albedo of 0.69, 0.03 higher than from ALS data, the standard deviations are similar. However, visual inspection of the differences shows that ALS overestimated albedo at locations where darker glacier debris showed through the thin layer of snow and underestimated albedo at areas with higher snow cover. In north-exposed slopes of the accumulation area and around large crevasses, ALS overestimated albedo compared to the reference albedo.

5.5 Discussion

5.5.1 Measurement and correction of in-situ data

To provide accurate and absolute in-situ reference albedo data, multiple corrections of the raw albedometer and spectro-radiometric data were required. Without these corrections, the values measured on the ground contained a strong topographic bias because of the measurement setup and could not be compared with ALS measurements.

Calculation of the broadband albedo from the albedometer's measured incident and reflected radiation led to a strongly changing albedo (+0.14) over the course of the day as consequence of the inclined local surface and the horizontal measurement setup (Jonsell et al. 2003; Mannstein 1985). Although the evolution of the albedo values over time was improved by this first correction step, a temporal trend remained, showing an increase of the albedo in the afternoon over the initial values present in the morning. Taking the influence of the terrain into account, at the same time obstructing the diffuse irradiance from the sky and reflecting radiation back into the upward-looking pyranometer, led to a more reasonable result. In this second correction step, the sunlit fraction of raster cells within the viewshed of the top pyranometer was the dominating factor: Due to the highly undulated topography present in our study site, the ratio of visible cells illuminated by the sun was 0.97 at the beginning of the measurements and decreased to 0.70 at the end of the measurements, with a more rapid decrease towards the end. In the late afternoon, the high mountain range to the southwest of the albedometer position started to cast shadows onto areas in the viewshed of the instrument, reducing the incident radiation. The evolution of this shadow fraction was therefore responsible for the increase in albedo in the afternoon.

The high proportion of the snow covered part of the terrain with a corresponding high albedo led to sky view correction factors larger than 1. This indicated that the amount of radiation reflected from the snow covered terrain was larger than the amount of diffuse radiation obscured by the mountains. Consequently, the measured incident radiation was too high compared to the topography corrected result. Accordingly, the corrected albedo values increased after the sky view correction.

The conversion of spectro-radiometric field measurements to broadband albedo depended on more assumptions. Applying equation (2) is not fully correct as we integrate spectral reflectance (HCRF) rather than spectral albedo (BHR). Furthermore, the spectral irradiance is taken from the white reference measurements also based on the HCRF measurement setup. As albedo is defined as a BHR property, one should measure and integrate reflectance values from all possible incidence angles at a single location. However, this is only possible using either a BRDF snow model or in-situ goniometer measurements, which were not available. Hemispherical snow measurements available at a different locations and dates were not used, as multiple assumptions to fit the model to our measurements would have been needed. Instead, we assumed a Lambertian behavior of the surface and corrected the spectro-radiometer derived albedo topographically using equation (1), as for the albedometer measurements. Additionally, the spectral ranges of the FieldSpec (350-2500 nm) and the albedometer (305-2800 nm) were not entirely the same. Consequently, to further homogenize the resulting albedo, we calculated the albedo difference between the spatially closest FieldSpec measurement and the albedo value of the albedometer taken at the same time. Due to similar environmen-

tal variables (altitude, location, exposition, slope, snow cover) at the two sites, we assumed the snow properties to be similar and therefore shifted the values of the FieldSpec based measurements to the ones of the albedometer and applied this offset to all other FieldSpec albedo values.

5.5.2 From raw to physically corrected intensities

We homogenized the ALS intensity data using multiple physically based correction steps (cf. section 5.3.2). Despite these correction steps, which homogenized the ALS intensity values considerably, a striped pattern of intensity values remained, most apparent in the accumulation area (Fig. 5-6a). This pattern was likely due to a combination of effects that it is most apparent in the south-west area of the glacier and could be attributed to the low point density and to the lower overlap of different flight strips with different viewing geometries. Therefore, the corrected intensity values per raster cell in these areas were only a mean of returns observed with the same laser geometry (i.e. incidence angle and range distance), whereas in all other cases, ground returns stemmed from at least two different flight paths and consequently, incidence angles. Thus, the deficiency in the result is most likely to be associated with the recorded raw intensity values or the insufficiencies in the physical correction process.

When examining the raw intensity values, we found that the ALS instrument recorded weak intensity returns in increments of 1 DN, whereas stronger return intensities were sampled in increments of 20 DN. In our data set, all low- to mid-altitude flight configurations produced data with a majority of increments of 20 DN. Although this instrument setup facilitates to cover a broad range of intensities, it resulted in only a few unique values, e.g. only about 10 different intensity values were recorded on a homogeneous part of the glacier. Values that would have been situated in between the unique interval numbers were rounded to the next increment. Consequently, small changes in the measured intensity might have resulted in large differences when registered. This effect was therefore impossible to correct for. Lutz and others (2003) reported that the use of the maximum intensity value per raster cell evaded the striped pattern. However, extensive experiments with highest and lowest values per raster cell did not improve the result, most likely due to the aforementioned influence of the sampling intervals.

We found that not all corrected intensity values in a single raster cell were the same. Possible sources of these differences are the local snow BRDF, possible stray light from the sun reflected into the sensor (in particular in the forward scattering domain), and variations in the energy of the emitted laser pulse. To quantify the influence of the BRDF, we applied two BRDF models: the first by assuming a Lambertian reflection behavior and the second by training Li-Ross kernels on a test site of snow. The Lambertian model overcorrected the average intensities for increasing angles of incidence (Fig. 5-5). Although the Li-Ross correction performed better than the Lambertian correction in the snow sample area (Fig. 5-1), it is based on the assumption of a specific BRDF for a test site, which may not be correct for different regions or snow types, hindering the transferability of the method. As the snow properties were expected to change from higher to lower altitudes (e.g., as indicated by snow grain size measurements), applying the model to regions exhibiting a different snow surface will result in a bias. Therefore, the Li-Ross correction did not outperform the Lambertian correction according to our statistical analysis (Table 5-2). However, the amount of variance explained by the topographic corrections remained small or even impaired the standard

deviations compared to the considerable amount of variance attached to the range and PRF corrections. Note that the remaining standard deviation of for example 30% (glacier snow with Li-Ross correction) is not to be evaluated worse than the 28% of the glacier tongue. This difference in standard deviations is due to the remaining natural variations inherent to the different surface areas and therefore not comparable. Furthermore, after an additional correction was applied, the changes could lead to a qualitative improvement of the raster representation, although the change in standard deviation was small.

Based on a qualitative visual inspection of single ALS flight strips, the influence of sun-induced snow BRDF effects seemed possible, though extensive simulation with solar stray light did not improve the results. ALS intensity values were therefore assumed to be not affected by solar radiation which is in support of findings by Wagner et al. (2006).

The emitted laser pulse energy was assumed to be stable over the period of the surveys. However, measurements of the emitted intensity recorded in full-waveform digitizing systems suggest considerable variation of the pulse energy in between pulses. Due to the discrete digitizing system used, which did not record the outgoing laser pulse, this additional uncertainty remained in the data but is considered to be small.

5.5.3 From intensity to a spatially distributed albedo proxy

Correlating ALS intensity values with in-situ measured albedo values showed a coefficient of determination (R^2) of 0.74. The small number of in-situ measurements (N=7) were limiting us from testing other possible correlation functions, as the range of different in-situ albedo values was small and the use of a higher order function (e.g. a polynomial) to fit the data would likely result in overfitting. The small spatial variation of the measured albedo values was due to a snowfall event a few days prior the campaign and limited melt thereafter. Snow characteristics were therefore similar on larger parts of the glacier area and did not exhibit the characteristic end-of-summer facies types such as snow, firn, and bare ice. Due to the size of the glacier, it was not possible to collect more in-situ reference measurements, e.g. on the partially melted snow parts on the glacier tongue. However, precisely because the glacier surface was rather homogeneous in large areas, most ALS intensity values are in close agreement with the field reference measurements and mitigate the challenge of converting ALS intensities to an albedo proxy outside the interval of reference measurements. Overall, the resulting values were within the expected range, e.g. around 0.6 on the glacier tongue with partially molten and aged snow, along with mineral and biogenic dust starting to show through the snow and values up to 0.9 in the accumulation area with greater snow depths. This is in line with results comparing snow depth, snow age and albedo on another glacier in the Swiss Alps (Morteratschgletscher; Oerlemans and Knap (1998)).

Finally, we compared the ALS albedo proxy with a broadband albedo from synchronous multispectral ADS 80 airborne imagery (Fig. 5-6). The statistical results, as well as a first qualitative assessment, look generally promising. The mean difference of the albedo values is only 0.01 with a slightly larger difference at the tongue due to the impure surface being visible through the thin snow layer. The albedo difference in the accumulation area, where the ALS proxy is higher than the ADS 80 reference albedo, could be explained by the large local solar zenith angle on the north-exposed slopes, being an

indication that the BRDF correction of ADS 80 imagery did not perform adequately at extreme solar angles.

At the survey date, the glacier was still entirely snow covered. However, for a typical end-of-summer situation with one third or more of the glacier being snow-free, the narrowband to broadband conversion becomes more challenging. At the near-infrared wavelength of the ALS, the reflectance is mostly dependent on the snow grain size. The broadband albedo, though, is dominated by impurities in the visible part of the electromagnetic spectrum. Figure 5-7 demonstrates the challenge by providing results from a simulation of hemispheric albedo based on fine (0.1 mm radius) and coarse grained snow (1 mm), each without, with moderate, and with high dust concentrations (based on the SNICAR simulator, Flanner et al. 2007).

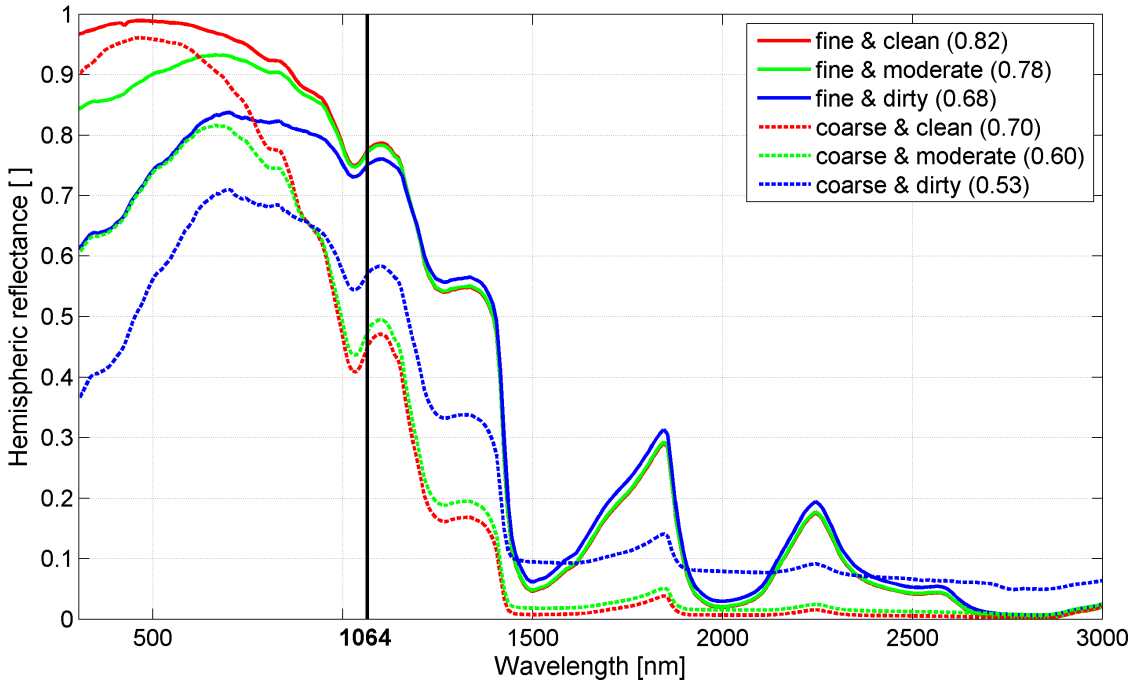

Figure 5-7 Simulation of broadband albedo influenced by two snow grain sizes and three dust concentrations based on the SNICAR model (Flanner et al. 2007). Note the non-linear relationship between the ALS reflectance (vertical line at 1064 nm) and the broadband albedo (in brackets in the legend) when dust concentrations increase.

In the case of surface impurities, the relationship between broadband albedo and reflectance at 1064 nm becomes non-linear. Therefore, at the tongue, the ALS albedo proxy was not entirely able to mimic the influence of debris being visible through the thin snow layer and overestimated albedo. Our study has therefore limited transferability. To overcome this limitation in the narrowband to broadband conversion, more in-situ measurements on the different surface types must be conducted or additional multispectral imaging is required.

5.5.4 Implications for glacier modeling

Literature references of glacier surface albedo used for energy and mass balance modeling usually consist of assumed values for snow, firn, and ice (e.g. Machguth et al. 2006b). Some models allow snow albedo to evolve with time using a snow aging func-

tion partly including the growing influence of underlying facies types (e.g. Oerlemans and Knap 1998). However, these approaches do not take into account the local variability of albedo. In the case of Findelengletscher, a snowfall took place only four days prior to the in-situ and ALS measurements; the modeled albedo will thus result in snow albedo values very similar to the assumed initial snow albedo. Consequently, a bias between the calculated albedo in this study and the modeled values exists. Table 5-3 shows the snow albedo value from Machguth and others (2006b), as used for Findelengletscher (among other glaciers), compared to the calculated snow albedo for different regions from this study. The average albedo for the entire Findelengletscher derived from in-situ and ALS measurements is 0.09 higher than the model value, leading to slower melting of the fresh snow surface compared to the model. At the same time, the tongue's albedo is lower, leading to increased melting and finally being snow-free earlier than calculated by the model. Subsequently, the melt will be even faster due to this albedo feedback mechanism.

Table 5-3 Comparison of three albedo products. The literature snow albedo (a) is taken from Machguth and others (2006b). Product (b) is an albedo normalized to the literature values using the average corrected ALS intensity and the median absolute deviation (MAD). The last column (c) shows average and MAD of the radiometrically calibrated ALS intensity.

Area	a) Literature albedo	b) Scaled ALS variability	c) Measured ALS variability
Findelengletscher, tongue	0.70 +/- 0	0.70 +/- 0.04	0.66 +/- 0.06
Findelengletscher, main part	0.70 +/- 0	0.70 +/- 0.02	0.79 +/- 0.04
Entire Findelengletscher	0.70 +/- 0	0.70 +/- 0.03	0.79 +/- 0.04
Northern side glacier (Adlergletscher)	0.70 +/- 0	0.70 +/- 0.06	0.77 +/- 0.09

As in-situ albedo measurements are only available on few glaciers, the direct application of the proposed method on a different glacier is difficult. However, assuming the average corrected ALS intensity represented the snow albedo from the literature and using the median absolute deviation (MAD, used in Tab. 5-3) or another suitable measure of statistical dispersion of the ALS values, enables to attribute a variability value to the literature albedo and consequently allows deriving a distributed albedo map. In the case of a glacier with multiple facies types visible, local maxima in the ALS intensity's histogram for snow and ice surfaces could be used to link intensity with albedo values from the literature. Therefore, the ALS intensity data could be used to map the variation of albedo for an entire glacier without in-situ measurements. The resulting albedo can then be checked for validity when the albedo ranges between 0 and 1. From the three albedo products, the radiometrically calibrated ALS intensity (Tab. 5-3, c) provided the best albedo product for modeling purposes.

5.6 Conclusions and outlook

We measured and corrected on-glacier spectro-radiometric and albedometer measurements to serve as reference broadband albedo in preparation for deriving a glacier-wide spatially distributed albedo proxy map based on ALS intensity data. First, we show that it is essential to correct in-situ measurements for topographic biases. For instrument inter-comparison, a transformation to broadband albedo is required. Second, ALS intensity data - once corrected for range, PRF, atmospheric, and topographic artifacts – can be combined with literature values to a distributed, relative albedo proxy. Third, ALS intensity data, radiometrically calibrated with in-situ measurements, provided a distributed albedo proxy for snow. However, care must be taken on bare ice and impure surface regions.

Nowadays, ALS is increasingly used to map topographic changes in glaciology, in order to derive a geodetic glacier mass balance. As these measurements are usually only performed in a decadal interval, the mass balance in between this interval has to be calculated using either in-situ glaciological mass balance measurements or by modeling, relying on meteorological measurements. However, one of the most important factors for glacier melt is the surface albedo which is spatially and temporally highly variable. Being able to complement glacier volume change measurements from ALS with a calibrated albedo proxy provides an important input variable for glacier mass balance models. It enables using the high resolution albedo information as a starting point of models by using only a few in-situ albedo measurements and data provided by ALS anyway. As ALS is an active instrument measuring in the hotspot configuration, ALS reflectance is not affected by shadowing and to a lesser degree subject to directional effects than passive optical imagery.

For future applications, we recommend using albedometer measurements on all surface types present as the measurements can be performed quickly and evade the transformation of spectro-radiometric measurements into broadband albedo. Still, all of these measurements must be carefully evaluated and corrected for potential topographic influences.

Although provided with only one narrow spectral band, the spectral response of glacial surfaces at this wavelength enabled to distinguish areas with different albedo. Overall, the results obtained in this study encourage exploiting the intensity information present in ALS data to support glacier energy and mass balance modeling.

Acknowledgements

We thank Jeff Dozier and an anonymous reviewer for their constructive and helpful comments, Alexander Damm for providing atmospheric attenuation values, Andreas Hueni for providing data from the Specchio data base, Hendrik Wulf for valuable advice, and Optech Inc. for laser scanner calibration values. We acknowledge BSF Swissphoto for the acquisition of the ALS data and continued support. Karl Schroff from the Institute for Atmospheric and Climate Science (ETH Zurich) provided the albedometer and technical support. We are grateful to Wilfried Haeberli for his valuable support. This project was supported by the Swiss energy utility Axpo.

6 SYNOPSIS

6.1 Main results and discussion

The main results of this research (see section 1.5 for the research questions) are presented here summarizing the papers in chapters 2-5.

6.1.1 Assessment of ALS topographic information for glaciology

Publication 1 (chapter 2):

Joerg, P.C., Morsdorf, F., & Zemp, M. (2012). Uncertainty assessment of multitemporal airborne laser scanning data: A case study on an Alpine glacier. *Remote Sensing of Environment*, *127*, 118-129

- What changes in the Findelengletscher were observed in the period 2005-2010?

The application of ALS DEM differencing on Findelengletscher allowed the accurate derivation of multiple glacier change key figures. During the investigated 5-year period, the data revealed that the Findelengletscher's surface area diminished by 2% and the terminus retreated by about 200 m. The average annual thickness change was -0.7 m, with up to -7 m elevation change at the tongue and -0.2 m in the accumulation area. A distinctive ripple pattern in the accumulation area was detected, with marked elevation decreases followed closely by strong increases. This indicated the dynamics of the glacier by showing the down-valley propagation of crevasses. The vertical dynamic additionally present can be seen by comparing the in-situ ablation stakes and snow pit measurements. The conversion factor from elevation change into meters water equivalent (w.e.) would exceed the physically possible ice density (ablation area), and the average in-situ surface accumulation of approx. 1.1 m w.e. was counteracted by the firn densification and the submergence of the ice.

The reported direct glaciological mass balance of the Findelengletscher in the same period considerably differed from the derived geodetic glacier change measured. Assuming an average density of 850 kg m^3 for converting the elevation change into the geodetic mass balance, the results from both methods differ by more than 30%, with the geodetic balance being more negative than the in-situ derived mass balance. We suspect this bias originates from a combination of uncertainties: a) the density conversion factor, b) the under-sampling of the large accumulation area with in-situ measurements not fully capturing the variability present, and c) the extrapolation method used to inter-/extrapolate from the in-situ point measurements to account for the entire glacier.

The well-defined setup of the ALS surveys for glaciological purposes resulted in high-resolution and highly accurate DEMs to investigate the topographic changes in the Findelengletscher. The large difference between the results of the two measuring methods shows the importance of accurate geodetic reference measurements to account for the accumulation of systematic errors. It is therefore essential to thoroughly reassess the in-situ observation measurements. This is currently being done based on the results of this study, using a distributed mass balance model incorporating meteorological and

other data to derive the mass balance of the Findelengletscher (results not yet published). At the same time, the uncertainties in the in-situ measurement network are being carefully investigated (Machguth et al., in prep.). However, for ALS DEM differencing, the uncertainty of the choice of the density conversion factor makes the derivation of the geodetic mass balance difficult. Ongoing research based on the excellent ALS data sets and in-situ data time-series is contributing to a better understanding of the dynamics of the Findelengletscher and of other glaciers in the world.

Changes in glacier volume have been studies for many years, typically by differencing DEMs using photogrammetric methods (Haug et al. 2009; Koblet et al. 2010). ALS promises to increase the accuracy of volumetric change measurements by providing much more accurate DEMs as it directly measures surface elevations (Geist 2005; Kennett and Eiken 1996). The application of ALS in glacier research started in the mid-1990s when the first attempts were made to derive DEMs on glacier surfaces (Favey et al. 1999; Kennett and Eiken 1996), but ALS systems were not usable for operational glacier mapping. ALS DEMs were first used to measure glacier volume changes within the framework of the EC-funded Operational Monitoring system for European Glacier Areas (OMEGA) project in Austria and Norway (Geist et al. 2003). The possibility of measuring of glacier change using multi-temporal ALS DEMs was demonstrated on the Hintereisferner and Engabreen (Geist 2005). Since then, ALS has become established as a method to operationally measure glacier change and contribute to glacier inventories (Abermann et al. 2009; Knoll and Kerschner 2010).

Our research focused on data from state-of-the-art ALS systems and on the evaluation of the data for multiple effects not considered very thoroughly in the existing literature. We were able to evaluate the volume change of the Findelengletscher using ALS. To compare glacier volume change with synchronous data from in-situ measurements, however, the systematic and stochastic uncertainties in the data must be known. This topic is discussed in more detail in addressing the following research questions.

- How accurately can glacier topography and glacier changes be reproduced using ALS? How significant are the uncertainties involved for estimating volume change?

To extract the local elevation and overall volume change of a glacier, accurate DEMs are important, especially if the change signal is small. A systematic vertical error in one (or both) of the DEMs used can quickly lead to major misinterpretations of the volume change. Although the mass turnover and local elevation changes in the Findelengletscher are considerable, a systematic vertical uncertainty of just a decimeter will lead to the overestimation of more than a million cubic meters of volume change. A systematic evaluation of the accuracy of each DEM is therefore mandatory.

Our study showed that ALS with an emitted wavelength of 1064 nm could map the complete surface of the Findelengletscher, without being influenced by varying surface characteristics. Some of the problems with DEMs produced photogrammetrically, such as few correlation points in snow covered and shadow areas, were absent in the ALS data. Consequently, a complete DEM of the glacier could be produced without uncertain areas due to interpolation effects. In addition, although it is widely assumed that ALS data are very accurate, the accuracy of the ALS DEMs had to be evaluated. Previous studies often relied on a priori accuracies from the data provider or used flat test areas such as a football field to check for vertical uncertainties (Geist 2005). Further-

more, the term “uncertainty” was often not used consistently. For example, only the single-emission vertical and horizontal stochastic uncertainties from a calibration report were used. It is, however, only systematic uncertainties in DEMs that influence the elevation change, but they are often not thoroughly investigated. The high elevations and undulating topography of our study site, led us to decide to take a multi-layered approach to evaluate our data for systematic and stochastic uncertainties directly in the study site. We surveyed the glacier forefield in-situ to establish reference surfaces, used already present ground control points, and developed an error propagation model to evaluate the accuracy on different scales.

Comparing single laser returns with reference surfaces and points indicated that systematic vertical shifts of about 0.25 m were present in every single DEM. Although horizontal shifts were detected as well, the magnitude and direction of such shifts was not consistent throughout the whole study area. Consequently, we modeled systematic and stochastic uncertainties for every laser return in the study site using a physical and statistical error propagation model. Subsequently, these results were combined to reveal the overall uncertainty of the elevation change for the entire glacier. The stochastic uncertainty for the glacier change was found to be negligibly small, but systematic uncertainties resulted in changes in thickness of up to 35%.

ALS DEMs have been evaluated for accuracy in various studies using reference surfaces (Favey et al. 1999; Geist 2005), ground control points (Geist 2005; Hodgson and Bresnahan 2004a; Hopkinson and Demuth 2006), and error modeling (Filin 2003; Goulden and Hopkinson 2010; Huising and Gomes Pereira 1998). Most such studies relied on uncertainties from data providers or did not measure them directly in the study site. These estimates may therefore differ markedly from the uncertainties actually present. Additionally, the scale to which the stochastic uncertainties refer to is often not clear. For example, is it a single laser return, single raster elevation, or the entire DEM? Furthermore, systematic uncertainties are assumed not to be present although such uncertainties do influence DEM elevations and subsequently thus the resulting calculation of volume change.

We were able to show how to evaluate the accuracy of ALS data using reference points, reference surfaces, and physical error propagation modeling. The last method allowed us to calculate the uncertainties for each part of a study site. It attributed errors to their sources and projected these uncertainties onto the glacier’s surface. By using this error propagation, we were able to predict all the stochastic uncertainties actually measured. However, only about half of the systematic uncertainties could be explained by the model. This limitation shows that additional errors are present that cannot be attributed to the ALS system. Possible sources of the remaining error could originate from the coordinate transformation, atmospheric effects, or from changes in the terrain originally assumed to be stable outside the glacier. Errors from the relative georeferencing of adjacent flight lines (strip adjustment) were not investigated quantitatively, but by qualitatively inspecting the point cloud. No differences between flight strips were detected, however, and it is possible that small errors will remain present due to imperfect strip adjustment.

Although ALS DEMs provide high-precision elevation data, we recommend in this paper using independent reference data to evaluate the data for systematic uncertainties.

As the study also assigned uncertainties to its sources, it could therefore help instrument providers to improve critical equipment in the ALS system.

- What is the origin of these uncertainties?

The physical error propagation method developed was able to explain stochastic uncertainties with magnitudes similar to those measured on reference surfaces. For the systematic errors, about half of the uncertainty was attributed to the ALS system, mainly introduced by IMU and GPS uncertainties. Some of the unassigned systematic uncertainty probably originates from coordinate transformation parameters, atmospheric effects, or from the way potential differences between the composition of the atmosphere and the calibrated atmosphere alter the speed of light and therefore the measured range. Such effects are typically not resolvable as the vendor-specific calibration routines are considered industrial secrets.

The error propagation model developed seems to be a valuable way to simulate uncertainties in areas without reference surfaces or points. However, unresolvable systematic uncertainties may exist and could possibly degrade the quality of a volume change assessment. Again, we recommend using an independent reference surface near a test site and preferably at a similar elevation to exclude possible atmospheric influences.

Publication 2 (chapter 3):

Joerg, P.C., & Zemp, M. (2014). Evaluating volumetric glacier change methods using airborne laser scanning data. *Geografiska Annaler: Series A Physical Geography*, *96*, 135-145

- How can using an economically optimized ALS flight setup influence the volume change accuracy?

After evaluating the validity and systematic and stochastic uncertainties in the first paper (chapter 2), we used this extensive data set for a series of volume change computation tests. Currently, the high economic and computational costs of very high point density data mean that their use is restricted to research applications. The investments necessary for an operational use of ALS data in glacier monitoring must be carefully analyzed for cost-benefit. We therefore decided, in addition to the high point density data, to perform a low-cost acquisition with a considerably lower point density, which still had one return per 2.5 m^2. Our evaluations showed a small bias of only 1.1% in the volume change compared to the high point density model. This result is promising since this less expensive acquisition setup seems to significantly reduce costs. We therefore suggest using ALS more widely in glaciology since lower point densities still seem to be able to adequately capture the glacier change signal with a high enough accuracy.

- What systematic and stochastic uncertainties are introduced when using different methods to derive the geodetic volume change? On what spatial scale are systematic uncertainties of concern?

The second aim of the paper was to investigate if traditional geodetic volume change methods were prone to systematic errors and what influence scale had on the calculated volume changes. Such methods have a long tradition in glaciology, dating back to the late nineteenth century (Finsterwalder 1897; Mercanton 1916). The results from geodetic volume change assessments were used to validate and calibrate measurements from

the glaciological method (Zemp et al. 2013), and to spatially and temporally extrapolate from glaciological results derived in-situ (Cogley 2009; Zemp et al. 2009). However, discriminating between errors from the acquisition and from different methods is difficult and has only been assessed in a few studies up to now (Reinhardt and Rentsch 1986).

We used our ALS DEMs with well-known uncertainties (cf. Ch. 2) to test for possible differences and uncertainties from traditional geodetic volume change methods. Our contribution allows uncertainties in older data sets and volume change calculations to be estimated without having to conduct additional uncertainty assessments. In addition, the advantages and limitations of each method and the influences of scales were discussed, which should help in choosing the most appropriate method for a given topographic data set.

Our results showed that, by using highly accurate measurements (ALS or any other DEM-generating method), very few systematic differences in the volume change persisted so long as the raster size used is kept small relative to the glacier size (e.g. raster size of 25 m for the 13 km^2 large glacier). However, using very large raster sizes (e.g. 250 m) on the Findelengletscher led to systematic errors of up to 8% in the 5-year period investigated. At such low resolutions, the location of the raster grid and the shape of the glacier play a more important role. The absolute systematic error was found to be independent of the time period, a shorter investigation period or a glacier with a low annual mass turnover will exhibit higher relative systematic errors. Therefore, before starting data acquisition, the spatial resolution of a DEM for the glacier to be investigated should be carefully considered.

In addition to the raster DEM differencing method, we simulated the volume change by using two traditionally used volume change methods. The first uses elevation contour lines from two points in time and geometrically approximates the 3-D body of the changed volume (Finsterwalder 1953; Hofmann 1958). Our results show that, with a high contour line density, the result differed only slightly from the reference volume change. If fewer contours were used, the melt will be underestimated due to the undersampling of the strongly changing topography at the tongue. Instead of directly working with the contours to derive the volume change, we generated a DEM from each set of contours and subsequently evaluated the DEM difference (Reinhardt and Rentsch 1986). Using 25 and 50 m contour equidistances provided a very accurate representation of the reference volume change, but using 100 m contours overestimated melt considerably and was therefore not able to entirely capture the elevation changes in the Findelengletscher.

The third method extrapolated the elevation change along a center flow line of the glacier to the entire area at each elevation band (Arendt et al. 2002). This method resulted in a strong underestimation of melt, primarily due to its inability to model the elevation changes in the accumulation area representatively, as another extensive study criticizing this profile method also found (Berthier et al. 2010). However, our study suggests the error source, unlike what has been reported previously, originates from overestimating the elevation change at the tongue. Consequently, the profile method should be employed with caution, as not only may the results differ greatly, but also the error source may not be consistent.

We found systematic errors if an inappropriate method or scale was used to assess the Findelengletscher. Since the size and shape of the glacier, however, influences the results, these might be different for other glaciers. However, our study provides useful information about the critical scales and methods used in glaciology and shows that key estimates from earlier volume change studies must be carefully evaluated, bearing our findings in mind.

Publication 3 (chapter 4):

Sold, L., Huss, M., Hoelzle, M., Joerg, P.C., & Zemp, M. (2013). Methodological approaches to inferring end-of-winter snow distribution on alpine glaciers. *Journal of Glaciology, 59*, 1047-1059

- How could winter accumulation measurements benefit from using ALS?

To model the annual mass balance of a glacier, not only must ablation processes be estimated, but also the snow accumulation. Ablation processes have generally been better investigated and are less difficult to model than the snow accumulation distribution (Dadic et al. 2010). Typically, extrapolated measurements of temperature, precipitation, and climate models are tuned to the characteristics of a study site (Hock 1999; Machguth et al. 2006b). However, the actual snow accumulation pattern is dependent on local influences such as avalanches, the topography, and wind (Dadic et al. 2010; Machguth et al. 2006a). Consequently, the snow accumulation can be spatially highly variable. To date, only few studies have attempted to perform end of winter snow depth measurements but their results could not be compared with independent methods to evaluate the uncertainty of the measurements.

Combining the distributed ALS topographic changes, linearly distributed helicopter-borne ground penetrating RADARgrams, and linearly distributed in-situ measurements of snow depths and density allowed the accurate measurement of the Findelengletscher's winter accumulation. It also provided useful information on the uncertainties and glacier dynamics. Each method has its limitations and benefits. ALS provided a distributed, complete elevation change pattern and the overall volume change, but not density measurements of the volume change to calculate the winter mass balance. In addition, ALS requires elevation corrections for the vertical flow components of the glacier to provide actual snow depths. These challenges can be overcome by using density measurements and local snow depths from in-situ snow probings and snow pits. In this paper, the vertical flow was also modeled using in-situ measurements and a 5-year period of end-of-summer ALS DEM differencing. As the time frame here was only half a year, a tuning factor to account for fraction of the winter flow and firn compaction had to be introduced. This tuning factor was derived by minimizing the error between ALS snow depths and in-situ snow probings.

If only the standard method of snow probing and snow density measurements is applied, the spatial variability can be only partially captured the number of measurements is small and dangerous areas cannot be probed. This limitation can be mitigated by using transects from airborne ground penetrating RADAR. Such snow depth measurements are not influenced by ice flow and firn compaction, but have to meet three challenges: a) the radio-wave velocity in snow chosen sets the spatial scale to transform the radio-wave's travel time to meters snow depth, which depends on material characteristics

such as snow wetness, b) the vertical spatial resolution depends on the signal bandwidth, and c) the RADARgrams to determine the boundary between snow and firn are difficult to interpret.

Combining these different methods leads to a more reliable winter accumulation balance. While in-situ measurements must be made, a single remote sensing assessment is sufficient to compensate for the limited sampling possible with the in-situ method.

- What conditions have to be fulfilled and what are the limitations?

ALS enabled the accurate determination of the glacier-wide volume change from end-of-summer to end-of-winter. It is independent of solar illumination and can, unlike airborne photogrammetry, map texture-less fresh snow and is thus the remote sensing method of choice for winter accumulation measurements. However, the dynamic processes involved make it difficult to obtain information on, e.g. the winter mass balance. The compaction of snow and firn before the measurements were taken can differ from those of the previous year, so that an inter-annual comparison of volume change is unreliable. Synchronous in-situ measurements are regarded as mandatory to measure the snow depth and density at different locations. With this additional information, a conversion into a mass balance is possible.

If the distribution of snow heights and local mass balances are of interest, the ice dynamics have to be corrected for the vertical components of submergence and emergence flow as well as for firn compaction. This can be done at well-distributed points of snow probing to measure the actual snow depth or by modeling the glacier's vertical flow.

Combining ALS and in-situ measurements is the best way to accurately measure the winter balance of a glacier and to derive the distribution of snow depths. However, having to have two data sets limits their feasibility and makes it difficult to transfer the results to other study sites. In addition, modeling the vertical flow requires annual data and therefore an additional data set, preferably several years apart, which could be a challenge. The tuning factor introduced to account for the fraction of the annual flow covering the winter period and the firn compaction was derived using ALS and in-situ data combined, which means both data sets need to have been collected. The transfer to another glacier with only one measured data set available could therefore be difficult.

6.1.2 Distributed glacier surface albedo from ALS

Publication 4 (chapter 5):

Joerg, P.C., Weyermann, J., Morsdorf, F., Zemp, M., & Schaepman, M.E. (re-submitted after revisions). Computation of a distributed glacier surface albedo using airborne laser scanning intensity data and in-situ spectro-radiometric measurements. *Remote Sensing of Environment*

- What is the benefit of using ALS intensity information?

In glacier energy and mass balance modeling, an important factor governing melt is the broadband albedo – the fraction of energy reflected from the glacier's surface, which is therefore not available for melt (Oerlemans et al. 2009; Ohmura et al. 2007). However, this factor is typically not measured but introduced into an energy/mass balance by an educated guess (Cuffey and Paterson 2010; Greuell et al. 1997; Klok and Oerlemans

2004; Machguth et al. 2006b). The starting or calibration point for such an energy and mass balance model is often a DEM. In the first three papers, we focused on the exploitation of DEMs generated by ALS. However, most ALS systems also record the intensity of each backscattered ALS return at the same time as measuring distances from the airplane to the ground. The scanning nature of ALS systems therefore additionally provides near-infrared backscatter of the surveyed area, which could be used to derive the reflective properties at every location.

Our study therefore focused on the extraction of information based on ALS intensity corrections for glaciological purposes. We found that applying multiple steps of corrections to ALS raw intensity information resulted in a homogenous map of the near-infrared backscatter of the Findelengletscher's surface. However, to interpret these backscatter values physically, surface albedo reference measurements were needed and used to calibrate the corrected intensity data. Finally, this resulted in a distributed albedo proxy map of the Findelengletscher, which can be used as input for glacier energy/mass balance modeling.

- What is the information value of the albedo proxy derived from ALS intensity?

Our data set used the narrow, near-infrared band of the ALS system. The R^2 of 0.74 suggests a valid correlation between the corrected intensity values and the in-situ measurements. However, this result should be interpreted as a proxy for broadband albedo. The reflectance of snow in the near-infrared part of the electromagnetic spectrum is highly dependent on snow grain size, whereas in the visible part or the spectrum, the reflectance is more affected by impurities on the surface. The albedo proxy from ALS intensity thus provides better results in snow-covered areas of a glacier, whereas at the snow-free tongue, the significance is reduced. However, in the case of the data set used in our contribution, the Findelengletscher was almost entirely snow covered. In addition, the boundary conditions of albedo (between 0 and 1) were met confirming values reported in the literature for different areas and ages of snow.

This approach was improved by introducing a reference broadband albedo derived from a multi-spectral airborne digital camera (Leica ADS-80; RGB and near-infrared bands) acquired on the same date. This broadband albedo was then compared to the albedo proxy from the ALS data and showed a good agreement for the overall mean albedos and on the main part of the glacier. However, small systematic differences were detected on the glacier tongue, where the ALS albedo proxy overestimated the broadband albedo due to the restriction to accordingly map surface impurities in the ALS' near-infrared wavelength. In contrast, the broadband albedo was lower than the ALS albedo proxy in some parts of the accumulation area. As systematic differences in this entirely snow covered part were unlikely to originate from the ALS data, we suspected an inadequate topographic correction in the ADS 80 data. The comparatively low broadband albedo values were present in steep north-exposed slopes where the local solar zenith angles were very large. The BRDF correction applied might therefore be at its limit.

Our contribution went one step further than existing publications working with ALS intensity data (Geist 2005; Höfle and Pfeifer 2007; Lutz et al. 2003; Vain et al. 2009) by linking physically corrected intensity data to reference measurements with an observable physical quantity. Although the results for the entirely snow covered glacier look promising, additional research is needed to show that such data and methods also work well for a typical end-of-summer glacier surface (snow, firn, and ice).

6.2 Lessons learned for ALS glacier research

Since ALS was first used on glaciers in the mid-1990s (Favey et al. 1999; Kennett and Eiken 1996), it has technologically evolved, e.g. by the improving the accuracy of the IMU/GPS systems, and its potential application in glaciology has been demonstrated (e.g. the OMEGA project; Geist 2005). Thus the time is ripe for a careful assessment of the state of the art systems in the more operational context of a glacier mass balance monitoring program. The aim of this dissertation was to advance glacier research by using airborne laser scanning data, to better understand the products and accuracies provided by ALS and to demonstrate its benefit in different research fields in glaciology. The main lessons learned were:

- ALS should currently be the method of choice for geodetic glacier volume change measurements because it is very accurate and can map the entire glacier surface.
- Stochastic uncertainties in the ALS DEMs are negligible, but systematic uncertainties must always be considered.
- Existing volume change calculation methods must be evaluated carefully for scale-dependent systematic and stochastic uncertainties.
- The cost of an ALS data set can be reduced by choosing a lower point density, with which DEMs of reasonable quality can be produced.
- Synchronous in-situ and airborne measurements provide excellent data sets for topographic and albedo comparisons without needing to assume change between the different measurements and systems used.
- ALS can provide the winter snow depth distribution with high accuracy, if it is corrected for glacier dynamics and firn compaction.
- Using physically corrected ALS intensity data can provide distributed albedo proxy maps, which can serve as useful data inputs to improve glacier energy/mass balance models.

Based on these findings, we formulate the following recommendations within the larger project framework:

- Long-term monitoring of glaciers is essential, with ALS as the geodetic method of choice to complement in-situ measurements.
- ALS data should be easily usable and understandable, particularly in terms of data format, metadata, and accuracy estimations.
- The largest error sources in ALS are within the IMU/GPS system, but at an already very high accuracy level. Gross errors (e.g. erroneous coordinate transformation) pose a much greater threat to the data quality than system error sources. Independent reference measurements are therefore regarded as indispensable.
- Trading higher ALS point densities for larger survey areas or multi-temporal campaigns on the same area is recommended.
- A careful planning of synchronous field and flight campaigns is highly recommended.

- The LASER wavelength needs to be carefully evaluated. A test with 1560 nm led to a large part of the glacier not being detected, whereas 1064 nm performed much better.
- Energy/mass balance models should be improved as geodetic campaigns can often only be performed at decadal intervals to eliminate systematic errors in glaciological (in-situ) measurements.
- Results from ALS in glaciology can be attractively presented to the general public. Third-party project support can therefore be a funding solution for both researchers and funding parties.

6.3 Conclusions

Glaciers are sensitive indicators of climate change. Their currently strong melt is contributing considerably to rises in global sea levels, so that they are a strong symbol of today's changing climate. The quantification of glacier change has a long tradition, dating back more than 100 years. While the first attempts to measure glacier changes were restricted to in-situ measurements, airborne and spaceborne remote sensing have increasingly contributed by providing distributed, independent methods to validate the mass change in glaciers. However, with continually evolving systems and methods, sound uncertainty assessments of each method are indispensable.

In this dissertation we describe the benefits and limitations of applying of high resolution airborne laser scanning data sets in glaciology. It contributes to an existing in-situ mass balance measuring program by providing an accurate geodetic volume change of the glacier (along with an extensive uncertainty assessment) to compare and calibrate with in-situ measurements. Uncertainties were measured and modeled in-depth for the first time using different methods and reference datasets, as well as physical error propagation modeling and geostatistical approaches. We have shown that ALS can considerably benefit glaciology and is stochastically very accurate. However, systematic errors may still persist and must be evaluated carefully in each data set.

These high quality datasets were used to compare systematic and stochastic uncertainties in several traditional volume change methods on different scales with the reference high resolution ALS volume change. This evaluation showed that random method- and scale-dependent errors exist. Low relative spatial resolutions coordinated with the geometric shape of a glacier may lead to exponentially larger random uncertainties. In addition, such measurements are strongly dependent on the mass turnover of a glacier, although the absolute uncertainty remains the same, independent of the mass turnover. Thus, a glacier with little mass turnover, such as found in glaciers in Svalbard, is prone to larger relative uncertainties. The contour methods to estimate volume change worked reasonably well, but the central profile method was unable to capture the variability of the glacier sufficiently. In conclusion, the choice of a volume change method can systematically influence the result, which should be considered when using results from older volume change measurement methods.

The annual volume or mass change of a glacier has been the focus of research of many studies. However, the snow accumulation distribution is equally important, but the glacier dynamics and temporal firn compaction involved are complex and have thus been

less investigated. The third study used, along with in-situ snow probings and ground penetrating RADAR measurements, an additional winter ALS digital elevation model at maximum snow depth. The inter-comparison of these different measuring methods showed that ALS, if it is vertically corrected for emergence velocity and firn compaction, can map the snow accumulation pattern with high accuracy and spatial resolution. This map presents a new data base to validate snow accumulation models and should help to improve glacier mass balance models.

Such distributed mass balance models depend on accurate digital elevation models that show the glacier change measured and also meteorological and glacier surface properties. The amount of energy absorbed on the glacier's surface is directly available for melt and dependent on the surface broadband albedo. Albedo is one of the most important variables for the energy and mass balance of a glacier. The fourth study thus researched the applicability of ALS intensity data to provide a distributed albedo proxy. The results suggest that physical corrections can lead to improved ALS intensities and correlate with in-situ albedo measurements to a distributed albedo proxy. The resulting map respected the boundary conditions of albedo (values between 0 and 1) and was in agreement with albedo values from the literature. In addition, broadband albedo derived from an independent multi-spectral airborne digital sensor data set provided a good validation source for the ALS albedo proxy. The method seems to be a workable way to derive an albedo proxy where, as here, the glacier is almost entirely snow covered. For impure ice surfaces, however, more research using in-situ albedo measurements is needed and the conversion from intensity to an albedo proxy must be carefully evaluated.

6.4 Outlook

ALS is the method of choice in geodetic glacier applications. However, the high costs compared to airborne photogrammetry and the spectral restriction to only a single narrow band of the electromagnetic spectrum is challenged by the evolution of new multi-spectral photogrammetric scanners. In the past few years, new airborne systems featuring additional multi-angular near-infrared bands have been developed, which are better able to cope with the low textures encountered in the accumulation areas of glaciers. A co-supervised Master's thesis comparing ALS and Leica ADS-80 photogrammetric DEMs on the Findelengletscher suggests that the two methods are of comparable high quality. Photogrammetric methods are better known and the data obtained may attract a larger community than ALS with its higher costs and complexity. The additional synchronous availability of RGB orthophotos is another benefit, which directly helps to estimate supplementary glacier information, such as the current location of the snow line and surface classification, e.g. debris cover or albedo distribution. However, the quality of photogrammetric methods still depends on the presence of solar illumination of the surface and is not able to surpass the quality of ALS DEMs.

A desirable future development of ALS systems would therefore be to develop operational airborne multi-spectral LiDAR systems. Such multiple wavelengths would allow more information about glacier surface properties to be obtained without relying on solar illumination as in photogrammetric systems. However, the laser emission power is restricted for eye safety reasons in the visible part of the electromagnetic spectrum,

which could hamper the development of such systems. If these restrictions can be overcome, it should be possible to extract more information from the glacier surface, such as snow grain size, debris and albedo distribution.

Topographic glacier changes will also benefit from the recent emergence of small remote sensing drones (unmanned aerial vehicles, UAV). These lightweight UAV could already contribute to glacier research by providing photogrammetric DEMs and RGB or near-infrared orthophotos of glaciers. The high altitude and the size of glaciers, and prevailing strong winds mean the platform's usefulness is currently limited by battery capacity and propulsion power. Small RADAR and ALS instruments are currently being developed with UAV use in mind. However, the instrument's size and weight (and possibly high power consumption) still limit its operational applicability. Possibly, these problems will be overcome in a matter of few years.

This research has improved our understanding of the Findelengletscher, but the projects on topographic changes and albedo distribution have to be regarded as case studies. Long-term glacier monitoring is essential for climate change studies. Fortunately, the continuation of the direct glaciological measuring program was guaranteed by a memorandum of understanding between the Universities of Fribourg and Zurich, and should eventually lead to an invaluable long-term mass balance measurement program. Today, partly stimulated by this research and dissertation, the Findelengletscher has become the focus of several other research projects. These include automated snow line detection using a webcam (Huss et al. 2013), tests with terrestrial laser scanning, and investigations of spectral snow characteristics by the newly established Swiss Earth Observatory Network (SEON) using the imaging spectrometer APEX, and various field measurements. Thus, the Findelengletscher will continue to contribute to many different research fields and monitoring projects.

Although the Findelengletscher catchment contains only two glaciers, and excellent interdisciplinary research is being performed there, the representativeness of research and monitoring results is limited. Longer time-series of mass balance measurements are available for only a few glaciers worldwide. Improving glacier mass change measurements is therefore very important. However, operational glacier monitoring is not regarded as high priority research and it is consequently hard to obtain funding. On the other hand, if glacier monitoring from remote sensing platforms is to be improved, it requires more research into methods and better data from sensors is required to make it operational.

The excellent data and results from this research were used in training of Andean and Himalayan glaciologists. The know-how transfer to countries with far fewer options to mitigate the consequences of climate change and glacier melt than Switzerland will lead to more and better data from these sparsely sampled regions. However, the difficulty of obtaining decent remote sensing equipment makes it hard to assess uncertainty, which limits the quality of these measurements, particularly as in-situ measurements are not easy to perform. As a consequence, more effort must be made to develop new ways of remote sensing technologically.

6.5 References

Abermann, J., Fischer, A., Lambrecht, A., & Geist, T. (2010). On the potential of very high-resolution repeat DEMs in glacial and periglacial environments. *The Cryosphere, 4*, 53-65

Abermann, J., Lambrecht, A., Fischer, A., & Kuhn, M. (2009). Quantifying changes and trends in glacier area and volume in the Austrian Ötztal Alps (1969–1997–2006). *The Cryosphere, 3*, 415-441

Arendt, A.A., Echelmeyer, K.A., Harrison, W.D., Lingle, C.S., & Valentine, V.B. (2002). Rapid wastage of Alaska glaciers and their contribution to rising sea level. *Science, 297*, 382-386

Baltsavias, E.P. (1999). Airborne laser scanning: basic relations and formulas. *ISPRS Journal of Photogrammetry and Remote Sensing, 54*, 199-214

Begert, M., Schlegel, T., & Kirchhofer, W. (2005). Homogeneous temperature and precipitation series of Switzerland from 1864 to 2000. *International Journal of Climatology, 25*, 65-80

Beniston, M., Stoffel, M., & Hill, M. (2011). Impacts of climatic change on water and natural hazards in the Alps: Can current water governance cope with future challenges? Examples from the European "ACQWA" project. *Environmental Science and Policy, 14*, 734-743

Berk, A., Anderson, G.P., Acharya, P.K., Bernstein, L.S., Muratov, L., Lee, J., Fox, M., Adler-Golden, S.M., Chetwynd, J.H., Hoke, M.L., Lockwood, R.B., Gardner, J.A., Cooley, T.W., Borel, C.C., Lewis, P.E., & Shettle, E.P. (2006). MODTRAN™ 5: 2006 update. In, *Proceedings of SPIE - The International Society for Optical Engineering*. Kissimmee, FL, USA

Berthier, E., Schiefer, E., Clarke, G.K.C., Menounos, B., & Rémy, F. (2010). Contribution of Alaskan glaciers to sea-level rise derived from satellite imagery. *Nature Geoscience, 3*, 92-95

Brock, B.W., Willis, I.C., & Sharp, M.J. (2000). Measurement and parameterization of albedo variations at haut glacier d'arolla, Switzerland. *Journal of Glaciology, 46*, 675-688

Cogley, J.G. (2009). A more complete version of the World Glacier Inventory. *Annals of Glaciology, 50*, 32-38

Collins, D.N. (1979). Quantitative determination of the subglacial hydrology of two Alpine glaciers. *Journal of Glaciology, 23*, 347-362

Corripio, J.G. (2004). Snow surface albedo estimation using terrestrial photography. *International Journal of Remote Sensing, 25*, 5705-5729

Cuffey, K.M., & Paterson, W.S.B. (2010). *The Physics of Glaciers*. (4 ed.). Oxford: Butterworth-Heinemann

Dadic, R., Mott, R., Lehning, M., & Burlando, P. (2010). Wind influence on snow depth distribution and accumulation over glaciers. *Journal of Geophysical Research F: Earth Surface, 115*

Dozier, J., Green, R.O., Nolin, A.W., & Painter, T.H. (2009). Interpretation of snow properties from imaging spectrometry. *Remote Sensing of Environment, 113*, 25-37

Dozier, J., & Painter, T.H. (2004). Multispectral and Hyperspectral Remote Sensing of Alpine Snow Properties. *Annual Review of Earth and Planetary Sciences, 32*, 465-494

Farinotti, D., Usselmann, S., Huss, M., Bauder, A., & Funk, M. (2011). Runoff evolution in the Swiss Alps: projections for selected high-alpine catchments based on ENSEMBLES scenarios. *Hydrological Processes, 26*, 1909-1924

Favey, E., Geiger, A., Gudmundsson, G.H., & Wehr, A. (1999). Evaluating the Potential of an Airborne Laser-scanning System for Measuring Volume Changes of Glaciers. *Geografiska Annaler: Series A, Physical Geography, 81*, 555-561

Filin, S. (2003). Recovery of systematic biases in laser altimetry data using natural surfaces. *Photogrammetric Engineering & Remote Sensing, 69*, 1235-1242

Finsterwalder, R. (1953). Die zahlenmässige Erfassung des Gletscherrückgangs an Ostalpengletschern. *Zeitschrift für Gletscherkunde und Glazialgeologie, 2*, 189-239

Finsterwalder, R. (1954). Photogrammetry and glacier research with special reference to glacier retreat in the Eastern Alps. *Journal of Glaciology, 2*, 306-315

Finsterwalder, S. (1897). Der Vernagtferner. *Wissenschaftliche Ergänzungshefte zur Zeitschrift des Deutschen und Österreichischen Alpenvereins, 1*, 1-96

Flanner, M.G., Zender, C.S., Randerson, J.T., & Rasch, P.J. (2007). Present-day climate forcing and response from black carbon in snow. *Journal of Geophysical Research D: Atmospheres, 112*

Frey, H., Haeberli, W., Linsbauer, A., Huggel, C., & Paul, F. (2010). A multi-level strategy for anticipating future glacier lake formation and associated hazard potentials. *Natural Hazards and Earth System Science, 10*, 339-352

Geist, T. (2005). Application of airborne laser scanner technology in glacier research. In, *Faculty of Geo- and Atmospheric Sciences, Institute of Geography* (p. 118). Innsbruck: University of Innsbruck

Geist, T., Lutz, E., & Stötter, J. (2003). Airborne laser scanning technology and its potential for applications in glaciology. *International Archives of Photogrammetry, Remote Sensing and Spatial Information Science, 34*, 101-106

Glaciological Reports (1881-2010). The Swiss Glaciers. In, *Yearbooks of the Cryospheric Commission of the Swiss Academy of Sciences (SCNAT)* published since 1964 by the Laboratory of Hydraulics, Hydrology and Glaciology (VAW) of ETH Zürich

Glennie, C. (2007). Rigorous 3D error analysis of kinematic scanning LIDAR systems. *Journal of Applied Geodesy, 1*, 147-157

Goulden, T., & Hopkinson, C. (2010). The Forward Propagation of Integrated System Component Errors within Airborne Lidar Data. *Photogrammetric Engineering & Remote Sensing, 76*, 589-601

Greuell, W., Knap, W.H., & Smeets, P.C. (1997). Elevational changes in meteorological variables along a midlatitude glacier during summer. *Journal of Geophysical Research D: Atmospheres, 102*, 25941-25954

Haeberli, W., Hoelzle, M., Paul, F., & Zemp, M. (2007). Integrated monitoring of mountain glaciers as key indicators of global climate change: The European Alps. *Annals of Glaciology, 46*, 150-160

Haug, T., Rolstad, C., Elvehøy, H., Jackson, M., & Maalen-Johansen, I. (2009). Geodetic mass balance of the western Svartisen ice cap, Norway, in the periods 1968-1985 and 1985-2002. *Annals of Glaciology, 50*, 119-125

Heinzel, J., & Koch, B. (2011). Exploring full-waveform LiDAR parameters for tree species classification. *International Journal of Applied Earth Observation and Geoinformation, 13*, 152-160

Hock, R. (1999). A distributed temperature-index ice- and snowmelt model including potential direct solar radiation. *Journal of Glaciology, 45*, 101-111

Hodgson, M.E., & Bresnahan, P. (2004a). Accuracy of airborne lidar-derived elevation: Empirical assessment and error budget. *Photogrammetric Engineering & Remote Sensing, 70*, 331-339

Hodgson, M.E., & Bresnahan, P. (2004b). *Accuracy of airborne lidar-derived elevation: Empirical assessment and error budget*. Bethesda, MD, ETATS-UNIS: American Society for Photogrammetry and Remote Sensing

Hoelzle, M., Darms, G., Lüthi, M.P., & Suter, S. (2011). Evidence of accelerated englacial warming in the Monte Rosa area, Switzerland/Italy. *Cryosphere, 5*, 231-243

Höfle, B., & Pfeifer, N. (2007). Correction of laser scanning intensity data: Data and model-driven approaches. *ISPRS Journal of Photogrammetry and Remote Sensing, 62*, 415-433

Hofmann, W. (1958). Der Vorstoss des Nisqually-Gletschers am Mt. Rainier, U.S.A., von 1952 bis 1956. *Zeitschrift für Gletscherkunde und Glazialgeologie, 4*, 47-60

Hopkinson, C., & Demuth, M.N. (2006). Using airborne lidar to assess the influence of glacier downwasting on water resources in the Canadian Rocky Mountains. *Canadian journal of remote sensing, 32*, 212-222

Hueni, A., Nieke, J., Schopfer, J., Kneubühler, M., & Itten, K.I. (2009). The spectral database SPECCHIO for improved long-term usability and data sharing. *Computers and Geosciences, 35*, 557-565

Huising, E.J., & Gomes Pereira, L.M. (1998). Errors and accuracy estimates of laser data acquired by various laser scanning systems for topographic applications. *ISPRS Journal of Photogrammetry and Remote Sensing, 53*, 245-261

Huss, M. (2013). Density assumptions for converting geodetic glacier volume change to mass change. *The Cryosphere, 7*, 877-887

Huss, M., Bauder, A., & Funk, M. (2009). Homogenization of long-term mass-balance time series. *Annals of Glaciology, 50*, 198-206

Huss, M., Bauder, A., Funk, M., & Hock, R. (2008). Determination of the seasonal mass balance of four Alpine glaciers since 1865. *Journal of Geophysical Research F: Earth Surface, 113*

Huss, M., Sold, L., Hoelzle, M., Stokvis, M., Salzmann, N., Farinotti, D., & Zemp, M. (2013). Towards remote monitoring of sub-seasonal glacier mass balance. *Annals of Glaciology, 54*, 75-83

Huss, M., Zemp, M., Joerg, P.C., & Salzmann, N. (2014). High uncertainty in 21st century runoff projections from glacierized basins. *Journal of Hydrology, 510*, 35-48

Iken, A., & Bindschadler, R.A. (1986). Combined measurements of subglacial water pressure and surface velocity of Findelengletscher, Switzerland: conclusions about drainage system and sliding mechanism. *Journal of Glaciology, 32*, 101-119

Joerg, P.C., Morsdorf, F., & Zemp, M. (2012). Uncertainty assessment of multi-temporal airborne laser scanning data: A case study on an Alpine glacier. *Remote Sensing of Environment, 127*, 118-129

Joerg, P.C., & Zemp, M. (2014). Evaluating volumetric glacier change methods using airborne laser scanning data. *Geografiska Annaler, Series A: Physical Geography, 96*, 135-145

Jonsell, U., Hock, R., & Holmgren, B. (2003). Spatial and temporal variations in albedo on Storglaciären, Sweden. *Journal of Glaciology, 49*, 59-68

Kaasalainen, S., Pyysalo, U., Krooks, A., Vain, A., Kukko, A., Hyyppä, J., & Kaasalainen, M. (2011). Absolute Radiometric Calibration of ALS Intensity Data: Effects on Accuracy and Target Classification. *Sensors, 11*, 10586-10602

Kaser, G., Fountain, A., & Jansson, P. (2003). A Manual for Monitoring the Mass Balance of Mountain Glaciers. In, *IHP-VI Technical Documents in Hydrology*. Paris, France: UNESCO

Keiler, M., Knight, J., & Harrison, S. (2010). Climate change and geomorphological hazards in the eastern European Alps. *Philosophical Transactions of the Royal Society A: Mathematical, Physical and Engineering Sciences, 368*, 2461-2479

Kennett, M., & Eiken, T. (1996). Airborne measurement of glacier surface elevation by scanning laser altimeter. *Annals of Glaciology, 24*, 293-296

Klok, E.J., & Oerlemans, J. (2004). Modelled climate sensitivity of the mass balance of Morteratschgletscher and its dependence on Albedo parameterization. *International Journal of Climatology, 24*, 231-245

Knap, W.H., Brock, B.W., Oerlemans, J., & Willis, I.C. (1999a). Comparison of Landsat TM-derived and ground-based albedos of Haut Glacier d'Arolla, Switzerland. *International Journal of Remote Sensing, 20*, 3293-3310

Knap, W.H., Reijmer, C.H., & Oerlemans, J. (1999b). Narrowband to broadband conversion of landsat TM glacier albedos. *International Journal of Remote Sensing, 20*, 2091-2110

Knoll, C., & Kerschner, H. (2010). A glacier inventory for South Tyrol, Italy, based on airborne laser-scanner data. *Annals of Glaciology, 50*, 46-52

Koblet, T., Gärtner-Roer, I., Zemp, M., Jansson, P., Thee, P., Haeberli, W., & Holmlund, P. (2010). Reanalysis of multi-temporal aerial images of Storglaciären, Sweden (1959-99); Part 1: Determination of length, area, and volume changes. *The Cryosphere, 4*, 333-343

Law, K.H., & Nichol, J. (2004). Topographic correction for differential illumination effects on IKONOS satellite imagery. *Proceedings of the XXth ISPRS Congress, Istanbul, Turkey*, 641-646

Lemke, P., Ren, J., Alley, R.B., Allison, I., Carrasco, J., Flato, G., Fujii, Y., Kaser, G., Mote, P., & Thomas, R.H. (Eds.) (2007). *Observations: Changes in snow, ice and frozen ground*. Cambridge, UK and New York, NY, USA: Cambridge University Press

Li, W., Stamnes, K., Eide, H., & Spurr, R. (2007). Bidirectional reflectance distribution function of snow: corrections for the Lambertian assumption in remote sensing applications. *Optical Engineering, 46*, 066201

Liang, S. (2001). Narrowband to broadband conversions of land surface albedo I algorithms. *Remote Sensing of Environment, 76*, 213-238

Liu, S., Liu, Q., Wen, J., & Li, X. (2010). The angular and spectral kernel model for BRDF and albedo retrieval. *IEEE Journal of Selected Topics in Applied Earth Observations and Remote Sensing, 3*, 241-256

Lutz, E., Geist, T.H., & Stötter, J. (2003). Investigations of airborne laser scanning signal intensity on glacial surfaces — Utilizing comprehensive laser geometry modeling and orthophoto surface modeling (A case study: Svartisheibreen, Norway). *International Archives of Photogrammetry, Remote Sensing and Spatial Information Sciences, 34*, 143-148

Luzum, B.J., Starek, M., & Slatton, K.C. (2004). Normalizing ALSM intensities. In, *Geosensing Engineering and Mapping (GEM) Center Report No. Rep 2004-07-001* (p. 8): Civil and Coastal Engineering Department, University of Florida

Lyapustin, A., Gatebe, C.K., Kahn, R., Brandt, R., Redemann, J., Russell, P., King, M.D., Pedersen, C.A., Gerland, S., Poudyal, R., Marshak, A., Wang, Y., Schaaf, C., Hall, D., & Kokhanovsky, A. (2010). Analysis of snow bidirectional reflectance from ARCTAS spring-2008 campaign. *Atmospheric Chemistry and Physics, 10*, 4359-4375

Machguth, H. (2008). On the Use of RCM Data and Gridded Climatologies for Regional Scale Glacier Mass Balance Modeling in High Mountain Topography; The Example of the Swiss Alps. In, *Department of Geography* (p. 176). Zurich: University of Zurich

Machguth, H., Eisen, O., Paul, F., & Hoelzle, M. (2006a). Strong spatial variability of snow accumulation observed with helicopter-borne GPR on two adjacent Alpine glaciers. *Geophys. Res. Lett., 33*, L13503

Machguth, H., Paul, F., Hoelzle, M., & Haeberli, W. (2006b). Distributed glacier mass-balance modelling as an important component of modern multi-level glacier monitoring. *Annals of Glaciology, 43*, 335-343

Mallet, C., & Bretar, F. (2009). Full-waveform topographic lidar: State-of-the-art. *ISPRS Journal of Photogrammetry and Remote Sensing, 64*, 1-16

Mannstein, H. (1985). The interpretation of albedo measurements on a snowcovered slope. *Archives for Meteorology, Geophysics, and Bioclimatology Series B, 36*, 73-81

Mercanton, P.L. (1916). Vermessungen am Rhonegletscher/Mensuration au glacier du Rhone: 1874-1915. *Neue Denkschrift der Schweizerischen Naturforschenden Gesellschaft, 52*, 189

Morsdorf, F., Meier, E., Kötz, B., Itten, K.I., Dobbertin, M., & Allgöwer, B. (2004). LIDAR-based geometric reconstruction of boreal type forest stands at single tree level for forest and wildland fire management. *Remote Sensing of Environment, 92*, 353-362

Negi, H.S., & Kokhanovsky, A. (2011). Retrieval of snow albedo and grain size using reflectance measurements in Himalayan basin. *Cryosphere, 5*, 203-217

Nelson, R., Krabill, W., & MacLean, G. (1984). Determining forest canopy characteristics using airborne laser data. *Remote Sensing of Environment, 15*, 201-212

Nuth, C., & Kääb, A. (2011). Co-registration and bias corrections of satellite elevation data sets for quantifying glacier thickness change. *The Cryosphere, 5*, 271-290

Oberli, A. (1979). Dufour-Karte und Siegfried-Atlas. *Unsere Landeskarten* (p. 72). Berne: Schweizerischer Alpen-Club in cooperation with the Federal Office of Topography

Oerlemans, J., Giesen, R.H., & Van Den Broeke, M.R. (2009). Retreating alpine glaciers: Increased melt rates due to accumulation of dust (Vadret da Morteratsch, Switzerland). *Journal of Glaciology, 55*, 729-736

Oerlemans, J., & Knap, W.H. (1998). A 1 year record of global radiation and albedo in the ablation zone of Morteratschgletscher, Switzerland. *Journal of Glaciology, 44*, 231-238

Ohmura, A., Bauder, A., Müller, H., & Kappenberger, G. (2007). Long-term change of mass balance and the role of radiation. *Annals of Glaciology, 46*, 367-374

Østrem, G., & Brugmann, M. (1991). *Glacier Mass-Balance Measurements: A Manual for Field and Office Work*. Oslo: NVE

Paul, F., Machguth, H., & Kääb, A. (2005). On the impact of glacier albedo under conditions of extreme glacier melt: The summer of 2003 in the Alps. *EARSeL eProceedings, 4*, 139-149

Rabus, B., Eineder, M., Roth, A., & Bamler, R. (2003). The shuttle radar topography mission - A new class of digital elevation models acquired by spaceborne radar. *ISPRS Journal of Photogrammetry and Remote Sensing, 57*, 241-262

Reinhardt, W., & Rentsch, H. (1986). Determination of changes in volume and elevation of glaciers using digital elevation models for the Vernagtferner, Ötztal Alps, Austria. *Annals of Glaciology, 8*, 151-155

Richter, R., & Schläpfer, D. (2002). Geo-atmospheric processing of airborne imaging spectrometry data. Part 2: Atmospheric/topographic correction. *International Journal of Remote Sensing, 23*, 2631-2649

Rignot, E., Echelmeyer, K., & Krabill, W. (2001). Penetration depth of interferometric synthetic-aperture radar signals in snow and ice. *Geophysical research letters, 28*, 3501-3504

Roujean, J.L., Leroy, M., & Deschamps, P.Y. (1992). A bidirectional reflectance model of the Earth's surface for the correction of remote sensing data. *Journal of Geophysical Research, 97*, 20455-20468

Sapiano, J.J., Harrison, W.D., & Echelmeyer, K.A. (1998). Elevation, volume and terminus changes of nine glaciers in North America. *Journal of Glaciology, 44*, 119-135

Schaepman-Strub, G., Schaepman, M.E., Painter, T.H., Dangel, S., & Martonchik, J.V. (2006). Reflectance quantities in optical remote sensing—definitions and case studies. *Remote Sensing of Environment, 103*, 27-42

Sold, L., Huss, M., Hoelzle, M., Andereggen, H., Joerg, P.C., & Zemp, M. (2013). Methodological approaches to infer end-of-winter snow distribution on alpine glaciers. *Journal of Glaciology, 59*, 1047-1059

Stroeve, J., Box, J.E., Gao, F., Liang, S., Nolin, A., & Schaaf, C. (2005). Accuracy assessment of the MODIS 16-day albedo product for snow: Comparisons with Greenland in situ measurements. *Remote Sensing of Environment, 94*, 46-60

Sugiyama, S., Yoshizawa, T., Huss, M., Tsutaki, S., & Nishimura, D. (2011). Spatial distribution of surface ablation in the terminus of Rhonegletscher, Switzerland. *Annals of Glaciology, 52*, 1-8

Tachikawa, T., Hato, M., Kaku, M., & Iwasaki, A. (2011). Characteristics of ASTER GDEM version 2. In (pp. 3657-3660)

Vain, A., Kaasalainen, S., Pyysalo, U., Krooks, A., & Litkey, P. (2009). Use of Naturally Available Reference Targets to Calibrate Airborne Laser Scanning Intensity Data. *Sensors, 9*, 2780-2796

Vain, A., Liba, N., & Sepp, K. (2011). Factors affecting the airborne laser scanning intensity data. In, *Environmental Engineering, 8th international conference*. Vilnius, Lithuania: Vilnius Gediminas Technical University

Wagner, W. (2010). Radiometric calibration of small-footprint full-waveform airborne laser scanner measurements: Basic physical concepts. *ISPRS Journal of Photogrammetry and Remote Sensing, 65*, 505-513

Wagner, W., Ullrich, A., Ducic, V., Melzer, T., & Studnicka, N. (2006). Gaussian decomposition and calibration of a novel small-footprint full-waveform digitising airborne laser scanner. *ISPRS Journal of Photogrammetry and Remote Sensing, 60*, 100-112

Wanner, W., Li, X., & Strahler, A.H. (1995). A new class of geometric-optical semiempirical kernels for global BRDF and albedo modeling. In, *Geoscience and Remote Sensing Symposium, IGARSS '95* (pp. 15-17)

Warren, S.G. (1982). Optical properties of snow. *Reviews of Geophysics and Space Physics, 20*, 67-89

Wehr, A., & Lohr, U. (1999). Airborne laser scanning-an introduction and overview. *ISPRS Journal of Photogrammetry and Remote Sensing, 54*, 68-82

WGMS (2012). *Fluctuations of Glaciers 2005-2010*. Zurich, Switzerland: ICSU(WDS)/IUGG(IACS)/UNEP/UNESCO/WMO, World Glacier Monitoring Service

Wiscombe, W.J., & Warren, S.G. (1980). A model for the spectral albedo of snow. I: pure snow. *Journal of the Atmospheric Sciences, 37*, 2712-2733

Zemp, M., Haeberli, W., Hoelzle, M., & Paul, F. (2006). Alpine glaciers to disappear within decades? *Geophysical research letters, 33*

Zemp, M., Hoelzle, M., & Haeberli, W. (2009). Six decades of glacier mass-balance observations: A review of the worldwide monitoring network. *Annals of Glaciology, 50*, 101-111

Zemp, M., Jansson, P., Holmlund, P., Gärtner-Roer, I., Koblet, T., Thee, P., & Haeberli, W. (2010). Reanalysis of multi-temporal aerial images of Storglaciären, Sweden (1959-99); Part 2: Comparison of glaciological and volumetric mass balances. *The Cryosphere, 4*, 345-357

Zemp, M., Thibert, E., Huss, M., Stumm, D., Rolstad Denby, C., Nuth, C., Nussbaumer, S.U., Moholdt, G., Mercer, A., Mayer, C., Joerg, P.C., Jansson, P., Hynek, B., Fischer, A., Escher-Vetter, H., Elvehøy, H., & Andreassen, L.M. (2013). Uncertainties and re-analysis of glacier mass balance measurements. *The Cryosphere Discussions, 7*, 789-839

Zwally, H.J., Schutz, B., Abdalati, W., Abshire, J., Bentley, C., Brenner, A., Bufton, J., Dezio, J., Hancock, D., Harding, D., Herring, T., Minster, B., Quinn, K., Palm, S., Spinhirne, J., & Thomas, R. (2002). ICESat's laser measurements of polar ice, atmosphere, ocean, and land. *Journal of Geodynamics, 34*, 405-445

CURRICULUM VITAE

Academic education

2009－2014 **Ph.D.** studies University of Zurich (Switzerland), Department of Geography, Glaciology and Geomorphodynamics Group (3G)/Remote Sensing Laboratories (RSL). Thesis: *Assessment of glacial changes, surface properties, and related uncertainties based on airborne laser scanning*.

2007－2008 **MSc** studies in Geography, University of Zurich (Switzerland). Thesis: *Processing of full waveform airborne laser scanning data in Southern France*.

2004－2007 **BSc** studies in Geography, University of Zurich (Switzerland). Thesis: *Fusion von LiDAR-Daten mit passiv-optischen Daten: Methoden und Anwendungen*.

1995－2002 **Matura** type E (economy and natural sciences) at the Kantonsschule Graubünden, Chur (Switzerland)

Teaching and supervisions

2013－present **Lecture and exercises:** GEO 233: Bachelor's course to basics in remote sensing.

2011－present **Lecture and exercises**: GEO 813: Surveying course for geography graduate students.

2013－2014 **MSc co-supervision**: Thierry Bossard, *Evaluation of the glaciological suitability of aerial image based digital elevation models through airborne laser scanning data at the Findelengletscher, Canton Valais*.

2012 **BSc supervision**: Nadia Signer, *Methoden zur Bestimmung der Massenbilanz von Gletschern: Vergleich und Kombination*.

2011 **BSc supervision**: Pascal Buri, *Methoden zur Messung und Modellierung der Winter-Massenbilanz von alpinen Gletschern*.

2010 **BSc supervision**: Thierry Bossard, *Methoden zur Messung und Modellierung der Albedo von Gletschern*.

Professional experience

2013－present **Research associate**, Head of the scientific National Point of Contact for Satellite Images (NPOC) at the University of Zurich, Department of Geography, Remote Sensing Laboratories (RSL), Zurich, Switzerland. Scientific consulting, experimental product development, and teaching.

2011－present **Lecturer**, surveying course for geography graduate students and Bachelor courses, University of Zurich, Department of Geography, Remote Sensing Laboratories (RSL), Zurich, Switzerland.

2009－2013 **Research assistant**, University of Zurich, Department of Geography, Glaciology and Geomorphodynamics Group (3G), Zurich, Switzerland.

2006－2008 **Tutor and semester assistant**, University of Zurich, Department of Geography, Remote Sensing Laboratories (RSL), Zurich, Switzerland.

2004 & 2005 **Internships,** surveyor, TRANSCO Sedrun (Batigroup), new Gotthard railway base tunnel, Switzerland.

Graduate courses and professional training

- Effective scientific presentations
- Principles and theories in geography
- Scientific writing
- Graduate Seminar I & II
- Project management
- Retreat seminars
- Karthaus summer school on ice sheets and glaciers in the climate system

Conferences and workshops

- Axporama glacier exhibit vernissage (Böttstein, Switzerland, 2013)
- Workshop on measurement and uncertainty assessment of glacier mass balance (Tarfala, Sweden, 2012)
- Andes+ Capacity Building (Zurich, Switzerland, 2012)
- Alpine Glaciology Meeting (Munich, Germany, 2011)
- 2° Ausstellung (Basle, Switzerland, 2011)
- Karthaus summer school on ice sheets and glaciers in the climate system (Karthaus, 2011)
- European Geosciences Union (Vienna, Austria, 2010)
- Nacht der Forschung (Zurich, Switzerland, 2009)
- Gletscherworkshop (Obergurgl, Austria, 2009)

Publications

Peer-reviewed publications

Joerg, P.C., Morsdorf, F., & Zemp, M. (2012). Uncertainty assessment of multi-temporal airborne laser scanning data: A case study on an Alpine glacier. *Remote Sensing of Environment, 127*, 118-129

Sold, L., Huss, M., Hoelzle, M., **Joerg, P.C.**, & Zemp, M. (2013). Methodological approaches to inferring end-of-winter snow distribution on alpine glaciers. *Journal of Glaciology, 59*, 1047-1059

Zemp, M., Thibert, E., Huss, M., Stumm, M., Rolstad Denby, C., Nuth, C., Nussbaumer, S.U., Moholdt, G., Mercer, A., Meyer, C., **Joerg, P.C.**, Jansson, P., Hynek, B., Fischer, A., Escher-Vetter, H., Elvehøy, H., & Andreassen, L.M. (2013). Reanalysing glacier mass balance measurement series. *The Cryosphere, 7*, 1227-1245

Joerg, P.C., & Zemp, M. (2014). Evaluating volumetric glacier change methods using airborne laser scanning data. *Geographiska Annaler: Series A Physical Geography, 96,* 135-145

Huss, M., Zemp, M., **Joerg**, **P.C.**, & Salzmann, N. (2014). High uncertainty in 21st century runoff projections from glacierized basins. *Journal of Hydrology, 510,* 35-48

Joerg, P.C., Weyermann, J., Morsdorf, F., Zemp, M., Schaepman, M. (re-submitted). Computation of a distributed glacier surface albedo using airborne laser scanning intensity data and in-situ spectro-radiometric measurements. *Remote Sensing of Environment*

Other scientific contributions

Joerg, P.C., Morsdorf, F., Zemp, M. (2010). Operational use of airborne laserscanning for glacier monitoring in Switzerland. EGU General Assembly, Vienna, AT.

Joerg, P.C. (2010). Gletschervermessung mit Licht. Exhibition on "2° - Weather, Humans and the Climate", Basel, CH.

Joerg, P.C., Machguth, H., Huss, M., Morsdorf, F., Zemp, M. (2011). Mass balance assessment using in-situ methods and airborne laserscanning at Findelengletscher, Switzerland. Alpine Glaciology Meeting, Munich, DE.

Joerg, P.C. (2011). Airborne Laser Scanning im Einsatz der Glaziologie am Findelengletscher. *Geomatik Schweiz, 109,* 444-447

Huss, M., Zemp, M., **Joerg, P.C.**, Sold, L., Salzmann, N. (2012). High uncertainty in 21st century runoff projections from glacierized catchments. EGU General Assembly, Vienna, AT.

Sold, L., Huss, M., Hoelzle, M., **Joerg, P.C.**, Salzmann, N., Zemp, M. (2012). Methodological approaches to inferring end-of-winter snow distribution on alpine glaciers. EGU General Assembly, Vienna, AT.

Sold, L., Huss, M., Hoelzle, M., **Joerg, P.C.**, Salzmann, N., Zemp, M. (2012). Measuring and understanding winter mass balance and snow depth distribution on alpine glaciers from LiDAR DEM differentiation, GPR and snow soundings. Swiss Geoscience Meeting, Bern, CH.

Joerg, P.C., Morsdorf, F., Zemp, M. (2012).Topographic Change of Findelengletscher, Valais, Switzerland, 2005-2010 (including map 1:15,000). Fluctuations of Glaciers, Vol. X (2005-2010).

Rastner, P., Zemp, M., **Joerg, P.C.**, Huss M. (2013). Scientific visualization of glacier changes for public communication: the example of Findelengletscher, Switzerland. EGU general assembly, Vienna, AT.

Huss, M., Zemp, M., **Joerg, P.C.**, Salzmann, N. (2013). High uncertainty in 21st century runoff projections from glacierized catchments. Davos Atmosphere and Cryosphere Assembly, CH.

Joerg, P.C., Weyermann, J. Morsdorf, F., Zemp, M., Schaepman, M.E. (2014). From airborne laser scanning intensity to a distributed glacier surface albedo product. EGU general assembly, Vienna, AT.

ACKNOWLEDGEMENTS

In the past four years, I was given the unique opportunity to perform research in an interdisciplinary project involving many fields I'm personally fascinated with. The topics of climate change, glaciology, and applied remote sensing always intrigued me and are also of great interest for the wider public. Despite my already sound geographical education, this PhD dissertation would not have been possible without the support of many people I'd like to express my gratitude to. Furthermore, I'm grateful for the support of the Axpo Holding AG which enabled the superior project and consequently my PhD studies.

My sincere thanks on the professional as well as on the personal side go to Wilfried Haeberli and Michael Schaepman for their inspiration and enthusiasm in their research fields of glaciology and remote sensing, and for continuously supporting my project. Michael Zemp and Felix Morsdorf for their friendliness, motivation, fruitful discussions of topics new to me, and the support in the exhausting publication processes, as well as for excellent company, also during field work – I learned a lot from you guys! Matthias Huss and Philipp Rastner for taking great care of the two side projects, fruitful discussions, and the derivation and presentation of stunning results. All my colleagues at UZH, foremost of both the 3G and RSL groups, for sharing a great time. The "Findelitos" group members at UZH and UFR for their strenuous efforts collecting in-situ data invaluable for my studies and for keeping an eye on good old Findelengletscher. Special thanks to Monika Müller and Christian Brogli of the Axpo Holding AG for demonstrating how to professionally deal with the public (in the media as well as for the Axporama exhibition), for their excellent collaboration and personal cordiality. BSF-Swissphoto for providing the study with excellent ALS data as well as documentation, and for linking us with Optech Inc., the instrument's manufacturer for sharing in-depth technical details of the scanner system. Sincere thanks to Stephan Landtwing and Lucas Clemenz for professionally leading the project on the data provider's side and answers to many questions never asked by the usual customer. Many thanks also to Silvia Dingwall for polishing the English of the dissertation.

I'm certainly indebted to my family members and friends, who had to share me with things like Lasers, Matlab, and the Findelengletscher. First and foremost thanks to my wife, Nadia, who was always supporting me more than I could ever have asked for. Thank you very much, you are the sunshine of my life! With you I feel confident to be able to tackle the adventure of our family with our son Adriano. I'd like to especially thank my parents Sandra and Silvio and my sister Annina for always wholeheartedly supporting me. Sincere thanks go also to other family members, my dear friends, and their partners: Martin, Beat, Daniel, Lars, Christine, Seraina, Annina, Christoph, Philippe, Désirée, Stephanie, Sonja, Luana, Philipp, Marcel, Jana, Djavi, Alexa, Charlotte, Christian, Nicola, Sina, Gianrico, Ervin, Elio, Yvonne, and many more I might have forgotten to mention here.

Thank you all!

ISBN Nr. 978-3-03703-031-8